博 士 論 文

Spectral Modeling of Reflective-Fluorescent Scenes

（反射と蛍光を含むシーンの分光特性モデリング）

東京大学大学院
情報理工学系研究科
電子情報学専攻

48-127421　付 瑩

指導教員　佐藤洋一　教授

平成 27 年 6 月

Abstract

Fluorescence frequently occurs in many objects, such as natural gems and corals, fluorescent dyes used for clothing, and plant containing chlorophyll to name a few. In fact, it was reported that fluorescent surfaces are present in 20% of randomly constructed scenes. This is a significant proportion of scenes that have not been considered in the past. Another important point is that reflective and fluorescent components behave very differently under different illuminants. Thus to accurately predict the color of objects, separate modeling of all spectral properties of both reflective and fluorescent components is essential. The goal of this research is to model the full spectral reflective and fluorescent components of an entire scene, and make use of the fluorescence with various computer vision techniques.

The first part of this thesis describes efficient separation and recovery of reflectance and fluorescence emission spectra through the use of two high frequency illuminations modulated in the spectral domain. With the obtained fluorescence emission spectra from the high frequency illuminants, it is then described how to estimate the fluorescence absorption spectrum of a material given its emission spectrum. In addition, I provide an in depth analysis of the method and also show that filters can be used in conjunction with standard light sources to generate the required high frequency illuminants. The proposed method is also tested under ambient light to demonstrate its applicability to synthetic relighting of real scenes.

In the second part, a more practical approach is presented to hyperspectral imaging of reflective-fluorescent scenes using only a conventional RGB camera and varied colored illuminants. The key idea of the proposed approach is to exploit a unique property of fluorescence: the chromaticity of fluorescent emissions are invariant under different illuminants. This allows to robustly estimate spectral reflectance and fluorescent emission chromaticity. Then, given the spectral reflectance and fluorescent chromaticity, the fluorescence absorption and emission spectra can also be estimated. Experimental results demonstrate that all scene spectra can be accurately estimated from RGB images. It

is also shown that the proposed method can be used to accurately relight scenes under novel lighting.

In the third part, a novel method is proposed for removing interreflections from only a single image using fluorescence. From a bispectral observation of reflective and fluorescent components recorded in distinct color channels, the proposed method separates direct lighting from interreflections. Experimental results demonstrate the effectiveness of the proposed method on complex and dynamic scenes. In addition, it is shown how the proposed method improves an existing photometric stereo method in shape recovery.

The main contributions of this dissertation are three folds: the spectral property under high frequency illumination is explored to model the spectral of reflective-fluorescent scenes; a more practical approach is presented to hyperspectral imaging of reflective-fluorescent scenes using only a conventional RGB camera and varied colored illuminants; the bispectral measurement of the fluorescent material is investigate to remove interreflection by using only a single image. The efforts and achievements in this thesis effectively model the spectra of reflective-fluorescent scenes under different capture conditions and equipments and promote the practical capabilities of interreflection removal by only a single image.

Acknowledgements

I would like to express my gratitude to all those who gave me the possibility to complete this dissertation.

I would first like to express deepest gratitude to my advisor, Prof. Yoichi Sato, for his excellent guidance, valuable suggestions, and kind encouragement he gave me through my Ph.D study in Graduate School of Information Science and Technology at the University of Tokyo. With his help, I learned how to find research problems and solve them and how to write papers and make a presentation.

I would also like to thank Prof. Imari Sato from National Institute of Informatics, Antony Lam from Saitama University, Prof. Takahiro Okabe from Kyushu Institute of Technology and Prof. Yasuyuki Matsushita from Osaka University. Their insight and passion for the research teach me how to face difficulties and enjoy research, and help me grow as a researcher with a positive and optimistic view of life. For their consistent and generous support, I thank them from the deepth of my heart.

I would also like to express grateful thank to all members of Sato Laboratory, for their kind advices, technical support and many helpful assistance in my life. I would like to thank the secretaries for their support and kindness. I also gratitude to all my friends in Japan and China. Without them, my life through the Ph.D course will not be so happy and harmonious.

I would appreciate the final defense committee members: Prof. Kiyoharu Aizawa, Prof. Shinichi Satoh, Prof. Toshihiko Yamasaki, and Prof. Takeshi Oishi, for their valuable comments and suggestions to my work.

Lastly, my deepest gratitude goes to my family for their perpetual support and unconditional love. It is to them that I dedicate this dissertation.

Contents

List of Figures

List of Tables

Chapter 1

Introduction

Fluorescence is general phenomenon and occurs in many objects, such as natural gems and corals, fluorescent dyes used for clothing, and plant containing chlorophyll to name a few. In fact, Barnard [Bar99] shows that 20 % of randomly constructed scenes is presented fluorescence. This is a significant proportion of scenes that rarely considered by past methods. In addition, Johnson *et al.*[JF99] and Zhang and Sato[ZS11] both showed the object's reflective and fluorescent components behave differently under different illuminations.

When a reflective surface is illuminated by incident light, it reflects back light of the same wavelength. Fluorescence typically transfers the energy from one wavelength to a longer wavelength which is known as Stokes shift [Ros92][Lak06], making fluorescence different from ordinary reflection that re-emits light at the same wavelength as the light source. As the properties of fluorescence are very different from ordinary reflectance, neglecting fluorescence can result in incorrect color estimation. Thus to accurately predict the color of objects, separate modeling of all spectral properties of both reflective and fluorescent components is essential.

Most fluorescent objects contain a combination of the very different reflective and fluorescent components so it is necessary to estimate them separately. Zhang and Sato [ZS11] provided a theory of fluorescent phenomenon and then separate the reflective and fluorescent components by using two images taken under different illuminants, but did not recover the full spectral

information of reflectance and fluorescence. Traditionally, to obtain the full spectral information of the fluorescent material, dense sampling is required in the spectral domain both for incident and emitted lights, which is called the bispectral method [Spr99]. To reduce the number of samplings, Lam *et al.* [LS13] recovered all spectra in a scene using sparsely captured band images with multi-band camera and variant narrow-band illuminations, but their method still requires 30 images captured under more than 10 narrow-band illuminations. In contrast, the goal of this thesis is to model the full spectral reflective and fluorescent components of an entire scene by using less images, and make use of fluorescence with various computer vision techniques.

In this dissertation, an efficient method is first presented to separate and measure the reflective and fluorescent spectra of a scene through the use of two high frequency illuminations in the spectral domain. In addition, based on the observation that materials with similar emission spectra tend to have similar absorption spectra as well, a method is devised for taking the recovered emission spectra from high frequency lighting and estimate their corresponding absorption spectra. Then, an efficient method based on RGB images is proposed for not only estimating the reflectance spectrum and the chromaticity of fluorescent components of a scene, but also to recover the fluorescent absorption and emission spectra of a scene. The scene is captured under general variant illuminations. It does not demand narrow-band light or programmable light source. Finally, a method for the separation of direct and indirect components is proposed, which can be achieved for dynamic scenes by capturing only a single image using fluorescence.

1.1 Background

1.1.1 Reflection and fluorescence models

This section begins with a brief review of how reflective-fluorescent materials are modeled [ZS13]. Due to reflection and fluorescence behaves differently, they need to be described by different models.

The radiance of a reflective surface depends on incident light and its reflectance. The observed radiance of an ordinary reflective surface at wave-

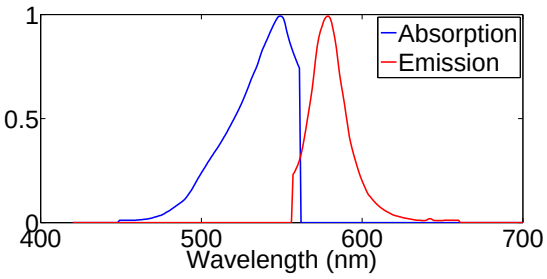

Figure 1.1: An example of absorption and emission spectra.

length λ is computed as

$$p_r(\lambda) = l(\lambda)s(\lambda), \tag{1.1}$$

where $l(\lambda)$ is the spectrum of the incident light at wavelength λ and $s(\lambda)$ is the spectral reflectance of the surface at wavelength λ.

The observed radiance of a pure fluorescent surface depends on the incident light, the material's absorption spectrum, and its emission spectrum. Fluorescence typically absorbs light at some wavelengths and emits them at longer wavelengths. The way this works is that when incident light hits a fluorescent surface, the surface's absorption spectrum will determine how much of the light is absorbed. Some of the absorbed energy is then released in the form of an emission spectrum at longer wavelengths than the incident light. The remainder of the absorbed energy is released as heat. The reason of this phenomenon is that fluorescent emission occurs after an orbital electron of a molecule, atom or nanostructure absorbs light and is excited, the electron relaxes to its ground state by emitting a photon of light and sends out heat after several nanoseconds. The higher the light frequency is, the more energy the light carries. Since some of the absorbed energy is lost as heat, the fluorescent emission will transmit to longer wavelength (or the low frequency). Figure 1.1 illustrates an example of the absorption and emission spectra for a fluorescent material over the visible spectrum.

Let $l(\lambda')$ represent the intensity of the incident light at wavelength λ', the observed spectrum of a pure fluorescent surface [ZS13] at wavelength λ

is described in terms of its absorption and emission spectra as

$$p_f(\lambda) = \left(\int l(\lambda^{'}) a(\lambda^{'}) \mathrm{d}\lambda^{'} \right) e(\lambda), \tag{1.2}$$

where $a(\lambda^{'})$ and $e(\lambda)$ represent the absorption and emission spectrum. $k = \left(\int l(\lambda^{'}) a(\lambda^{'}) \mathrm{d}\lambda^{'} \right)$ is determined by the absorption spectrum and the spectrum of the incoming light and independent of the emission spectrum. Replacing this part by a scale factor k. Equation (1.2)can be rewritten as

$$p_f(\lambda) = k e(\lambda), \tag{1.3}$$

which means that the shape or the distribution of the emitted spectrum is constant, but the scale k of the emitted spectrum changes under different illuminations. Namely, the radiance of the fluorescent emission changes under different illuminations, but its color stays the same regardless of illumination color.

The radiance of a reflective-fluorescent surface point can be expressed as a linear combination of the reflective component p_r and fluorescent component p_f, i.e. $p = p_r + p_f$. Thus,

$$p(\lambda) = l(\lambda) s(\lambda) + \left(\int l(\lambda^{'}) a(\lambda^{'}) \mathrm{d}\lambda^{'} \right) e(\lambda). \tag{1.4}$$

1.1.2 Reflectance and Fluorescence Capture Process

This section begins by briefly describing how reflectance and fluorescence absorption and emission spectra for a single point can be measured using bispectral measurements [LJA97].

Reflectance Measurement: Stokes shift indicates that a fluorescent point illuminated at wavelength $\lambda^{'}$ will generally emit light at longer wavelengths λ. The implication is that light will not generally emit at the same wavelength as the illuminant. Thus if a reflective-fluorescent point is illuminated at wavelength $\lambda^{'}$ and observed the point at wavelength λ when $\lambda^{'} = \lambda$, only the reflective component will be observed. An example of reflectance only recovery can be seen in Figure 1.2(a).

Emission Measurement: An emission spectrum will maintain the same shape regardless of the illuminant. The only affect an illuminant has on the

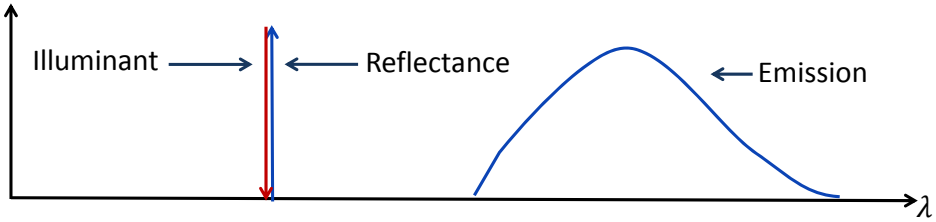

(a) Reflectance and Emission Capture

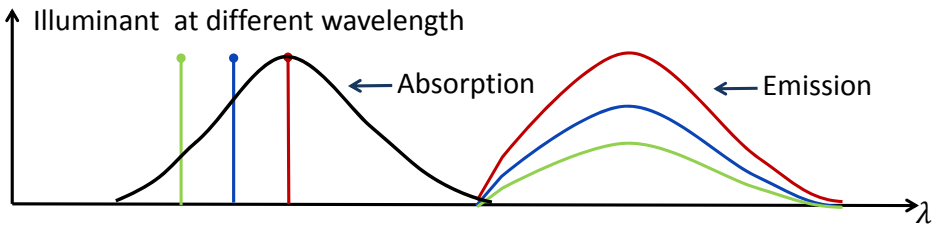

(b) Absorption Capture at Different Wavelengths

Figure 1.2: Capture of reflective-fluorescent spectra at a single point in a scene. (a) When the reflective-fluorescent scene is illuminated, the reflectance spectrum can be measured at the same wavelength as the illuminant while the emission spectrum can be captured at longer wavelengths. (b) Varying the illuminant over different wavelengths and measuring the fluorescence emission spectrum at the same wavelength. The observation of different scaled emissions allow us to infer the fluorescence absorption each wavelength.

observed emission spectrum is its scale. Since Stokes shift causes emissions to be observed at longer wavelengths than the illuminant, an illuminant is fixed at λ' and the emission is observed for all wavelengths $\lambda > \lambda'$. As long as λ' is set at a short enough wavelength, the entire emission spectrum can be observed. In the case of a reflective-fluorescent point, no reflectance would be observed at λ as reflectance only occurs at the same wavelength as the illuminant. Figure 1.2(a) shows an emission illuminated by a narrowband light.

Absorption Measurement: The absorption spectrum is just defined as how much the illuminant scales the emission at a given wavelength. Thus the scale of the emission can be simply observed at a wavelength λ while varying the illuminant wavelength λ' for $\lambda' > \lambda$. How much the strength of the observed emission changes at wavelength λ defines the absorption spectrum at wavelength λ'. Figure 1.2(b) shows the observation of different scaled emissions for inferring absorption at the illuminant wavelength.

In this study, bispectral measurement is used to obtain the ground truth to evaluate the accuracy of the proposed method.

1.1.3 Constant Chromaticity

From Equation (1.2), it can be seen that for a given fluorescent material, its emission spectrum always has the same spectral distribution regardless of the illuminant's spectral distribution (Figure 1.2(b)).

Thus when a pure fluorescent surface is captured by an RGB camera, the color of the pixel for the n-th channel under the m-th illuminant is

$$\begin{aligned} f_n^m &= \int c_n(\lambda) p_f^m(\lambda) \mathrm{d}\lambda \\ &= \left(\int l_m(\lambda') a(\lambda') \mathrm{d}\lambda' \right) \int c_n(\lambda) e(\lambda) \mathrm{d}\lambda. \end{aligned} \tag{1.5}$$

Here, $c_n(\lambda)$ $(n = (r, g, b))$ is the camera spectral sensitivity for the R, G, and B channels. Let

$$D_n = \int c_n(\lambda) e(\lambda) \mathrm{d}\lambda, \tag{1.6}$$

be called the reference value of the emission spectrum $e(\lambda)$.

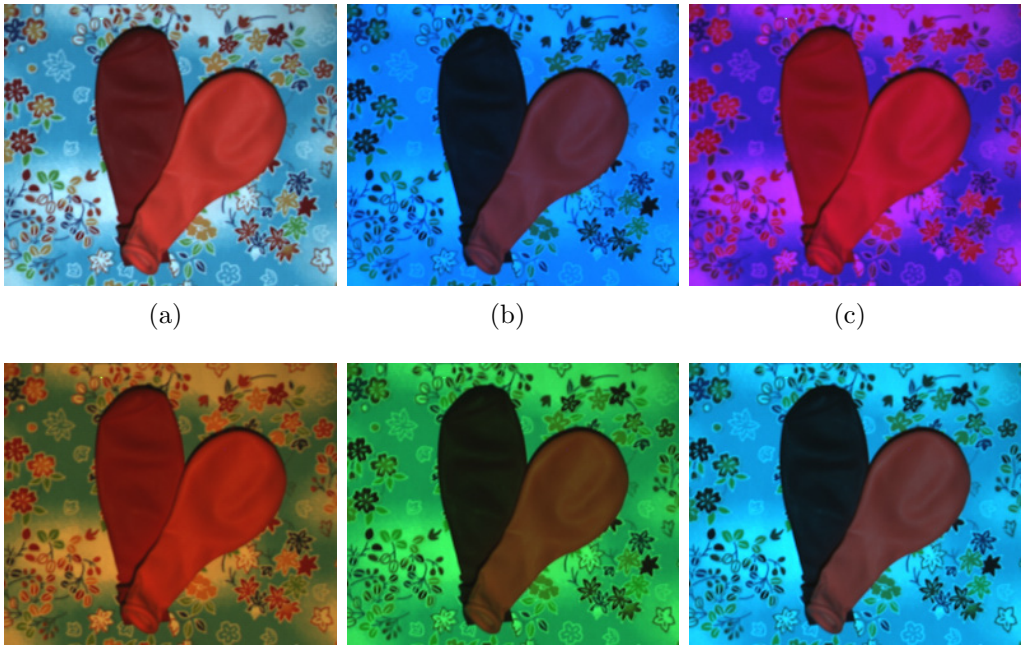

(a) (b) (c)

(d) (e) (f)

Figure 1.3: A reflective-fluorescent scene under different illuminations. The left ballon is ordinary reflective material, and the right ballon is fluorescent material.

The $\int l_m(\lambda')a(\lambda')\mathrm{d}\lambda'$ is determined by the absorption spectrum and incoming illumination spectrum, and independent from the spectrum of the outgoing fluorescence. Replacing this part by k_m and substituting Equation (1.6) into (1.5), Equation (1.5) can be rewritten as

$$f_n^m = k_m D_n. \tag{1.7}$$

Note that k_m is the same for all three channels.

Then the chromaticity E_n^m of the fluorescent component for the n-th channel under the m-th illuminant becomes

$$E_n^m = \frac{k_m D_n}{\sum_{t=1}^{3} k_m D_t} = \frac{D_n}{\sum_{t=1}^{3} D_t} = E_n, \tag{1.8}$$

where E_n is called the reference chromaticity. The scale factor k_m can be eliminated, thus the chromaticity of the fluorescent material is independent of both the illuminant and absorption spectrum, and it only depends on the camera spectral sensitivity and emission spectrum.

Equation (1.8) implies chromaticity value E_n^m is constant under varying illuminations. It is a;so noted that since $\sum_n^3 E_n = 1$, $E_3 = 1 - E_1 - E_2$, the chromaticity can be uniquely expressed with only 2 values. However, for convenience in the derivations, the chromaticity will be expressed in terms of 3 values.

In summary, the color appearance of reflective component varies with illumination dramatically, whereas the appearance of fluorescent component stays constant except for intensity (Figure 1.3). Many objects we see every day are neither pure reflective nor pure fluorescent, they are composites of ordinary reflective and fluorescent components.

1.2 Chapter Organization

This dissertation introduces spectral modeling of reflective-fluorescent scence, within which two of them model the full spectral reflective and fluorescent components of an entire scene, and one of them applies the fluorescence in our computer vision field.

In Chapter 2, the reflective and fluorescent spectra of a scene can be efficiently separated and measured through the use of high frequency illumination in the spectral domain. In Chapter 3, a more practical approach is proposed for hyperspectral imaging of reflective-fluorescent scenes using only a conventional RGB camera and varied colored illuminants. In Chapter 4, a novel method is presented for the separation of direct and indirect components, which can be achieved for dynamic scenes by capturing only a single image using fluorescence. Chapter 5 concludes this dissertation by summarizing the proposed methods and discussing potential future research directions.

Chapter 2

Separating Reflective and Fluorescent Components Using High Frequency Illumination in the Spectral Domain

2.1 Overview

Hyperspectral reflectance data are beneficial to many applications including but not limited to archiving for cultural e-heritage [BPP+03], medical imaging [SCC+06], and also color relighting of scenes [JF99]. As a result, many methods for acquiring the spectral reflectance of scenes have been proposed [CYBE10, DXW01, MW86, Tom96, Gat00, PLGN07a]. Despite the success of these methods, they have all made the assumption that fluorescence is absent from the scene. However, fluorescence does frequently occur in many objects, such as natural gems and corals, fluorescent dyes used for clothing, and plant containing chlorophyll to name a few. In fact, Barnard shows that fluorescent surfaces are present in 20% of randomly constructed scenes [Bar99]. This is a significant proportion of scenes that have not been considered by past methods.

Another important point is that reflective and fluorescent components behave very differently under different illuminants [JF99, ZS11]. Thus to ac-

(a) White light (b) Reflection (c) Fluorescence

Figure 2.1: (a) The scene captured under white light. (b) The recovered reflective component. (c)The recovered reflective component.

curately predict the color of objects, separate modeling of all spectral properties of both reflective and fluorescent components is essential. Specifically, when a reflective surface is illuminated by incident light, it reflects back light of the same wavelength. Fluorescent surfaces on the other hand, first absorb incident light and then emit at longer wavelengths. This wavelength shifting property is known as Stokes shift [Ros92, SHC07] and the question of which wavelengths of light are absorbed and which wavelengths are emitted are defined by the fluorescent surface's absorption and emission spectrum. As the properties of fluorescence are very different from ordinary reflectance, neglecting fluorescence can result in completely incorrect color estimation. This in turn negatively affects many methods that rely on accurate color estimation. For example, algorithms for relighting and color constancy would be affected.

The goal of this chapter is to accurately recover the full spectral reflective and fluorescent components of an entire scene. Typical fluorescent objects exhibit both reflectance and fluorescence (Figure 2.1) that is the sum of the two components interacting with illumination differently. The intensity of the fluorescent material at the wavelength λ is

$$p(\lambda) = p_r(\lambda) + p_f(\lambda), \tag{2.1}$$

where $p_r(\lambda)$ and $p_f(\lambda)$ are the intensity of the ordinary reflective and fluo-

rescent components, respectively. So the question of how these components can be accurately separated also needs to be addressed.

In this chapter, it is shown that the reflective and fluorescent spectra of a scene can be efficiently separated and measured through the use of high frequency illumination in the spectral domain. The proposed approach only assumes that the absorption spectrum of the fluorescent material is a smooth function with respect to the frequency of the lighting in the spectral domain. With this assumption, it becomes possible to separate reflective and fluorescent components by just two hyperspectral images taken under a high frequency illumination pattern and its shifted version in the spectral domain. The reflective and fluorescent emission spectra can then be fully recovered by the proposed separation method.

In addition to recovering reflectance and fluorescent emission spectra, the observation is made the observation that materials with similar emission spectra tend to have similar absorption spectra as well. Using this observation, a method is devised for taking the recovered emission spectra from high frequency lighting and estimate their corresponding absorption spectra. There are well established methods for measuring fluorescent spectra. For example, bispectral methods [Spr99] are effective approaches that measure fluorescence in terms of incoming and outgoing wavelengths but only work for a single point in space. Thus making the capture of entire scenes very labor and time intensive.

In summary, the contributions in this study are that an efficient method is presented for the separation and recovery of full reflectance and fluorescent emission spectra and this is, to our knowledge, the first method for estimating the absorption spectrum of a material given its emission. Since the reflective and fluorescent emission and absorption spectra of the scene is completely recovered, the ability to accurately predict the relighting of scenes under novel lighting is also shown.

2.2 Related Work

As noted earlier, there have been a number of papers on recovering the spectral reflectance of scenes [CYBE10, DXW01, MW86, Tom96, Gat00,

PLGN07a]. Despite the effectiveness of these methods for spectral reflectance capture, they all do not take the effects of fluorescence into account.

Unfortunately, not accounting for fluorescence can have a detrimental affect on color accuracy. For example, Johnson and Fairchild [JF99] showed that considering fluorescence can dramatically improve color renderings. Later, Wilkie *et al.* [WWLP06] showed accurate results by rendering fluorescent emissions using diffuse surfaces that can reflect light at a wavelength different from its incident illuminant wavelength. Hullin *et al.* [HHA+10] showed the importance of modeling and rendering of reflective-fluorescent materials using their bidirectional reflectance and reradiation distribution functions (BRRDF). Besides color rendering, the observation of fluorescent emissions on an object's surface has also been applied to photometric stereo for shape reconstruction [SOS12, TMMK12]. As mentioned earlier, Barnard *et al.* concluded that fluorescent surfaces are present in 20% of randomly constructed scenes [Bar99]. Thus the presence of fluorescence is significant and warrants attention.

In practice, fluorescent objects typically exhibit both reflectance and fluorescence so the joint occurrence of these phenomenon in scenes needs to be considered. Some methods in the literature have given this issue attention. Lee *et al.* [LSC01] provided a mathematical description for fluorescent processes and recovered the additive spectra of reflective and fluorescent components but did not separate them. Alterman *et al.* [ASW10] separated the appearance of fluorescent dyes from a mixture by unmixing multiplexed images. Zhang and Sato [ZS11] derived an independent component analysis based method to estimate the RGB colors of reflectance and fluorescent emission but not their spectral distributions. They also did not estimate the absorption spectrum of the fluorescent component and so, cannot predict intensity changes in fluorescent emission due to different illumination spectra. Tominaga *et al.* [THK11] estimated fluorescent emission spectra using multispectral images taken under two ordinary light sources. A limitation is that they assumed fluorescent emissions to be constant for all absorption wavelengths and thus cannot accurately predict the brightness of fluorescent components under varying illumination. Finally, none of these methods fully recover all reflective and fluorescent spectral components of scenes.

In recent work, methods for hyperspectral imaging of reflective-fluorescent scenes have been proposed. Lam and Sato [LS13] provided a method for recovering the full spectral reflectance and fluorescence absorption and emission spectra of scenes but they need to capture the scene about 30 times using a multiband camera under multiple narrowband illuminants. Suo *et al.* [SBCD14] presented the bispectral coding scheme which is rooted in the classical bispectral measurement method [Spr99] where dozens of images also have to be captured under shifting narrow-band illuminations. Zheng *et al.* [ZSS14] also recovered all the different types of fluorescence and reflectance spectra but they still require three hyperspectral images. All these methods have to capture multi-channel images [LS13][SBCD14][ZSS14]. The proposed method only uses two hyperspectral images to effectively recover all these spectra, and can also separate reflective and fluorescent components for any number of narrow-band channels under two high frequency light spectra.

As mentioned earlier, one of the key challenges in this problem is the separation of reflective and fluorescent components from composite objects exhibiting both phenomenon. There have been a number of methods in the literature on separating components in images. For example, Farid and Adelson [FA99] used independent components analysis to separate reflections on glass and a painting on the side of the glass opposite the observer. Nayar *et al.* [NFB93] separated specular reflections from diffuse reflections.

What is interesting is that an analogy can be drawn between the proposed approach and that of Nayar *et al.* [NKGR06]. Nayar *et al.* devised a way to separate direct and indirect components using high frequency lighting patterns in the spatial domain. It is found that reflectance and fluorescence in the spectral domain can be thought of as similar to direct and indirect illumination in the spatial domain. More specifically, the reflective component p_r may be thought of as a direct component in the spectral domain because incident light is reflected back at the same wavelength. The fluorescent component p_f on the other hand, does not emit light at the same wavelength as incident light. This is because it always shifts incident light from shorter wavelengths to longer ones. So one can think of it as indirect lighting in the spectral domain. In this work, the effectiveness of using high frequency lighting is shown in the spectral domain, not the spatial domain,

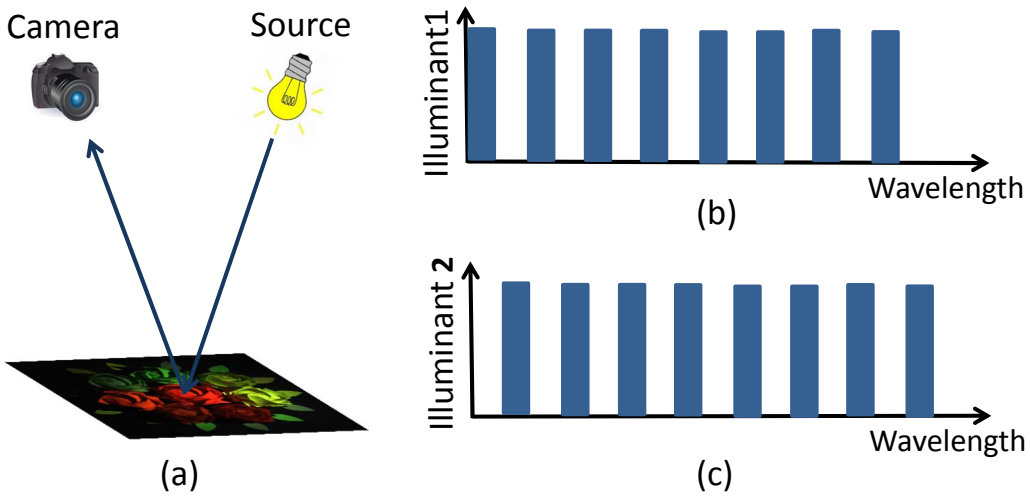

Figure 2.2: An example of a captured scene (a). When a reflective-fluorescent point in the scene is lit by the illuminant (b), which is a high frequency binary illumination pattern in the wavelength domain, each lit wavelength includes both reflective and fluorescent components while the unlit wavelengths have only the fluorescent component. (c) shows its complement.

for the separation and spectral recovery problem.

2.3 Separation of Reflection and Fluorescence

In this section, I present the separation method for reflective and fluorescent component by using the high frequency illumination, discuss the demand on the illumination frequency, and analyze the errors in the proposed method.

2.3.1 Separation Using High Frequency Illumination

In the experiments, high frequency illumination defined in the spectral domain is used for separating reflective and fluorescent components. Let us start with simple binary illuminants to describe the key idea of the proposed method. A high-frequency illumination pattern shown in Figure 2.2(b) is denoted by $l_1(\lambda)$ and its complement shown in Figure 2.2(c) by $l_2(\lambda)$. The illuminants are defined such that when $l_1(\lambda)$ has intensity, $l_2(\lambda)$ has no in-

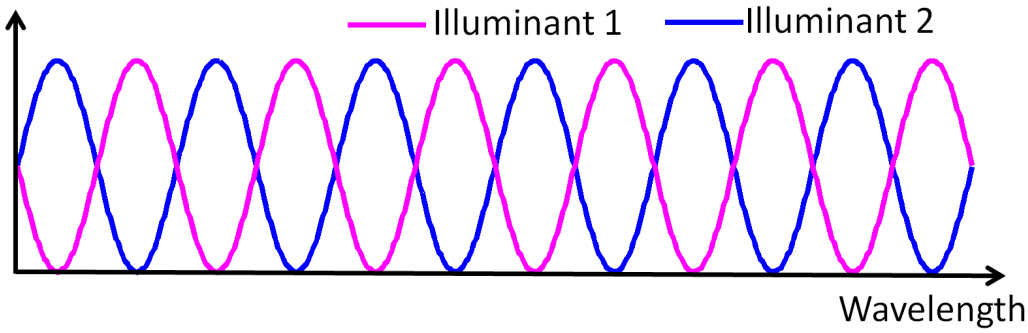

Figure 2.3: Sinusoidal illuminant patterns. The blue and pink solid lines denote two illumination patterns. There is a phase shift between them.

tensity and vice versa. Let us consider a certain wavelength λ_1, where the wavelength λ_1 is lit directly under the illuminant $l_1(\lambda)$, $l_1(\lambda_1) = 1$ and then it is not lit under the illuminant λ_2, $l_2(\lambda_1) = 0$. Since reflection preserves wavelength, it can be obtained that

$$\begin{aligned} p_1(\lambda_1) &= s(\lambda_1) + \frac{1}{2}k'e(\lambda_1), \\ p_2(\lambda_1) &= \frac{1}{2}k'e(\lambda_1). \end{aligned} \tag{2.2}$$

Here, $\int l_1(\lambda')a(\lambda')\mathrm{d}\lambda' = \int l_2(\lambda')a(\lambda')\mathrm{d}\lambda' = \int a(\lambda')\mathrm{d}\lambda'/2 = k'/2$ is assumed. That is, the absorptions due to the high-frequency illumination patterns are the same. It is shown later in this section this is true when the absorption $a(\lambda')$ is smooth with respect to the frequency of the illumination patterns in the spectral domain as is similarly discussed for the spatial domain by Nayar *et al.*[NKGR06]. With the same absorptions under the two illuminants, the reflectance and emission spectra at λ_1 are obtained as

$$\begin{aligned} s(\lambda_1) &= p_1(\lambda_1) - p_2(\lambda_1), \\ k'e(\lambda_1) &= 2p_2(\lambda_1). \end{aligned} \tag{2.3}$$

The reflectance and emission spectra at λ_2 where $l_1(\lambda_2) = 0$ and $l_2(\lambda_2) = 1$ can be obtained in a similar manner.

In this work, high frequency sinusoidal illuminants (Figure 2.3) in the spectral domain are used to achieve the same effect as the binary lighting

patterns because they are both more practical and fit into the theory of the proposed framework. The illuminants can be represented as

$$\begin{aligned} l_1(\lambda) &= \alpha + \beta \cos(2\pi f_l \lambda), \\ l_2(\lambda) &= \alpha + \beta \cos(2\pi f_l \lambda + \phi), \end{aligned} \tag{2.4}$$

where f_l is the frequency of illumination. The radiance of a surface under these two sinusoidal illuminants can be described as,

$$\begin{aligned} p_1(\lambda) &= l_1(\lambda)s(\lambda) + k_1 e(\lambda), \\ p_2(\lambda) &= l_2(\lambda)s(\lambda) + k_2 e(\lambda), \\ k_n &= \int l_n(\lambda^{'})a(\lambda^{'})\mathrm{d}\lambda^{'}. \end{aligned} \tag{2.5}$$

Here, assuming that k_n are constant for l_1 and l_2, that is to say, $k_1 = k_2 = k$, the reflectance $s(\lambda)$ and fluorescent emission $ke(\lambda)$ can be recovered as

$$\begin{aligned} s(\lambda) &= \frac{p_1(\lambda) - p_2(\lambda)}{l_1(\lambda) - l_2(\lambda)}, \\ ke(\lambda) &= p_1(\lambda) - \frac{p_1(\lambda) - p_2(\lambda)}{l_1(\lambda) - l_2(\lambda)} l_1(\lambda). \end{aligned} \tag{2.6}$$

In practice, the scene will includes many kinds of fluorescent materials, it is almost impossible to keep k constant for any kinds of fluorescent materials. Also, due to the limitation of the light source, it is impossible to produce any high frequency illumination. Thereby, to make the proposed method more robust, the recovered $s(\lambda)$ is substituted into both $p_1(\lambda) = l_1(\lambda)r(\lambda) + k_1 e(\lambda)$ and $p_2(\lambda) = l_2(\lambda)r(\lambda) + k_2 e(\lambda)$, and mean the recovered $k \cdot e(\lambda)$ from these two equations. So it can be obtained that

$$\begin{aligned} ke(\lambda) = \frac{1}{2}\Big[& p_1(\lambda) - \frac{p_1(\lambda) - p_2(\lambda)}{l_1(\lambda) - l_2(\lambda)} l_1(\lambda) + \\ & p_2(\lambda) - \frac{p_1(\lambda) - p_2(\lambda)}{l_1(\lambda) - l_2(\lambda)} l_2(\lambda) \Big]. \end{aligned} \tag{2.7}$$

2.3.2 Discussion on the Illumination Frequency

To recover the reflectance $r(\lambda)$ and fluorescent emission $ke(\lambda)$ completely, it first need to make $k_1 = k_2 = k$. In this section, how to satisfy the

condition $k_1 = k_2 = k$ is discussed. In the following, it is considered that the requirements for the illuminants based on the Nyquist sampling theorem [OWH96] and on an analysis of the McNamara and Boswell fluorescence spectral dataset [MGR+06].

Let $a_n(\lambda) = l_n(\lambda)a(\lambda)$ $\{n = 1, 2\}$, where $l_n(\lambda)$ can be considered as sampling or modulate function of $a(\lambda)$. The sampling theorem, which is most easily explained in terms of impulse-train sampling, establishes the fact that a band-limited signal is uniquely represented by its samples. In practice, however, narrow, large-amplitude pulses, which approximate impulses, are relatively difficult to generate and transmit. Instead, sinusoidal illuminant patterns in wavelength range (as shown in Figure 2.4) are used. These patterns are similar to amplitude modulation in communication system.

The spectrum of sinusoidal illumination $l_1(\lambda)$ in the frequency domain [OWH96] then becomes

$$L_1(f) = \frac{1}{2}[\beta\delta(f - f_l) + 2\alpha\delta(f) + \beta\delta(f + f_l)], \tag{2.8}$$

where $\delta(f)$ is the Dirac delta function. Let $A(f)$ and $A_n(f)$ denote the Fourier transform of $a(\lambda)$ and $a_n(\lambda)$, respectively. Since the product $l_n(\lambda)a(\lambda)$ in the spectral domain corresponds to a convolution in its Fourier domain,e.g.

$$A_n(f) = [L_n(f) * A(f)], \tag{2.9}$$

the Fourier transform of $a_1(\lambda)$ is

$$A_1(f) = \frac{1}{2}\left[\beta A(f - f_l) + 2\alpha A(f) + \beta A(f + f_l)\right]. \tag{2.10}$$

That is, a replication of the Fourier transform of the original signal $A(f)$ is centered around $+f_l$ and 0 and $-f_l$, as shown in Figure 2.4.

The Fourier transform of $l_1(\lambda)$ and $l_2(\lambda)$ with the phase offset ϕ are related as $L_2(f) = e^{i\phi}L_1(f)$, and thus the frequency spectrum of $a_2(\lambda)$ is

$$\begin{aligned} A_2(f) = \frac{1}{2}[&\beta e^{i\phi}A(f - f_l) + 2\alpha A(f) \\ &+ \beta e^{-i\phi}A(f + f_l)]. \end{aligned} \tag{2.11}$$

From the definition of the Fourier transform $A_n(f) = \int_{-\infty}^{+\infty} a_n(\lambda)e^{-i2\pi f\lambda}\mathrm{d}\lambda$, substituting $f = 0$ into this definition, it is obtained that

$$A_n(0) = \int_{-\infty}^{+\infty} a_n(\lambda)\mathrm{d}\lambda = \int_{-\infty}^{+\infty} l_n(\lambda)a(\lambda)\mathrm{d}\lambda = k_n. \tag{2.12}$$

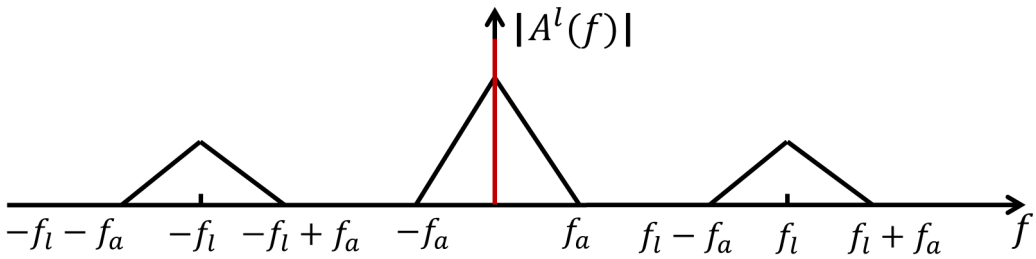

Figure 2.4: Spectrum of sampled signal under sinusoidal illuminant pattern in the frequency domain.

Therefore, k_n corresponds to $A_n(f)$'s zero-frequency component. This tells that it is necessary to satisfy the condition $A_1(0) = A_2(0)$ so that $k_1 = k_2 = k$. In Equations (2.10) and (2.11), substituting $f = 0$, it is obtained that

$$\begin{aligned} A_1(0) &= \frac{1}{2}\left[\beta A(-f_l) + 2\alpha A(0) + \beta A(f_l)\right], \\ A_2(0) &= \frac{1}{2}[\beta e^{i\phi} A(-f_l) + 2\alpha A(0) + \beta e^{-i\phi} A(f_l)]. \end{aligned} \tag{2.13}$$

Let us define f_a as $a(\lambda)$'s maximum frequency. Then $A(-f_l)$ and $A(f_l)$ become zero for $f_l > f_a$. This means that $A_1(0) = A_2(0) = 2\alpha A(0)$ for $f_l > f_a$ is achieved to make $k_1 = k_2 = k$. Thus, the frequency of the illuminants in the wavelength domain f_l needs to be greater than $a(\lambda)$'s maximum frequency or bandwidth f_a.

Now. the maximum frequency of $a(\lambda)$ on the McNamara and Boswell fluorescence spectral dataset is discussed. The maximum frequencies of all 509 materials are examined in the dataset, and obtain the maximum frequency of each absorption spectrum while retaining 99% of the energy[1]. The mean of the maximum frequency for all absorption spectra in the dataset is $1/45.9[nm^{-1}]$ and its standard deviation is $1/24.1[nm^{-1}]$. As mentioned previously, the illumination frequency f_l needs to be greater than $a(\lambda)$'s maximum frequency f_a, and the period is the reciprocal of the frequency, so the period of the illumination – which is called "sampling interval" – in the spectral domain needs to be less than the minimum sampling interval of all

[1]Since there exists some noise in the original spectra, ignoring some high frequency components is reasonable.

absorption spectra of fluorescent materials in the scene. Figure 2.5 shows the percentage of absorption spectra in the McNamara and Boswell fluorescence spectral dataset that satisfy the condition $k_1 = k_2$ under different sampling intervals. The period of the illumination is set as $40nm$ in the experiments due to limitations of the light source. However, this is still less than the mean minimum sampling interval of all absorption spectra ($45.9nm$) found in the dataset and works well in practice.

2.3.3 Analysis on the Errors

Due to limitations of the light source, ideal and arbitrary high frequency illuminations cannot be produced . It is thus unlikely for k to be the exact constant for all kinds of fluorescent materials in the scene under realistic conditions. Therefore, to reduce errors, the recovered $s(\lambda)$ is substituted into both $p_1(\lambda) = l_1(\lambda)s(\lambda) + k_1e(\lambda)$ and $p_2(\lambda) = l_2(\lambda)s(\lambda) + k_2e(\lambda)$, and average the recovered $ke(\lambda)$ from these two equations. Thus, the fluorescence emission $ke(\lambda)$ is recovered by

$$\begin{aligned} ke(\lambda) =& \frac{1}{2}\left[k_1e(\lambda) + k_2e(\lambda)\right] \\ =& \frac{1}{2}\Big[p_1(\lambda) - \frac{p_1(\lambda) - p_2(\lambda)}{l_1(\lambda) - l_2(\lambda)}l_1(\lambda) + \\ & p_2(\lambda) - \frac{p_1(\lambda) - p_2(\lambda)}{l_1(\lambda) - l_2(\lambda)}l_2(\lambda)\Big]. \end{aligned} \tag{2.14}$$

If $k_1 \neq k_2$,

$$s(\lambda) = \frac{(p_1(\lambda) - p_2(\lambda)) - (k_1 - k_2)e(\lambda)}{l_1(\lambda) - l_2(\lambda)}. \tag{2.15}$$

Let $s_{error}(\lambda)$ and $e_{error}(\lambda)$ denote the errors of $s(\lambda)$ and $ke(\lambda)$ (where $k = (k_1 + k_2)/2$ when $k_1 \neq k_2$). These errors can be expressed as

$$\begin{aligned} s_{error}(\lambda) &= abs\left[\frac{(k_1 - k_2)e(\lambda)}{l_1(\lambda) - l_2(\lambda)}\right], \\ e_{error}(\lambda) &= abs\left[(k_1 - k_2)e(\lambda)\frac{l_1(\lambda) + l_2(\lambda)}{2\left[l_1(\lambda) - l_2(\lambda)\right]}\right]. \end{aligned} \tag{2.16}$$

For the sinusoidal illuminant $l_n(\lambda)$ in Equation (2.4), the maximum and minimum intensities over all wavelengths λ are $\alpha + \beta$ and $\alpha - \beta$. Each value in an illuminant's spectrum has to be positive, so $\alpha/\beta \geq 1$.

In Equation (2.16), the errors for the reflective and fluorescence emission are directly proportional to $k_1 - k_2$. This means that the less difference between k_1 and k_2 there is, the smaller the errors. As α/β becomes larger, $A_1(0)$ and $A_2(0)$ in Equation (2.13) are less affected by the $\beta A(-f_l)$ and $\beta A(f_l)$ terms. As a result, the difference between k_1 and k_2 can be decreased under the same illumination frequency. Thus the k term is more robust under different illumination conditions, when α/β is large.

Nevertheless, when the scene is captured by the camera, the noise from the camera cannot be totally avoided. As $l_1(\lambda) - l_2(\lambda)$ shrinks, $s(\lambda)$ and $e(\lambda)$ are increasingly affected by noise, as can be seen in Equation (2.6). In order to make the proposed method more robust to noise, it is necessary to make the difference $l_1(\lambda) - l_2(\lambda)$ greater. In practice, the phase shift of illuminations $l_1(\lambda)$ and $l_2(\lambda)$ is set to π (Figure 2.3) and capture the scene at the illumination's peaks or crests to maximize the observed difference in $l_1(\lambda) - l_2(\lambda)$.

It is also interesting to note that the need to maximize $l_1(\lambda) - l_2(\lambda)$ also means that α/β should be closer to 1, which is at odds with the need to make α/β large to allow for a more robust k as discussed above. Sections 2.6 and 2.7 will discuss the influence and tradeoffs of the value of α/β in real data.

2.4 Estimating the Absorption Spectra

This section will explain how the absorption spectrum of a material is estimated from its emission spectrum that was obtained using the proposed method in Section 2.3.1.

The basic observation behind the proposed method is that fluorescent materials with similar emission spectra tend to have similar absorption spectra (Figure 2.6). From this observation, an effective method is derived that uses a dictionary of known emission and absorption spectrum pairs to estimate an absorption spectrum from a given novel emission.

Specifically, let $\hat{\boldsymbol{e}}$ be a known emission spectrum whose absorption spectrum $\hat{\boldsymbol{a}}$ is unknown. Let $\{\boldsymbol{e}_j\}$ be a dictionary of emission spectra and $\{\boldsymbol{a}_j\}$ be the known corresponding absorption spectra. Representing all these spectra as vectors, it is first determined the linear combination of $\{\boldsymbol{e}_j\}$ to reconstruct

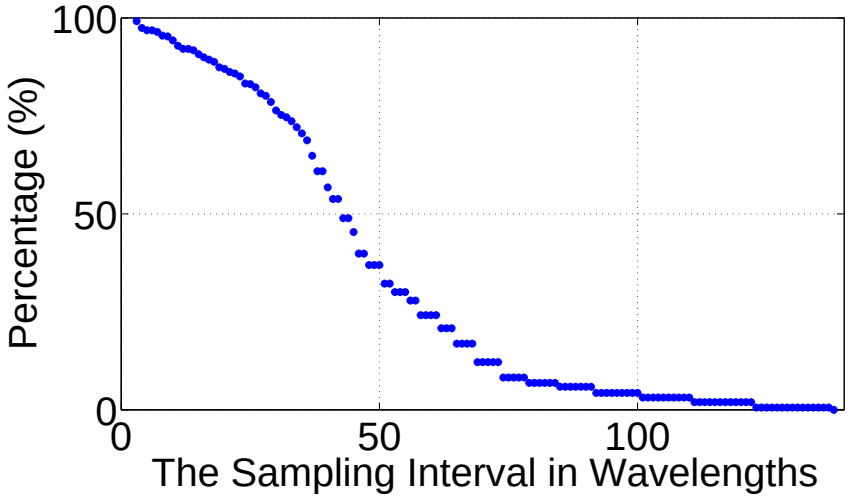

Figure 2.5: The percentage of absorption spectra in the McNamara and Boswell fluorescence spectral dataset where $k_1 = k_2$ given different sampling intervals. The smaller the sampling interval, the more absorption spectra satisfy the requirement that $k_1 = k_2$.

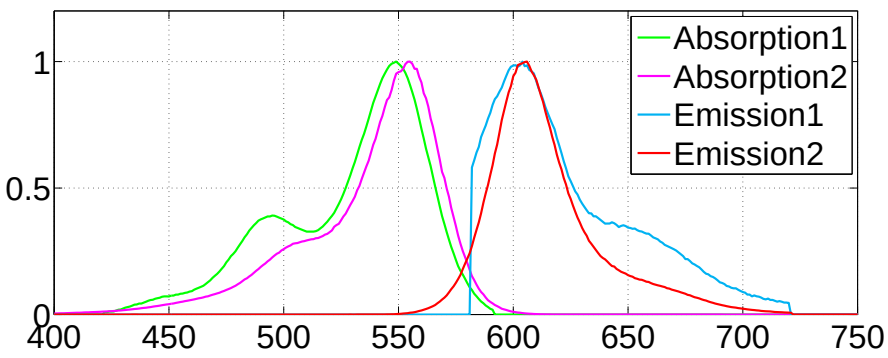

Figure 2.6: Absorption and emission spectra of two fluorescent materials.

$\hat{\boldsymbol{e}}$ by solving

$$\hat{\boldsymbol{e}} = \sum\nolimits_j w_j \boldsymbol{e}_j. \tag{2.17}$$

The weights $\{w_j\}$ are then used to calculate the corresponding excitation spectrum $\hat{\boldsymbol{a}}$ by

$$\hat{\boldsymbol{a}} = \sum\nolimits_j w_j \boldsymbol{a}_j. \tag{2.18}$$

Let $\{\boldsymbol{e}_j^{'}\}$ and $\{\boldsymbol{a}_j^{'}\}$ denote the subsets of $\{\boldsymbol{e}_j\}$ and $\{\boldsymbol{a}_j\}$ whose corresponding weights $\{w_j \neq 0\}$. Note that using the same $\{w_j\}$ in Equation (2.17) and (2.18) requires the linear combination be kept between the subspaces spanned by $\{\boldsymbol{e}_j^{'}\}$ and $\{\boldsymbol{a}_j^{'}\}$. It is asserted that an emission spectrum can typically be well-represented by a sparse basis. To show this, leave-one-out cross-validation is performed for each emission spectrum in the McNamara and Boswell fluorescence spectral dataset. $\hat{\boldsymbol{e}}$ is set as the testing sample and the remaining emission spectra in $\{\boldsymbol{e}_j\}$ are used as the dictionary. It is found find that any given emission $\hat{\boldsymbol{e}}$ can on average be well represented by 10 emission spectra from the dictionary, which is very sparse compared to the size of the whole dictionary, Thus $\hat{\boldsymbol{e}}$ can considered to live in a low-dimensional sub-space spanned by $\{\boldsymbol{e}_j^{'}\}$. Therefore, to minimize the number of basis vectors used from $\{\boldsymbol{e}_j\}$, $\hat{\boldsymbol{e}}$ is reconstructed by sparse weights $\boldsymbol{w}$ through l_1-norm minimization [DTDS12, CT06, EHJT04], according to

$$\min \|\boldsymbol{w}\|_1 \quad s.t. \quad w_j \geq 0 \text{ and } \left\|\hat{\boldsymbol{e}} - \sum\nolimits_j w_j \boldsymbol{e}_j\right\|_2^2 \leq \epsilon. \tag{2.19}$$

To test the accuracy of the proposed method, a subset of materials is chosen from the McNamara and Boswell fluorescence spectral dataset where both the emission and absorption spectra were present in the visible range (400 - 720 nm). This resulted in a collection of 183 materials. Leave-one-out cross-validation is performed in the 183 emission and absorption spectra. The estimated absorption spectrum was then compared against the ground truth using the root-mean-square-error (RMSE),

$$RMSE = \sqrt{\left(\int \left(a^{gt}(\lambda) - a^{re}(\lambda)\right)^2 d\lambda\right)/N}, \tag{2.20}$$

where $a^{gt}(\lambda)$ and $a^{re}(\lambda)$ are the ground truth and recovered spectra at wavelength λ, respectively. N is the length of the wavelength. The ground truth

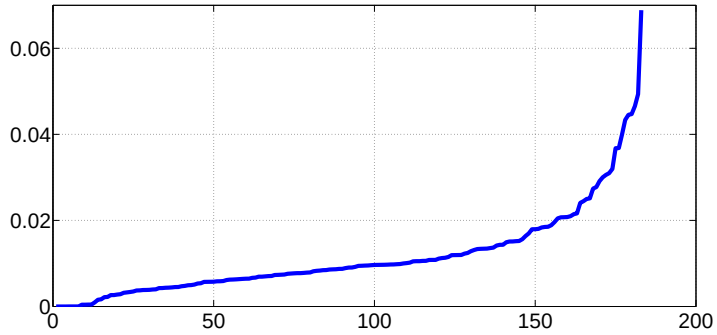

Figure 2.7: All test errors sorted in ascending order. 67% of cases were below the average error of 0.012.

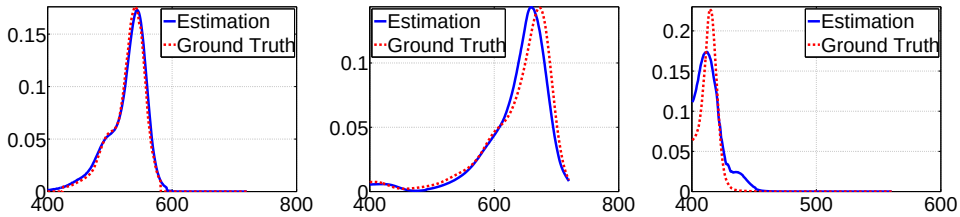

0.005 0.012 0.019

Figure 2.8: Examples of estimated absorption spectra and their root-mean-square-errors.

and estimation were also normalized for scale by setting them to be unit length vectors.

In the results, an average error of 0.012 is obtained. See Figure 2.7 for a plot of all the errors for the 183 estimated absorption spectra. It is found a minority of cases with high errors that violated the assumption that similar emission spectra map to the same absorption spectra. Despite this, the majority of materials fit the assumption and absorption is accurately estimated as can be seen in Figure 2.8. It is also noted that absorption only determines the scale of the emission and not the color of the material. Thus some minor loss in accuracy for estimated absorption does not have a dramatic effect on the predicted color of scenes.

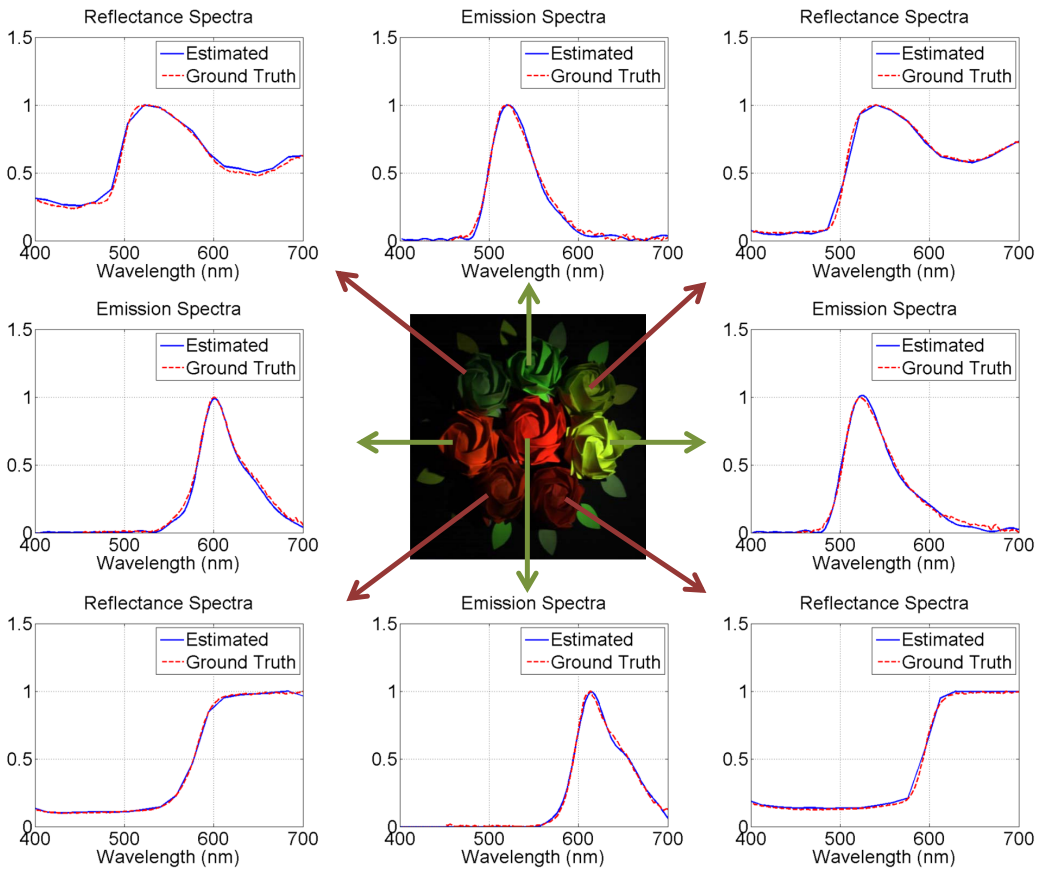

Figure 2.9: Recovered reflectance spectra for the ordinary reflective materials (red arrows) and fluorescent emission spectra for the fluorescent materials (green arrows).

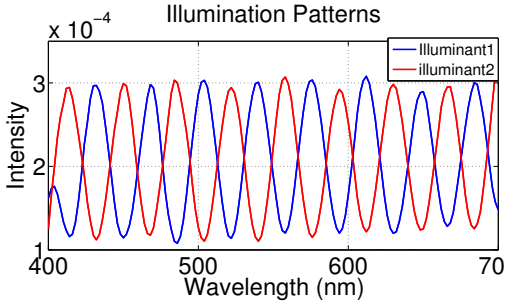

(a) High frequency illuminants produced by ELS

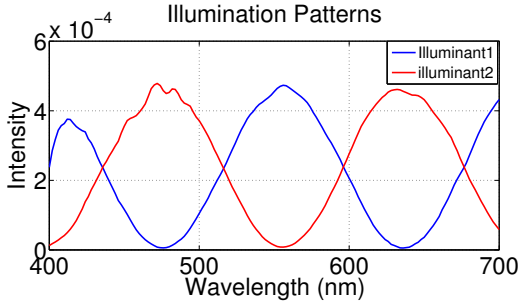

(b) Low frequency illuminants produced by ELS

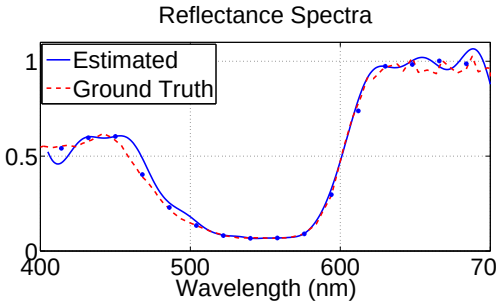

(c) Recovered $s(\lambda)$ under high frequency illuminants

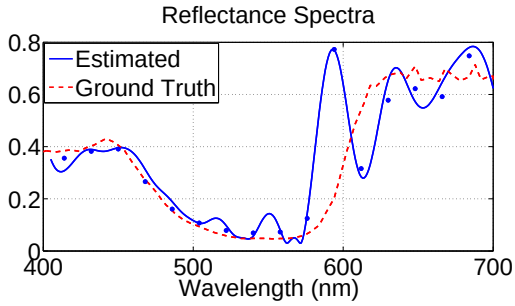

(d) Recovered $s(\lambda)$ under low frequency illuminants

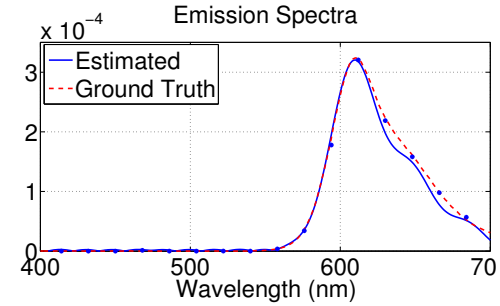

(e) Recovered $e(\lambda)$ under high frequency illuminants

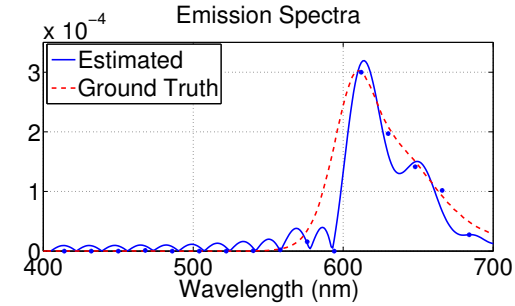

(f) Recovered $e(\lambda)$ under low frequency illuminants

Figure 2.10: Evaluate the separation method on pink sheet captured. (a)Two high frequency illuminations. (c) and (e) show the recovered reflectance and fluorescent emission spectra under these high frequency illuminations, respectively. (b)Two low frequency illuminations. (d) and (f) show the recovered reflectance and fluorescent emission spectra under these low frequency illuminations, respectively. Red line shows the ground truths and blue point shows the estimated results.

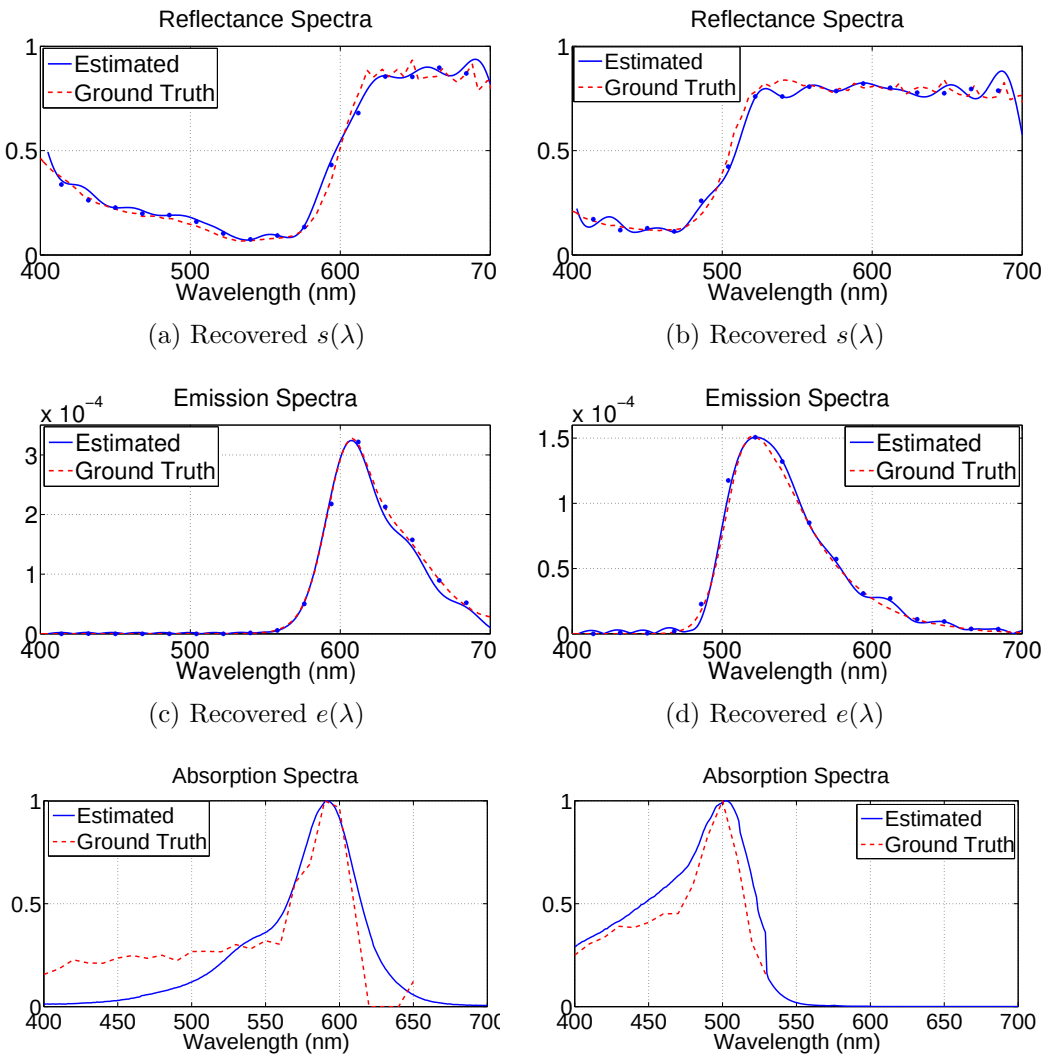

(a) Recovered $s(\lambda)$ (b) Recovered $s(\lambda)$

(c) Recovered $e(\lambda)$ (d) Recovered $e(\lambda)$

(e) Recovered $a(\lambda)$ (f) Recovered $a(\lambda)$

Figure 2.11: Recovered reflectance $s(\lambda)$, fluorescent emission $e(\lambda)$ and absorption $a(\lambda)$ spectra of the red and yellow sheets.

2.5 Experimental results and analysis

In the experiments, the importance of high frequency illumination is first demonstrated by using quantitative results on the recovery of reflectance and fluorescence spectra from real scenes. Then, visual examples of separated reflective and fluorescent components as RGB images are presented. In addition, the recovered spectra are used to accurately relight fluorescent scenes.

2.5.1 Experimental Setup

With the exception of the near UV light, Nikon Equalized Light Source (ELS) is used to produce all other illuminants in this section. The ELS is a programmable light source that can produce light with arbitrary spectral patterns from 400 nm to 720 nm. PR-670 SpectraScan Spectroradiometer is used to collect ground truth spectra. For the proposed method, a hyperspectral camera (EBA Japan NH-7) is used to capture whole scenes.

Figure 2.10(a) shows two high frequency illuminants produced by the ELS. Under these illuminants, the hyperspectral camera is used to capture the scene at wavelengths where either one of these illuminants have peaks so that the difference between l_1 and l_2 would be large and allow for reliable separation.

2.5.2 Quantitative Evaluation

For the ordinary reflective material, the reflectance spectrum can be easily recovered by capturing the scene under the white light across all visual spectra, While the emission spectrum for the fluorescent material can be easily captured the scene in longer wavelength under near UV light. Generally, the scene consists of both ordinary reflective material and fluorescent material. Here, the recovered reflectance spectrum for the ordinary reflective material and the emission spectrum for the fluorescent material are first evaluated. Their Ground Truth are captured under white light and the near UV light, respectively. In the proposed method, the reflectance spectrum $s(\lambda)$ and the emission spectrum $e(\lambda)$ are estimated by Equation (2.6) at the same time.

(a) Captured 4 channels under illuminant l_1

(b) Captured 4 channels under illuminant l_2

(c) Separated reflective components on 4 channels

(d) Separated fluorescent components on 4 channels

Figure 2.12: The separation results on 4 channels for a scene with fluorescent and non-fluorescent roses. These 4 channels, from left to right, are at 520 nm, 540 nm, 600 nm and 620 nm.

Figure 2.9 shows recovered reflectance spectrum for the ordinary materials (red arrows) and fluorescent emission spectra for the fluorescent material (green arrows) by using high frequency illuminations. It can be seen that all recovered spectra (Blue line) can approximate the Ground Truth (Red line) well. It demonstrate that the proposed method can also works for the ordinary reflective materials, in which $e(\lambda) = 0$, $s(\lambda)$ can be recovered by the first Equation in (2.6).

Then, quantitative results are compared on recovering the reflective and fluorescent spectral components using high and low frequency light on fluorescent colored sheets. Figure 2.10(a) and (b) show spectral distributions of the high frequency and low frequency illuminants used in the experiments.

The Ground Truth reflectance and fluorescence absorption and emission spectra of the fluorescent material are captured by bispectral measurements [Spr99]. The narrow band illuminations are employed across the visual light wavelength. The reflectance spectra are measured at the same wavelength with the the narrow band illuminations, fluorescent emission spectra are measured at the longer wavelength than the illuminations, and fluorescent absorption spectra are measured by observing the emission at a wavelength λ while varying the illuminant wavelength $\lambda^{'}$ for $\lambda^{'} < \lambda$.

In Figure 2.10(c)-(f), the recovered reflectance and fluorescent emission spectra of a pink fluorescent sheet under different illuminants. The recovered reflectance (Figure 2.10(c)) and fluorescent emission spectra (Figure 2.10(e)) under the high frequency illuminants approximate ground truth well. When the object is captured under the low frequency illuminants, the recovered reflectance (Figure 2.10(d)) and fluorescent emission (Figure 2.10(f)) have obvious errors. Figure 2.11(a)-(d) shows the recovered reflectance and fluorescent emission spectra of red and yellow fluorescent sheets under the high frequency illuminants. All these results demonstrate that the proposed method is able to recover reflectance and fluorescent emission spectra efficiently under high frequency illuminants.

In Figure 2.11(e) and (f), the recovered fluorescent absorption spectra of the red and yellow fluorescent sheets are shown. Due to limitations of the capture equipment, the ground truth could not be accurately measured in the short wavelength region in cases where absorption was relatively weak.

This issue can be seen in the the shorter wavelengths for the red sheet (Figure 2.11(e)). However, the recovered absorption spectra and the ground truth measurements still agree quite well.

2.5.3 Visual Separation and Relighting Results

In this section, experimental results for the separation of reflectance and fluorescence as well as accurate relighting performance are shown on visual images. The original results are in the form of hyperspectral images. Figure 2.12 shows the captured 4 channels of hyperspectral images and separated results by using high frequency illuminations for a fluorescent scene. From the left to the right columns, Figure 2.12(a) shows the scene captured at the peak, crest, peak and crest of the illuminant l_1, correspondingly Figure 2.12(b) shows the scene captured at the crest, peak, crest and peak of the illuminant l_2 at the same wavelength. The wavelength becomes longer from left to right columns. Their separated reflective and fluorescent components are shown in Figure 2.12(c) and (d), respectively. The separated fluorescent components (Figure 2.12(d)) only contain the fluorescent material, and demonstrate that the proposed method can effectively separate the reflective and fluorescent components. The green and yellow fluorescent roses are explicit shown in the shorter wavelength (the first and second columns in Figure 2.12(d)) and the orange and red fluorescent roses are explicit shown in the longer wavelength (the third and fourth columns in Figure 2.12(d)). But to easily visualize hyperspectral images, all of them have been converted to RGB images in the following.

The first scene is an image consisting of fluorescent and non-fluorescent roses and is taken under two high frequency illuminants (Figure 2.13(a) and (f)). Figure 2.1(b) and (c) are the corresponding recovered reflective and fluorescent components. The rose in 4 corners (the red arrows in Figure 2.9) only has ordinary reflectance so its colors in the recovered reflective component (Figure 2.1(b)) is the same as those seen under white light (Figure 2.1(a)). Looking at the center rose that is made of the red sheet in Figure 2.1(a), the recovered fluorescent component appears to be red. The measured emission spectrum of the red sheet (Figure 2.11(e)) indicates that the color of the

(a) Illuminant l_1 (b) Illuminant l_2 (c) Near UV light

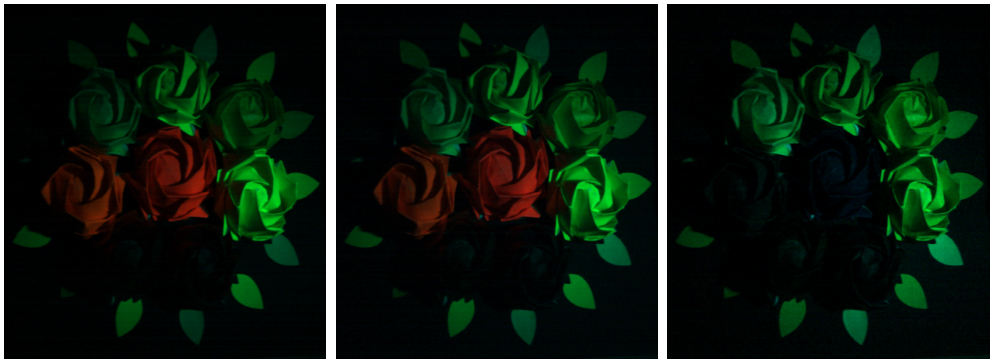

(d) Green light (e) Relighted (f) Relighted(Ref)

(g) Blue light (h) Relighted (i) Relighted (Ref)

Figure 2.13: The relighting results for a scene with fluorescent and non-fluorescent roses.

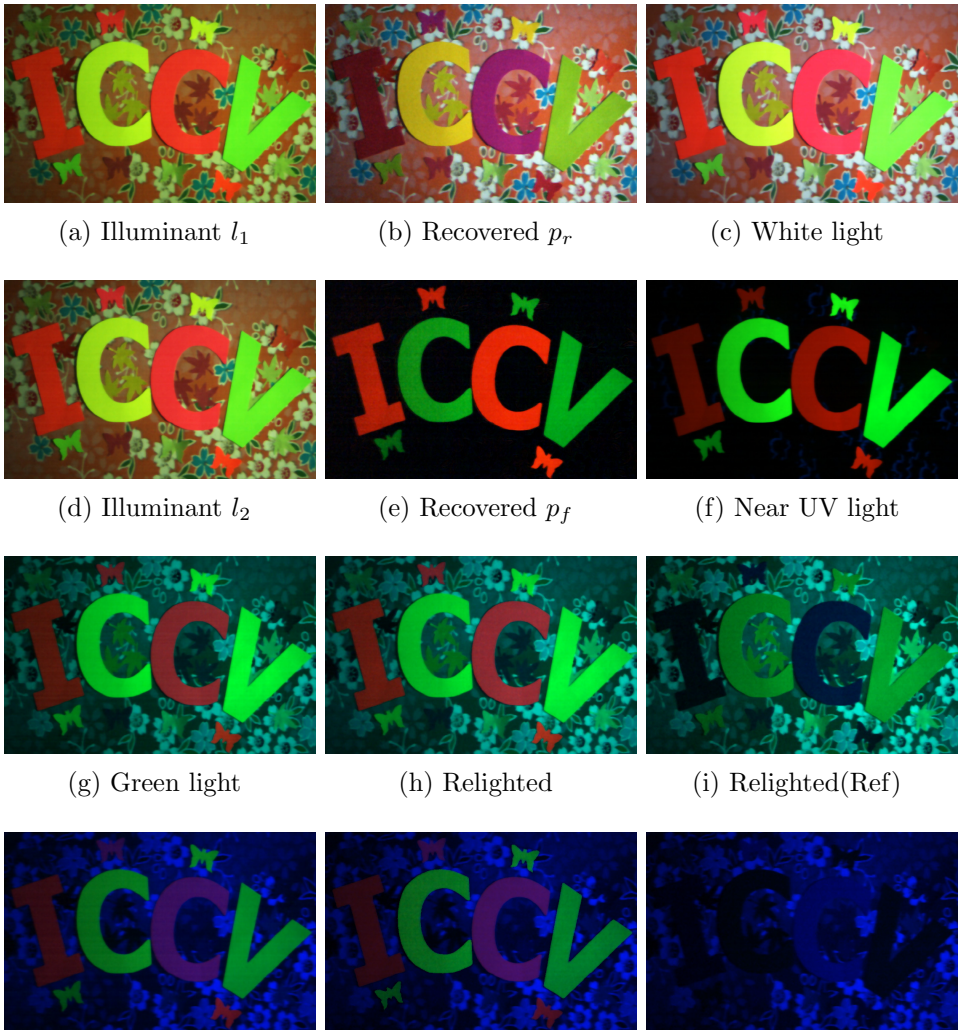

(a) Illuminant l_1 (b) Recovered p_r (c) White light

(d) Illuminant l_2 (e) Recovered p_f (f) Near UV light

(g) Green light (h) Relighted (i) Relighted(Ref)

(j) Blue light (k) Relighted (l) Relighted(Ref)

Figure 2.14: The separation and relighting results for fluorescent materials with complex background.

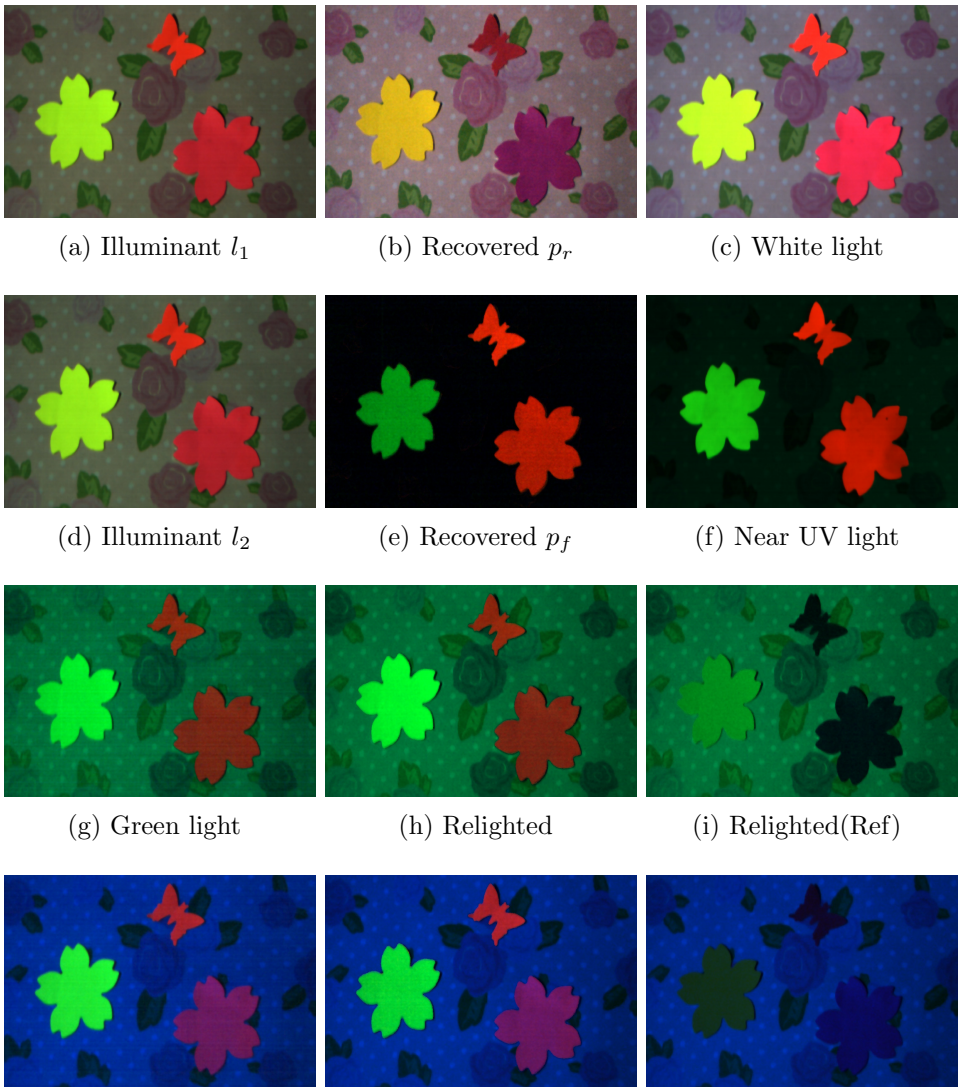

(a) Illuminant l_1 (b) Recovered p_r (c) White light

(d) Illuminant l_2 (e) Recovered p_f (f) Near UV light

(g) Green light (h) Relighted (i) Relighted(Ref)

(j) Blue light (k) Relighted (l) Relighted(Ref)

Figure 2.15: The separation and relighting results for fluorescent materials with complex background.

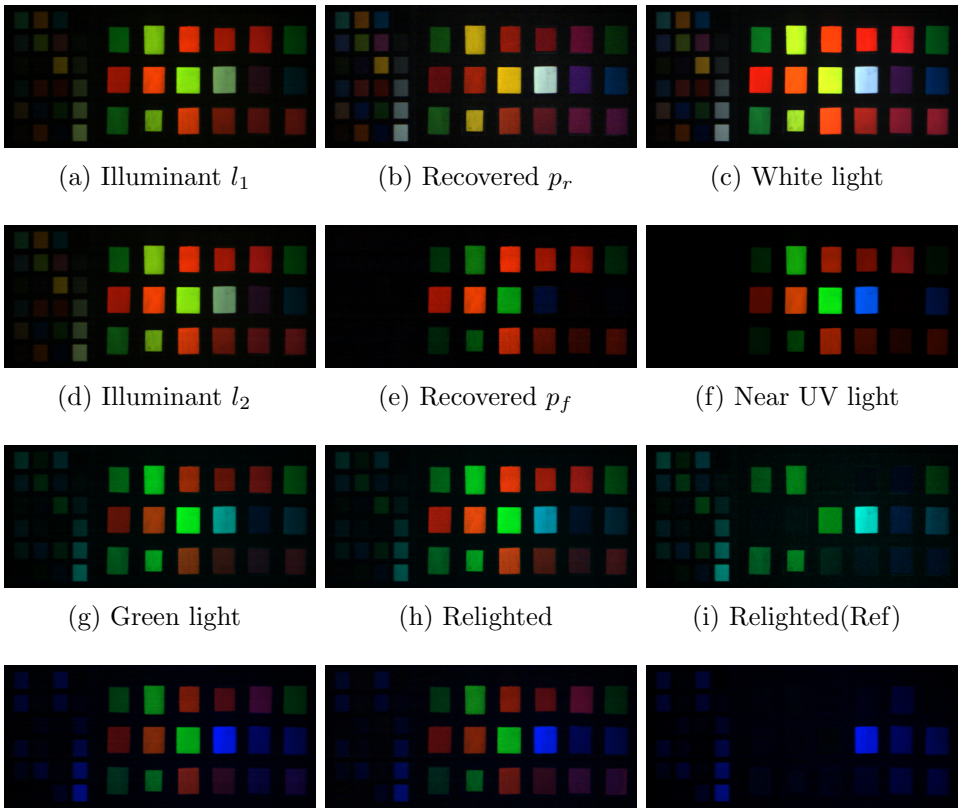

(a) Illuminant l_1 (b) Recovered p_r (c) White light

(d) Illuminant l_2 (e) Recovered p_f (f) Near UV light

(g) Green light (h) Relighted (i) Relighted(Ref)

(j) Blue light (k) Relighted (l) Relighted(Ref)

Figure 2.16: The separation and relighting results for fluorescent and non-fluorescent color chart.

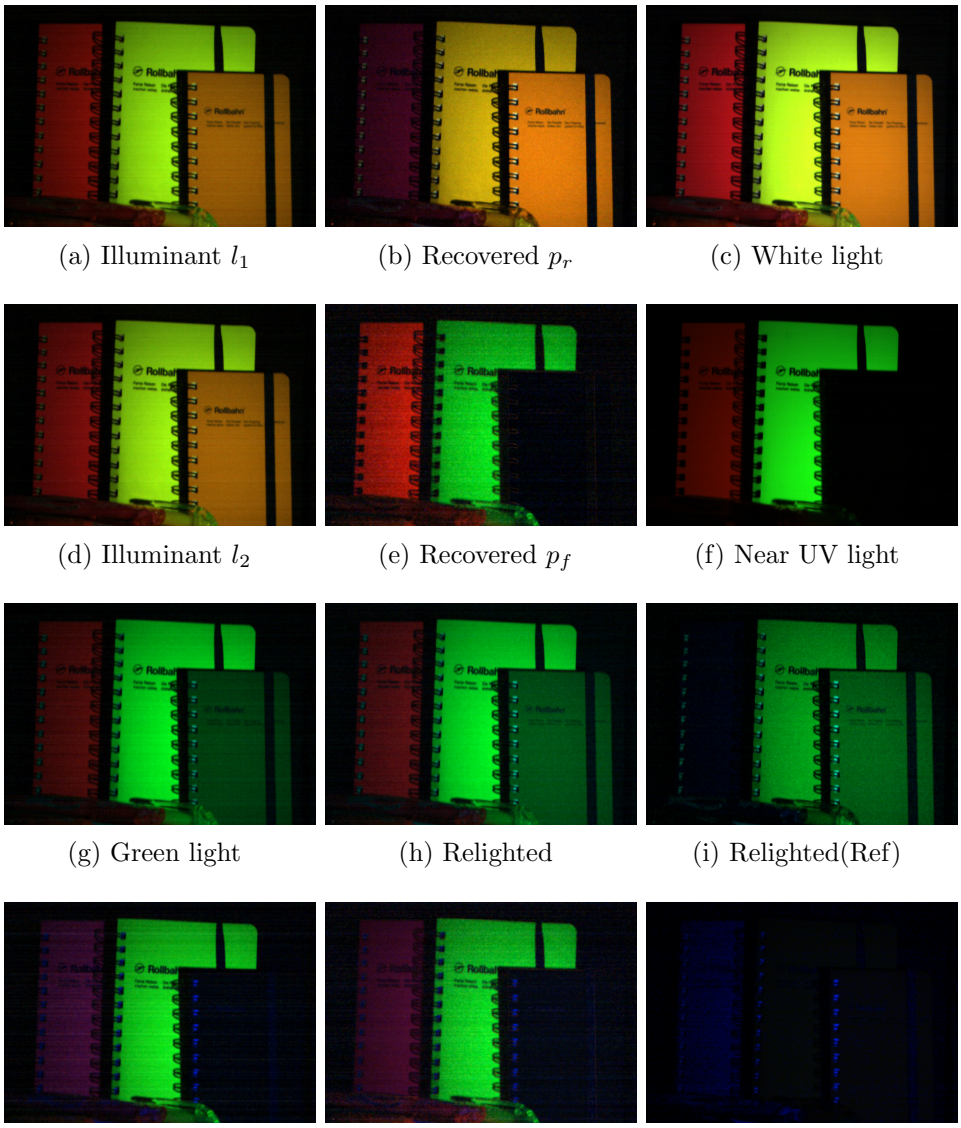

(a) Illuminant l_1 (b) Recovered p_r (c) White light

(d) Illuminant l_2 (e) Recovered p_f (f) Near UV light

(g) Green light (h) Relighted (i) Relighted(Ref)

(j) Blue light (k) Relighted (l) Relighted(Ref)

Figure 2.17: The separation and relighting results for a scene with fluorescent and non-fluorescent objects.

fluorescent component is indeed red. In addition, the scene captured under near UV light (Figure 2.13(b)) shows nearly pure fluorescent emission colors that also agree with the results. It is noted that since each fluorescent material has its own absorption spectrum, the value for $\left(\int l(\lambda')a(\lambda')\mathrm{d}\lambda'\right)$ is different between fluorescent materials captured under near UV light and high frequency light. As a result, under different lighting, fluorescent objects can exhibit different scales of emission, but the chromaticities match well under near UV light (Figure 2.13(b)) and recovered fluorescent component (Figure 2.1(c)).

Since the proposed method is able to recover the full reflectance, fluorescent emission, and fluorescent absorption spectra for an entire scene, the scenes can also been relighted. Figure 2.13 shows that real scenes can be accurately relighted using the proposed method. The scenes are captured under green (Figure 2.13(g)) and blue (Figure 2.13(d)) illuminants. The corresponding relighting results are shown in Figure 2.13(c) and (i). It can be seen that, the relighting results are very similar to the ground truths (Figure 2.13(g) and (d)), and demonstrate the effectiveness of the proposed method to recover the reflectance and fluorescent emission and absorption spectra. When the scene is relighted using the reflective component only (Figure 2.13(h) and (e)), this leads to many fluorescent materials appearing as black, especially under blue light (Figure 2.13(i)).

Figures 2.14-2.17 show additional separation of reflectance and fluorescence on 4 other fluorescent scenes and their relighting results. These scenes contain that color fluorescent sheet on a complex colored sheet, colored fluorescent flowers and butterfly on a complex colored background, fluorescent color checker with Macbeth chart, and the fluorescent and non-fluorescent notebooks. The separated reflective component (Figure 2.14-2.17(b)) for the ordinary reflective material is the same as those seen under white light (Figure 2.14-2.17(c)), and the separated fluorescent component (Figure 2.14-2.17(e)) also approximate the scene captured under near UV light (Figure 2.14-2.17(f)) which shows nearly pure fluorescent emission colors. The relighting results (Figure 2.14-2.17(h)(k)) were all close to the ground truth (Figure 2.14-2.17(g)(j)) and the fluorescent parts were well separated from the reflective parts. These additional results on real scenes show that the

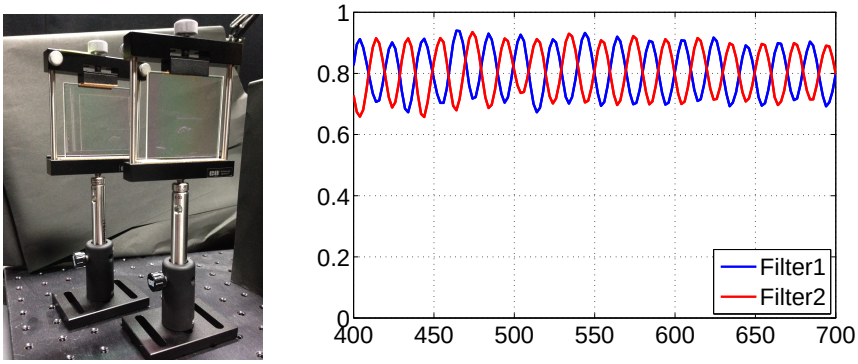

(a) Filters (b) Spectra

Figure 2.18: The two high frequency filters (a) and their spectra (b).

proposed method can effectively work for different scenes.

2.6 Separation by using high frequency filters

In section 2.5, a programmable light source known as the ELS is employed to produce complementary high frequency illuminants, by which the excellent experimental results can be obtained. However, programmable light sources such as the ELS are prohibitively expensive for many laboratories and consumers. They are also heavy and thus not portable. Due to these limitations, two complementary high frequency filters are designed, which are inexpensive and portable, as shown in Figure 2.18. These two filters are put in front of a light source to modulate an illuminant into high frequency illuminations that are the same as the lights produced by the programmable light source. They are designed as two complementary sinusoidal patterns with periods of 20 nm [1].

Let us denote one of filters as F_1 and its complement as F_2. So the illumination $l(\lambda)$ after going through the filters can be described as

$$\begin{aligned} l_1^f(\lambda) &= F_1(\lambda)l(\lambda), \\ l_2^f(\lambda) &= F_2(\lambda)l(\lambda). \end{aligned} \tag{2.21}$$

[1]Due to limitations in manufacturing of the filters, the exact sinusoidal spectra in the filters cannot be produced.

Table 2.1: The mean percent difference between k_1 and k_2 for 183 absorption spectra on CIE Standard Illuminants [HP11] with the ideal sinusoidal pattern filters, rectified real filters and real filters for 183 absorption spectra in the McNamara and Boswell Fluorescence Spectral Dataset. "Ideal (20 nm)" and "Ideal (40 nm)" denote filters with ideal sinusoidal patterns and periods of 20 nm and 40 nm. "Rectified Filters " are the "Real Filters" with maximum and minimum values normalized to range from [0,1]. The spectra of the the real filters are shown in Figure 2.18.

Illuminant	Ideal (40 nm)	Ideal (20 nm)	Rectified Filters	Real Filters
E	2.56	0.34	2.36	0.44
A	2.79	0.33	1.99	0.37
B	2.64	0.29	1.92	0.36
C	2.59	0.28	1.91	0.36
D50	2.70	0.46	2.22	0.42
D55	2.66	0.45	2.25	0.42
D65	2.61	0.44	2.30	0.43
D75	2.57	0.43	2.33	0.44
F1	8.06	1.41	2.31	0.44
F2	9.57	1.74	3.08	0.59
F3	11.25	2.13	3.98	0.77
F4	13.00	2.56	4.98	0.97
F5	7.92	1.36	2.18	0.41
F6	9.92	1.80	3.21	0.62
F7	7.82	1.33	2.27	0.43
F8	8.74	1.50	2.84	0.54
F9	9.86	1.74	3.39	0.65
F10	14.56	3.12	4.96	1.02
F11	16.58	3.73	5.88	1.21
F12	19.20	4.52	7.10	1.47

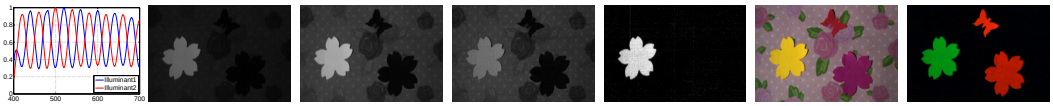

(a) ELS

(b) E light with filters

(c) C light with filters

(d) D55 light with filters

(e) D65 light with filters

(f) F5 light with filters

Figure 2.19: The separation results with the high frequency filters. The spectra of illuminants are shown in the first column. Taking a channel at 550nm as an example, the second and third columns show the captured images under 2 high frequency illuminations, and their separated reflective and fluorescent components are shown in third and fourth columns. The fifth and sixth columns show reflective and fluorescent components over all captured spectra in RGB images. To make comparison, the first row shows the separation results under high frequency illuminations produced by ELS. From second to sixth rows, the separation results under E, C, D55, D65 and F5 light with the high frequency filters are shown, respectively.

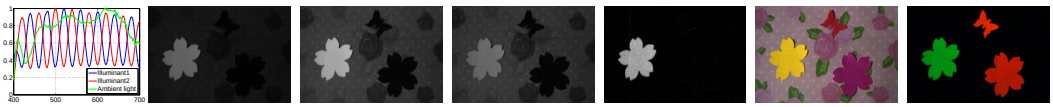

(a) ELS + Flat light

(b) E light with filters + Flat light

(c) C light with filters + Flat light

(d) ELS + Non-flat light

(e) E light with filters + Non-flat light

(f) C light with filters + Non-flat light

Figure 2.20: The separation results with ambient light. The spectra of illuminants are shown in the first column, where the green curves in the first and third rows are the spectra of the flat and unflat ambient light. Taking a channel at 550nm as an example, the second and third columns show the captured images under 2 high frequency illuminations, and their separated reflective and fluorescent components are shown in third and fourth columns. The fifth and sixth columns show reflective and fluorescent components over all captured spectra in RGB images. From the first to sixth rows, they are separation results under high frequency illuminants produced by ELS with flat ambient light (D50), E light through high frequency filters with flat ambient light, C light through high frequency filters with flat ambient light, high frequency illuminants produced by ELS with non-flat ambient light (typical fluorescent lamp), E light through high frequency filters with non-flat ambient light, and C light through high frequency filters with non-flat ambient light, respectively.

When the spectrum of light $l(\lambda)$ is flat (constant for all wavelengths λ), it can be seen that l_n^f $(n = 1, 2)$ are equivalent to the l_n $(n = 1, 2)$ discussed in Section 2.3.

However, common light sources such as daylight and off-the-shelf lights are not exactly flat, so it is necessary to evaluate how an arbitrary light source affects the resultant high frequency illuminations. $l_n(\lambda)$ is first replaced by $l_n^f(\lambda)$ in Equation (2.5) and obtain

$$\begin{aligned} p_1(\lambda) &= F_1(\lambda)l(\lambda)s(\lambda) + k_1 e(\lambda), \\ p_2(\lambda) &= F_2(\lambda)l(\lambda)s(\lambda) + k_2 e(\lambda), \\ k_n &= \int F_n(\lambda')l(\lambda')a(\lambda')\mathrm{d}\lambda'. \end{aligned} \tag{2.22}$$

As discussed in Section 2.3.3, the errors for the recovered reflective and fluorescent emission spectra is directly proportional to $k_1 - k_2$. In this case, the difference between k_1 and k_2 is affected by the spectra of the filters $F_n(\lambda)$, illuminant $l(\lambda)$ and fluorescent absorption $a(\lambda)$. Table 2.1 shows the mean percent difference between k_1 and k_2 for 183 absorption spectra, where each row corresponds to a CIE standard illuminant.

To explore the influences due to the frequency, distortion, and value α/β ratio of the filters (described in Section 3.4), the mean percentage is calculated on 4 kinds of filters, "Ideal (40 nm)", "Ideal (20 nm)", "Rectified Filters" and "Real Filters".

"Ideal (40 nm)" and "Ideal (20 nm)" denote ideal sinusoidal patterned filters with 40 nm and 20 nm periods and $\alpha/\beta = 1$. According to the discussion in Section 2.3.2, when the frequency of the filters is higher, the difference between k_1 and k_2 will be lower. Thus, the differences under "Ideal (20 nm)" are less than those under "Ideal (40 nm)" under the same illuminant $l(\lambda)$.

The real filters shown in Figure 2.18 exhibit spectral distortion, which cannot exactly described by Equation (2.4). these filters are partially remedied by normalizing the values of their spectra between minimum and maximum to be in the range [0,1], and denote this as the "Rectified Filters". Their spectra are shown in 2.18 (c). The "Rectified Filters" have the same period as the "Ideal (20 nm)" and a proportion of $\alpha/\beta = 1$, but they still

exhibit some distortion. Compared with "Ideal (20 nm)", the distortion in the "Rectified Filters" can enlarge the difference between k_1 and k_2.

The difference between k_1 and k_2 relies on the high frequency component $\beta \cos(2\pi f_l \lambda)$ in the illuminant and is not related to the direct current (DC) component α as discussed in Section 2.3.3. "Real Filters" denote the difference value between k_1 and k_2 on the real filters in Figure 2.18. "Real Filters" have the same period as the "Rectified Filters" and distortion but not a proportion of $\alpha/\beta = 1$. As α/β is larger for "Real Filters", their DC component of the filters is much larger than the high frequency components compared with "Rectified Filters". As shown in Table 2.1, the difference between k_1 and k_2 under "Real Filters" is lower compared with the "Rectified Filters" under the same standard illuminant, but the "Real Filters" case is easily affected by noise, as the maximum difference between the two complementary high frequency illuminants is small, which will be shown in Figure 2.19.

Another point, in terms of the discussion in Section 2.3.2 is that the frequency of the filter $F(\lambda)$ should be higher than the maximum frequency of $l(\lambda')a(\lambda')$ to keep $k_1 = k_2$. Therefore, for all these 4 cases, the higher frequency components the illuminants $l(\lambda)$ contain, the larger the difference between k_1 and k_2 will be. Examples of such lights are F10, F11, and F12.

Figure 2.19 shows the separated reflective and fluorescent components under different illuminants through the high frequency filters. The first column shows the high frequency illuminations' spectra, resulting from using different light sources. Taking a channel at 550 nm as an example, the second and third columns show the captured images under two high frequency illuminations, and their separation results are shown in the third and fourth columns. The fifth and sixth columns show separation results over all captured spectra in RGB images. Figure 2.19(b)-(f) show the separation results under E, C, D55, D65 and F5 lights with the high frequency filters, respectively. Compared with the separation results under the high frequency illuminations produced by the ELS (Figure 2.19(a)), the separation results using the high frequency filters are competitive but there is more noise, for example, in the two fluorescent flowers. The decreased amount of light going through the filters likely caused the camera to exhibit more noise. The ratio α/β for the high frequency filters is also much larger than for the spectra produced by

the ELS, which makes the separation results more sensitive to the noise from the camera and also contributes to the noise.

2.7 Ambient illumination

Until now, the proposed method have been extended to more general light source by using high frequency filters instead of ELS, but did not consider the ambient light. In the following, the effect from the ambient light is discussed and the proposed method is extended to the scene with the ambient light. Let us denote ambient illuminant as $l_a(\lambda)$. Without loss of generality, the illuminants produced by ELS or flat light source with filters are defined as $l_1(\lambda)$ and $l_2(\lambda)$. So the illuminations with ambient light can be described as

$$\begin{aligned} l_1^a(\lambda) &= l_1(\lambda) + l_a(\lambda), \\ l_2^a(\lambda) &= l_2(\lambda) + l_a(\lambda). \end{aligned} \tag{2.23}$$

Replacing the $l_n(\lambda)$ by $l_n^a(\lambda)$ in Equation (2.5), it can be obtained

$$\begin{aligned} p_1(\lambda) &= [l_1(\lambda) + l_a(\lambda)]s(\lambda) + k_1 e(\lambda), \\ p_2(\lambda) &= [l_2(\lambda) + l_a(\lambda)]s(\lambda) + k_2 e(\lambda), \\ k_n &= \int [l_n(\lambda) + l_a(\lambda)]a(\lambda^{'})\mathrm{d}\lambda^{'}. \end{aligned} \tag{2.24}$$

Since the ambient illuminant l_a is the same under the two different high frequency illuminants $l_1^a(\lambda)$ and $l_2^a(\lambda)$, the difference between k_1 and k_2 is only related to the high frequency illuminants $l_1(\lambda)$ and $l_2(\lambda)$. Intuitively, the intensity of the ambient illuminant can be considered as a part of the DC component α, which is also the same under two complementary high frequency illuminations. Thus, the proposed method can be directly used on scenes with ambient light, and the reflectance and fluorescence emission spectra can be recovered by Equation (2.6), in which the illuminations $l_n(\lambda)$ are replaced by $l_n^a(\lambda)$.

Figure 2.20 shows the separation results under different high frequency illuminants and ambient light. The spectra of flat and non-flat ambient light are shown as green lines in the first and fourth rows of Figure 2.20(a). It can be seen that all separation results under flat ambient light (the first to

(a) Illuminations (b) p_r (c) p_f (d) p_r (e) p_f (f) p_r (g) p_f

Figure 2.21: The separation results under strong ambient light, which is typical of fluorescent lamps. (a) shows the two illuminations used to illuminate scene. (b) and (c) show separation results at crests of the ambient light spectrum at 520 nm, (d) and (e) show results at peaks of the ambient light spectrum 540 nm, and (f) and (g) show results over the visible spectrum as RGB images.

third rows in Figure 2.20) and non-flat ambient light (the fourth to sixth rows in Figure 2.20) are good enough. These results demonstrate that our method can work well under flat and non-flat ambient light source. Besides, compared with the results under the high frequency illuminations produced by ELS (The first and fourth rows in Figure 2.20), the separation results from E (the second and fifth rows in Figure 2.20) and C (the third and sixth rows in Figure 2.20) light through the high frequency filter contain much noise like in Figure 2.19, but are also acceptable.

The scene is also captured under a strong ambient illuminant which is typical of a fluorescent lamp, and show the separation results in Figure 2.21. The results on the crest located at 520 nm of the ambient light spectrum show clear separation of the components (Figure 2.21(b) and (c)), while the results on the peak at 540 nm of the ambient light spectrum are clearly wrong (Figure 2.21(d) and (e)). This is because the DC component in the $l_n^a(\lambda)$ is larger and the observation of two high frequency illuminations will be almost same under the strong ambient illuminant spectrum in that range. The separation results are easily affected by camera noise. Therefore, it is necessary to choose a higher intensity light source when the ambient illuminant is strong in practice.

2.8 Summary

In this chapter, a efficient method is proposed to simultaneously recover the reflectance and fluorescence emission spectra of an entire scene by using high frequency illumination in the spectral domain. Afterward, it is presented the method for estimating the fluorescence absorption spectrum of a material given its emission spectrum. Through this method, it is also shown that similar emission spectra tend to map to similar absorption spectra. The effectiveness of the proposed method was successfully demonstrated with experiments using real data taken by a spectroradiometer and camera, both in conjunction with a programmable light source. To extend the proposed method to much more general light sources, two high frequency filters are designed and employed under CIE standard illuminants. It is demonstrated that when the light source is flat enough compared with the frequency of the filters, the proposed method also works well. The proposed method is also implemented under high frequency illuminations with flat/non-flat ambient light, and the results show that the proposed method works well under different types of ambient light.

There are still a few limitations in this research that are worth attention and further investigation. First, the two high frequency filters used in the experiments affect the separation results, due to their distortions of the sinusoidal patterns and the differences between the peaks and crests of the light spectra. In the future, I expect to design/employ much better high frequency filters, which have much smaller distortions, and especially smaller values of α/β, to make them more robust to noise. Second, shading from the light source and specularity from the materials were not considered in this work. More importantly, shading and specularity can provide more information about a scene. Therefore, it is worth investigating a more comprehensive model for reflective and fluorescent separation to make it applicable to more real cases.

Chapter 3

Reflectance and Fluorescence Spectral Recovery via Actively Lit RGB Images

3.1 Overview

Fluorescence is also very different from ordinary reflectance in the way they respond to incident light [JF99, ZS11]. In particular, hyperspectral images of reflective-fluorescent scenes provide a rich amount of data for these two components. However, directly capturing such components from hyperspectral reflective-fluorescent images is challenging due to the very different ways that reflectance and fluorescence respond to incident light [JF99, ZS11].

As the properties of fluorescence are very different from ordinary reflectance, neglecting fluorescence can result in completely incorrect estimation of photometric properties. This in turn negatively affects many methods that rely on accurate color estimation. As shown in Figure 3.1, a scene is captured under blue and green lights (Figure 3.1(a)). When the effects of fluorescence are considered (Figure 3.1(b)), the simulated relighting results are close to the ground truth. However, when it is assumed that the scene does not include fluorescent materials, the relighting results for the fluorescent materials are wrong (Figure 3.1(c)).

It is also the case that in practice, most fluorescent objects are not purely

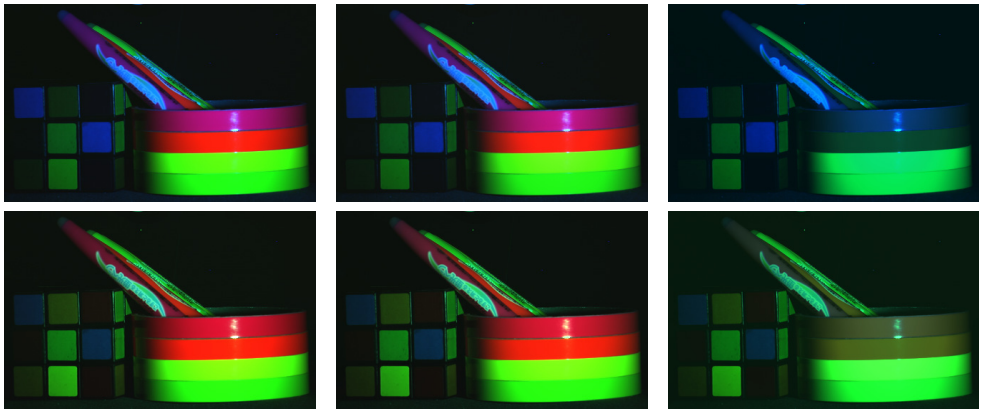

(a) Ground Truth (b) Relit with Fluorescence (c) Relit without Fluorescence

Figure 3.1: (a) The scene captured under blue and green light. (b) Simulated relighting results with consideration of fluorescent effects. (c) The relighting results without considering fluorescence.

fluorescent. Instead, they contain a combination of reflective and fluorescent components so both components need to be considered.The conventional approach to capturing these two components is to exhaustively measure different combinations of reflecting, absorbing and emitting wavelengths [LJA97]. This process is labor intensive and more efficient approaches for imaging scenes is desired. Zhang and Sato [ZS11] proposed a method that uses an RGB camera and independent component analysis (ICA) to separate reflective and fluorescent components but their method does not capture the spectral distributions of reflectance, fluorescence absorption and emission. In recent work, methods for hyperspectral imaging of reflective-fluorescent scenes have been proposed [LS13, FLS+13]. These methods are effective but require specialized cameras and specialized illuminants such as narrow-band light or high frequency light spectra.

A more practical approach is proposed for hyperspectral imaging of reflective-fluorescent scenes using only a conventional RGB camera and varied colored illuminants. The proposed method takes as input RGB images under different lighting and effectively separates reflectance and fluorescence in the spectral domain. These separated results can then be used for tasks such as

accurate color relighting of scenes under novel lighting (Figure 3.2).

The key idea in the proposed approach is to exploit a unique property of fluorescence: the chromaticity of fluorescence emissions are invariant under different illuminants. Based on this property, a method is formulated that takes RGB images and performs pixel-wise estimation of spectral reflectance and fluorescent chromaticity. The method works by iteratively improving estimates of the spectral reflectance and fluorescent chromaticity in turn. It is shown that the proposed method is robust to initialization conditions and converges onto accurate spectral reflectance and fluorescent chromaticity for real scenes. Then, the method is proposed for estimating the fluorescence absorption and emission spectra of the scene given the estimated spectral reflectance data and fluorescent chromaticities.
In summary, the main contributions are that we

1. Exploit the illuminant-invariant chromaticity of fluorescence to estimate both spectral reflectance and fluorescent chromaticity from RGB images,
2. Devise a means for estimating fluorescence absorption and emission spectra from given spectral reflectance and fluorescent chromaticity,
3. Ultimately, presenting the first system capable of imaging all reflective and fluorescence absorption and emission spectra of real scenes using only a conventional RGB camera and varied colored illuminants.

It is shown that the proposed method is accurate and demonstrate its effectiveness in predicting color relighting of real scenes.

3.2 Related Work

There have been a number of effective methods for estimating the spectral reflectance of scenes. For example, Tominaga [Tom96] recovered reflectance spectra from images captured by a monochrome camera with sequentially placed band-pass filters. Park *et al.* [PLGN07b] employed multiplexed illumination produced by sets of LEDs for fast spectral imaging of dynamic scenes. Chi *et al.* [CYBE10] obtained the spectral information of a scene in the presence of unknown ambient illumination by optimizing wide band

filtered illumination. Han *et al.* [HSOS10] recovered spectral reflectance using multiple illuminations produced by the color wheel in a DLP projector. Jiang and Gu [JG12] recovered spectral reflectance from two images taken with conventional consumer cameras under commonly available lighting conditions. These methods are practical and effective for imaging spectral reflectance but their limitation is they cannot accurately capture scenes with fluorescent surfaces. The reason for this loss in accuracy is because reflective and fluorescent surfaces react to incident light very differently.

The detrimental effects of not considering fluorescence is nicely illustrated in Johnson and Fairchild [JF99] where they showed that taking fluorescence into account dramatically improved color renderings. Lee *et al.* [LSC01] provided a mathematical description for fluorescent processes and recovered the additive spectra of reflective and fluorescent components but did not separate them. Furthermore, Barnard [Bar99] proposed improvements to color constancy algorithms which included spectral data from several fluorescent materials. Later, Wilkie *et al.* [WWLP06] showed accurate results by rendering fluorescence emissions using diffuse surfaces that can reflect light at a wavelength different from its incident illuminant wavelength. Hullin *et al.* [HHA+10] also demonstrated the importance of modeling different reflective-fluorescent materials by introducing the bidirectional reflectance and reradiation distribution function (BRRDF).

A conventional way to measure fluorescence in the spectral domain is to use Bispectral measurements [LJA97]. However, exhaustively measuring different combinations of absorption and emission wavelengths is labor intensive. In addition, such measurements only work for a single surface point. Thus they are impractical for imaging scenes.

Instead, a camera based approach is more desirable. Zhang and Sato [ZS11] proposed an ICA based reflective-fluorescent separation method. Tominaga *et al.* [THK11] used two light sources and multispectral imaging to estimate fluorescence emission spectra. Alterman *et al.* [ASW10] separated the appearance of each fluorescent dye from a mixture by unmixing multiplexed images. Fuchs [Fuc01] estimated the reflectance and fluorescence emission spectra of coral. None of these methods fully recover all reflective and fluorescent components of scenes.

In recent work, methods for hyperspectral imaging of reflective-fluorescent scenes have been proposed. Lam and Sato [LS13] provided a method for recovering the full spectral reflectance and fluorescence absorption and emission spectra of scenes but they required a multiband camera and multiple narrow-band illuminants. Fu *et al.* [FLS+13] also recovered the full spectral reflectance and fluorescence spectra of scenes by using high frequency light spectra but they require a hyperspectral camera and a programmable light source: a device that can be programmed to produce arbitrary light spectra. Zheng *et al*. [ZSS14] recovered all the different types of spectra by using 3 Ordinary Illuminants, but they still require a hyperspectral camera. While effective, all these methods require specialized equipment so their use in applications is limited. A more practical approach is proposed to fully capturing the reflectance and fluorescence absorption and emission spectra of scenes using an RGB camera and varied illuminants.

The wavelength shifting phenomenon of fluorescence has been studied and used for solving computer vision problems. Han *et al.* [HMS+12] utilized separated fluorescent components to estimate camera spectral sensitivity under unknown illumination. Sato *et al.* [SOS12] used the fluorescent component for photometric stereo. Treibitz *et al.* [TMMK12] constructed 3D models from fluorescence. Hullin *et al.* [HFI+08] utilized the fluorescent component for fluorescent immersion range scanning. Lam and Sato [LS13] and Fu *et al.* [FLS+13] predicted the appearance of relit fluorescent scenes after all information of spectra were recovered in the scene. Fu *et al.* [FLM+14] removed scene interreflection using fluorescence.

3.3 Reflectance and Fluorescence Spectra Estimation

In this section, an efficient method is proposed to recover the full spectra of reflectance and fluorescence. First, the reflectance spectrum and the chromaticity of the fluorescent component are estimated in an alternating process with an initialization of the fluorescent chromaticity. Then, the fluorescence absorption and emission spectra are recovered. Finally, we discuss how the

fluorescent chromaticity can be initialized in the proposed method.

3.3.1 Problem Formulation

When taking an image of a scene with reflective-fluorescent components using an RGB camera, the intensity of each pixel for the n-th channel under the m-th illuminant is

$$p_n^m = r_n^m + f_n^m. \tag{3.1}$$

r_n^m is the reflective component for the n-th channel under the m-th illuminant and can be described by

$$r_n^m = \int c_n(\lambda) l_m(\lambda) s(\lambda) \mathrm{d}\lambda, \tag{3.2}$$

where $s(\lambda)$ is the spectral reflectance of the material at wavelength λ, $l_m(\lambda)$ is the m-th illuminant's intensity and $c_n(\lambda)$ $(n = 1, 2, 3)$ is the corresponding camera spectral sensitivity for the R, G, and B channels.

Substituting Equations (3.2) and (1.5) into Equation (3.1),

$$\begin{aligned} p_n^m = &\int c_n(\lambda) l_m(\lambda) s(\lambda) \mathrm{d}\lambda \\ &+ \left(\int l_m(\lambda^{'}) a(\lambda^{'}) \mathrm{d}\lambda^{'} \right) \int c_n(\lambda) e(\lambda) \mathrm{d}\lambda. \end{aligned} \tag{3.3}$$

Equation (3.3) describes how the components of a reflective-fluorescent surface jointly appear in a camera image under illuminant $\boldsymbol{l_m}$. The task is to determine the full spectral reflectance $\boldsymbol{s}$ and fluorescence absorption spectrum $\boldsymbol{a}$ and emission spectrum $\boldsymbol{e}$ given the observed p_n^m under different illuminants $\boldsymbol{l_m}$ and camera spectral sensitivity $\boldsymbol{c_n}$, which can be estimated by

$$\{\hat{\boldsymbol{s}}, \hat{\boldsymbol{a}}, \hat{\boldsymbol{e}}\} = \arg\min_{s,a,e} G(\boldsymbol{s}, \boldsymbol{a}, \boldsymbol{e}), \tag{3.4}$$

where

$$\begin{aligned} G(\boldsymbol{s}, \boldsymbol{a}, \boldsymbol{e}) &= \sum_m \sum_n \| p_n^m - \hat{p}_n^m(\boldsymbol{s}, \boldsymbol{a}, \boldsymbol{e}) \|_2^2 \\ &= \sum_m \sum_n \| \int p_n^m - c_n(\lambda) l_m(\lambda) s(\lambda) \mathrm{d}\lambda - \\ &\left(\int l_m(\lambda^{'}) a(\lambda^{'}) \mathrm{d}\lambda^{'} \right) \int c_n(\lambda) e(\lambda) \mathrm{d}\lambda \|_2^2 \end{aligned} \tag{3.5}$$

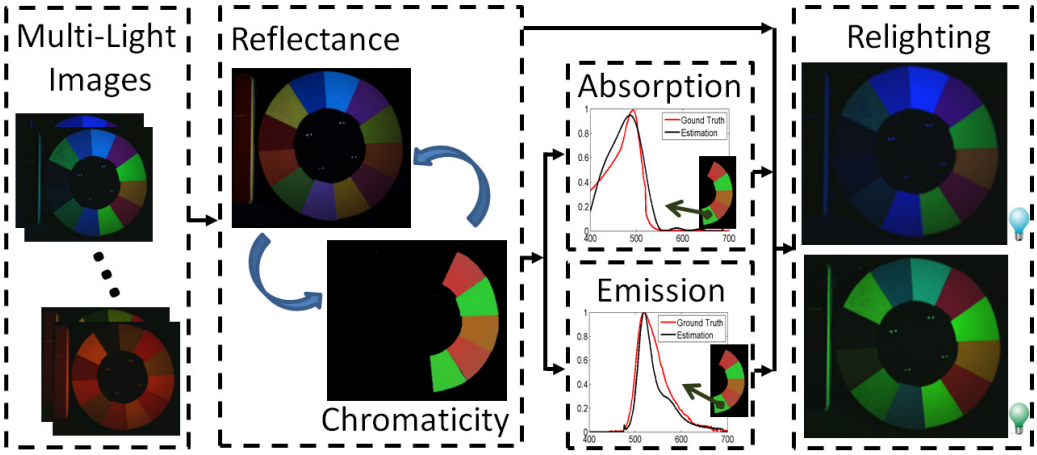

Figure 3.2: Overview of the method. The input images are captured under varied illuminants. The reflectance spectrum and the chromaticity of the fluorescent component are optimized in a process of alternating iterations that exploits the illuminant-invariant chromaticity of fluorescence. After that, the fluorescence absorption and emission spectra are estimated. All these recovered spectra can be used to relight the reflective-fluorescent scene under new illuminants.

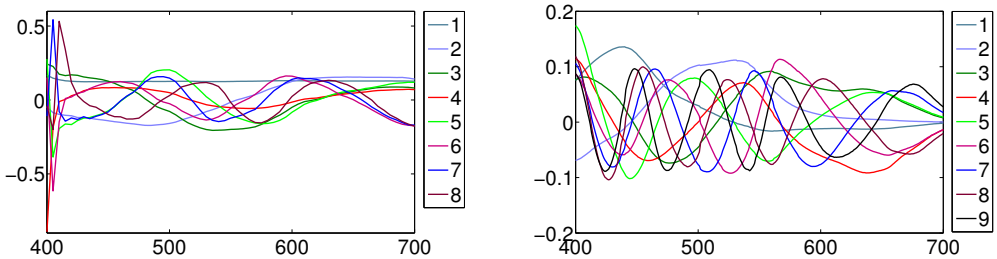

(a) Basis for the reflectance spectrum. (b) Basis for the absorption spectrum.

Figure 3.3: The bases are used to describe (a) reflectance and (b) fluorescence absorption spectra.

and $\hat{p}_n^m(\boldsymbol{s}, \boldsymbol{a}, \boldsymbol{e})$ is the estimated parameterization of p_n^m.

The proposed method for optimizing Equation (3.4) makes use of the illuminant-invariant chromaticity property of fluorescence. Therefore, all spectral components can be determined in two stages. It is started by using the illuminant-invariant chromaticity of fluorescence to estimate the reflectance spectrum $\boldsymbol{s}$ and the fluorescent chromaticity values E_n for all channels n. After that, the fluorescence absorption spectrum $\boldsymbol{a}$ and emission spectrum $\boldsymbol{e}$ can be recovered. Figure 3.2 shows an overview of the proposed method.

3.3.2 Reflectance Spectrum Recovery

In Section 1.1.3, it is shown that the chromaticity of fluorescence is invariant under different illuminants. I now show how to use the illuminant-invariant chromaticity of fluorescence in conjunction with basis functions for spectral reflectance to estimate the spectral reflectance of the scene.

According to a previous study [PHJ89], the spectral reflectance of various materials can be approximately represented by using a small number of basis functions as

$$s(\lambda) = \sum_{j=1}^{J} \alpha_j b_j(\lambda), \tag{3.6}$$

where $b_j(\lambda)$ $(j = 1, 2, \cdots, J)$ are the basis functions (Figure 3.3(a)) for spectral reflectance and α_j are the corresponding coefficients. From Equation

(3.6), Equation (3.2) can be rewritten as

$$r_n^m = \sum_j \alpha_j \int c_n(\lambda) l_m(\lambda) b_j(\lambda) \mathrm{d}\lambda = \sum_j \alpha_j q_{n,j}^m, \tag{3.7}$$

where $q_{n,j}^m = \int c_n(\lambda) l_m(\lambda) b_j(\lambda) \mathrm{d}\lambda$.

The illuminant-invariant chromaticity of fluorescence makes it possible to estimate the spectral reflectance $\boldsymbol{s}$ without knowing absorption spectrum $\boldsymbol{a}$ and emission spectrum $\boldsymbol{e}$. First note that $f_n^m = p_n^m - r_n^m = p_n^m - \sum_j \alpha_j q_{n,j}^m$. According to Equation (1.8), the chromaticity value E_n^m for channel n under illumination m can be computed by

$$E_n^m = \frac{f_n^m}{\sum_t f_t^m} = \frac{p_n^m - \sum_j \alpha_j q_{n,j}^m}{\sum_t (p_t^m - \sum_j \alpha_j q_{t,j}^m)} = E_n. \tag{3.8}$$

By straightforward algebraic manipulation of Equation (3.8),

$$p_n^m = E_n \sum_t (p_t^m - \sum_j \alpha_j q_{t,j}^m) + \sum_j \alpha_j q_{n,j}^m = p_n^m(\boldsymbol{\alpha}, \boldsymbol{E}), \tag{3.9}$$

where $\boldsymbol{\alpha}$ is the set of coefficients α_j $(j = 1, 2, ...J)$ and $\boldsymbol{E}$ is the set of chromaticity values E_n $(n = 1, 2, 3)$, and $p_n^m(\boldsymbol{\alpha}, \boldsymbol{E})$ is the parameterization of p_n^m. Then instead of minimizing Equation (3.5), it can be minimized by

$$G(\boldsymbol{\alpha}, \boldsymbol{E}) = \sum_m \sum_n \|p_n^m - \hat{p}_n^m(\boldsymbol{\alpha}, \boldsymbol{E})\|_2^2, \tag{3.10}$$

where $\hat{p}_n^m(\boldsymbol{\alpha}, \boldsymbol{E})$ is called the estimated parameterization of p_n^m. Equation (3.10) shows that coefficients $\boldsymbol{\alpha}$ and chromaticity $\boldsymbol{E}$ can be estimated in place of $\boldsymbol{s}$, $\boldsymbol{a}$, and $\boldsymbol{e}$.

The parameters $\boldsymbol{\alpha}$ and $\boldsymbol{E}$ need to be chosen to minimize the error function in Equation (3.10). Determining $\boldsymbol{\alpha}$ would allow for recovering the spectral reflectance $\boldsymbol{s}$ according to Equation (3.6). Finding $\boldsymbol{E}$ would provide us with the fluorescent chromaticity which will be used in later steps to determine the fluorescence spectral components.

A simple and effective method is proposed for estimating parameters $\boldsymbol{\alpha}$ and $\boldsymbol{E}$ using alternating iterations to converge upon a solution. The fluorescent chromaticity $\boldsymbol{E}$ is first initialized and denoted as $\hat{\boldsymbol{E}}$. A more detailed

discussion on the initialization of $\boldsymbol{E}$ can be found in Section 3.3.5. Then, $\boldsymbol{\alpha}$ is solved by

$$\hat{\boldsymbol{\alpha}} = \arg\min_{\boldsymbol{\alpha}} \sum_m \sum_n \|p_n^m - \hat{p}_n^m(\boldsymbol{\alpha}, \hat{\boldsymbol{E}})\|_2^2. \tag{3.11}$$

One way to solve Equation (3.11) is to find $\boldsymbol{\alpha}$ such that

$$\begin{aligned} p_n^m &= \hat{p}_n^m(\boldsymbol{\alpha}, \hat{\boldsymbol{E}}) \\ &= \hat{E}_n \sum_t (p_t^m - \sum_{j=1}^J \alpha_j q_{t,j}^m) + \sum_{j=1}^J \alpha_j q_{n,j}^m. \end{aligned} \tag{3.12}$$

Then rearranging terms in the equation,

$$y_n^m = \sum_j \alpha_j w_{n,j}^m, \tag{3.13}$$

where

$$\begin{aligned} y_n^m &= p_n^m - \hat{E}_n \sum_t p_t^m, \\ w_{n,j}^m &= q_{n,j}^m - \hat{E}_n \sum_t q_{t,j}^m. \end{aligned} \tag{3.14}$$

Equation (3.13) can be solved for all m and n in matrix form by finding the vector $\boldsymbol{\alpha} = [\alpha_1, ..., \alpha_J]^T$ such that

$$\boldsymbol{y} = \boldsymbol{W}\boldsymbol{\alpha}, \tag{3.15}$$

where $\boldsymbol{y} = [y_1^1, y_2^1, y_3^1, ..., y_1^M, y_2^M, y_3^M]^T$, is a $3M \times 1$ vector and $\boldsymbol{W}$ is a $3M \times J$ matrix where $\boldsymbol{W}_{3(m-1)+n,j} = w_{n,j}^m$.

In this system, there actually exist $2M$ independent equations because chromaticity is uniquely expressed in only 2 values. M is selected, such that $2M > J$, so the problem of estimating coefficients $\boldsymbol{\alpha}$ is over-determined. We adopted the constrained minimization method employed in Park *et al.* [PLGN07a] with a non-negative constraint on the reconstructed reflectance spectrum and use the second derivative of the reflectance spectrum with respect to λ as a smoothness constraint,

$$\begin{aligned} \hat{\boldsymbol{\alpha}} = &\arg\min_{\hat{\alpha}} \left\{ \|\boldsymbol{y} - \boldsymbol{W}\boldsymbol{\alpha}\|_2^2 + \mu_r \int \left(\frac{\partial^2 s(\lambda)}{\partial \lambda^2} \right)^2 \mathrm{d}\lambda \right\}, \\ &s.t. \quad \boldsymbol{B}\boldsymbol{\alpha} \geq 0 \quad \text{for all } \lambda, \end{aligned} \tag{3.16}$$

where μ_r is a weight for the constraint term. $\boldsymbol{B}$'s columns are the reflectance spectral basis vectors b_j.

Given the estimated $\boldsymbol{\alpha}$, $\boldsymbol{E}$ can be estimated by minimizing the same error function in Equation (3.10) with the constraint that $\sum_n^3 E_n = 1$, after several alternating iterations between estimating $\boldsymbol{\alpha}$ and $\boldsymbol{E}$, they converge upon a solution where $\boldsymbol{\alpha}$ and $\boldsymbol{E}$ are well estimated. With $\boldsymbol{\alpha}$ estimated, spectral reflectance $\boldsymbol{s}$ can be reconstructed by Equation (3.6).

3.3.3 Fluorescence Absorption Spectrum Recovery

Using the obtained spectral reflectance $\boldsymbol{s}$ and Equation (3.1), the appearance of the fluorescent component under the m-th illuminant is computed as $f_n^m = p_n^m - r_n^m$. This section describes how the fluorescence spectral components can be estimated given f_n^m.

Previous work has also shown that absorption spectra can be well represented by basis functions [LS13]. In the investigation, it has been found that a large collection of absorption spectra from the McNamara and Boswell Fluorescence Spectral Dataset [MGR+06] can be well represented using 9 principal components. In the proposed method, 9 principal components are employed to describe the fluorescent absorption spectrum, as shown in Figure 3.3(b). Thus the observed absorption spectrum can be expressed as a linear combination of basis vectors

$$a(\lambda) = \sum_{i=1}^{9} \beta_i v_i(\lambda), \tag{3.17}$$

where $v_i(\lambda)$ $(i = 1, \cdots, 9)$ is the i-th basis vector at wavelength λ and β_i is the corresponding coefficient. From Equations (1.5) and (3.17) the fluorescent component f_n^m can be described as

$$\begin{aligned} f_n^m &= D_n \sum_i \beta_m \int l_m(\lambda) v_i(\lambda) \mathrm{d}\lambda \\ &= D_n \sum_i \beta_m h_i^m \\ &= \gamma E_n \sum_i \beta_m h_i^m, \end{aligned} \tag{3.18}$$

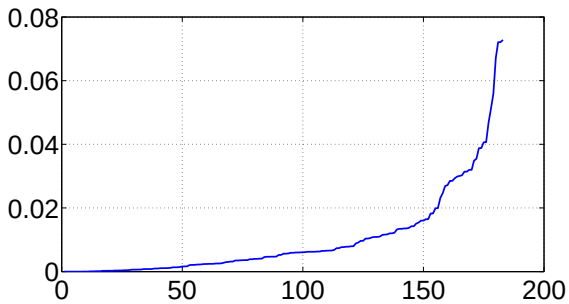

Figure 3.4: All test errors sorted in ascending order. 69% of cases were below the average error of 0.01.

where $h_i^m = \int l_m(\lambda) v_i(\lambda) \mathrm{d}\lambda$ and $\gamma = \sum_{t=1}^{3} D_t$.

E_n was determined from Section 3.3.2 so it can be used to recover the fluorescence absorption spectrum by estimating the coefficients β_i as

$$\hat{\boldsymbol{\beta}} = \arg\min_{\boldsymbol{\beta}} \sum_m \sum_n \| f_n^m - \gamma E_n \sum_i \beta_i h_i^m \|_2^2. \tag{3.19}$$

Similar to Equation (3.16), this is solved with a regularization term as

$$\begin{aligned} \hat{\boldsymbol{\beta}} = \arg\min & \left\{ \| \boldsymbol{f} - \boldsymbol{H}\boldsymbol{\beta} \|_2^2 + \mu_a \int \left(\frac{\partial^2 a(\lambda)}{\partial \lambda^2} \right)^2 \mathrm{d}\lambda \right\}, \\ s.t. \quad & \boldsymbol{V}\boldsymbol{\beta} \geq 0 \quad \text{for all } \lambda, \end{aligned} \tag{3.20}$$

where $\boldsymbol{f} = [f_1^1, \cdots, f_3^M]^T$, is a $3M \times 1$ vector, $\boldsymbol{\beta} = \gamma[\beta_1, \cdots, \beta_9]^T$ is a 9×1 coefficient vector, and $\boldsymbol{H}$ is a matrix where $\boldsymbol{H}_{3(m-1)+n,i}^m = h_i^m E_n$. $\boldsymbol{V}$ is a matrix whose columns are the absorption spectral basis vectors and γ is just a scale factor that does not affect the estimated shape of the fluorescence absorption spectrum. With the calculated results by Equation (3.20), the fluorescence absorption spectrum can be recovered by Equation (3.17).

3.3.4 Fluorescence Emission Spectrum Recovery

In this system, an RGB camera is used to capture the scene and only have 2 values for the fluorescent chromaticity $\boldsymbol{E}$ to recover the emission spectrum. Estimating an entire emission spectrum from only 2 values is a challenging problem but a data driven method is devised that is effective. I observe

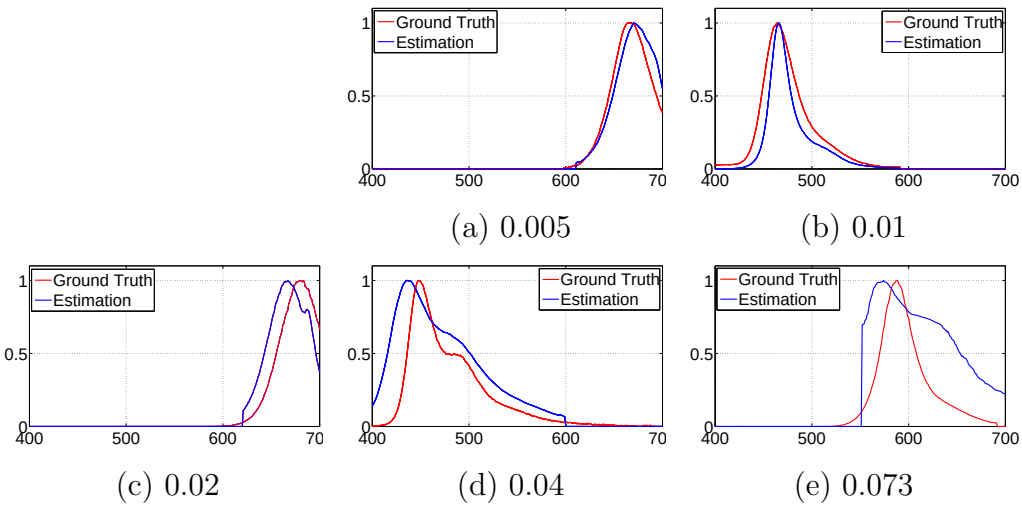

(a) 0.005 (b) 0.01

(c) 0.02 (d) 0.04 (e) 0.073

Figure 3.5: Examples of estimated emission spectra and their mean root square errors.

the emission spectra in the McNamara and Boswell Fluorescence Spectral Dataset, and find most of them have similar bell shapes (see Figure 3.5 for examples) but with different widths and peaks at different wavelengths, which is different from reflectance spectra that can be distributed over the entire visible spectrum (see Figure 3.8(a) for examples). Due to the restricted types of shapes exhibited by emission spectra, I have found that similar emission chromaticities generally map to similar emission spectra. This is because these restricted types of shapes reduce the possibility of metamerism between the fluorescent chromaticities and emission spectra.

This makes it possible to determine the corresponding emission spectrum to a given fluorescent chromaticity by performing a simple procedure. The known camera spectral sensitivity is used and integrated with each fluorescence emission spectrum in the dataset to obtain the corresponding chromaticity for each fluorescence emission. Then, the estimated fluorescent chromaticity $\boldsymbol{E}$ is compared with the fluorescent chromaticities from the dataset. The dataset emission spectrum's chromaticity with the lowest sum square error to the estimated fluorescent chromaticity $\boldsymbol{E}$ is then chosen as $\boldsymbol{E}$'s emission spectrum.

To test the effectiveness of the proposed method, tests are conducted

on the McNamara and Boswell Fluorescence Spectral Dataset. A subset of materials is first chose such that the emission and absorption spectra were both present in the visible spectrum (400 - 700 nm).[1] This resulted in a collection of 183 materials. Then proposed method is then tested by using leave-one-out cross-validation on the 183 emission spectra. In each case, the error between the estimated emission spectrum and its ground truth was computed using the mean root square error, $\sqrt{\sum_\lambda (e^{gt}(\lambda) - e^{es}(\lambda))^2}/d$, where d is the length of the visible spectrum, $e^{gt}(\lambda)$ is the ground truth emission spectrum and $e^{es}(\lambda)$ is the estimated emission spectrum. Before computing the errors, the estimation and ground truth were also normalized for scale by setting the maximum value of each emission spectrum to be 1.

In the results, the average error is 0.01. See Figure 3.4 for a plot of all the errors for the 183 estimated emission spectra. It is found that 69% of cases were below the average error of 0.01. Thus the results indicate that the majority of materials fit the assumption and emission spectra are accurately estimated as can be seen in Figure 3.5. In the 183 materials, 96% of the cases had an error of less than 0.04. It can be seen from Figure 3.5(d) that an error of 0.04 is quite reasonable. The worst case error is also shown in Figure 3.5(e). These results show that there were some high error cases that violated the assumption but these only constituted a small set.

3.3.5 Fluorescent Chromaticity Initialization

Equation (3.4) is a nonconvex function due to bilinear correlation between the reflectance spectrum $\boldsymbol{s}$ and fluorescent chromaticity $\boldsymbol{E}$. In practice, a standard alternating minimization scheme is used to solve this problem as described in Section 3.3.2. To estimate the reflectance spectrum, it is necessary to initialize the chromaticity $\boldsymbol{E}$ of the fluorescent component first.

To demonstrate the effectiveness of this alternating minimization scheme for the proposed method, the proposed method is tested under different possible initialization values for $\boldsymbol{E}$ by exhaustively trying different values for

[1] This subset is chosen because the experimental setup is currently focused on imaging in the visible spectrum. Although conceptually, the proposed method would extend to non-visible wavelengths as well.

Table 3.1: Average and standard deviations of the converged upon estimated chromaticities under all 66 initializations of $\boldsymbol{E}$ are shown in the second and third columns. The 66 initializations are densely and uniformly distributed in the space of possible initializations of $\boldsymbol{E}$. The low standard deviations indicate our estimation method is robust to different initializations of $\boldsymbol{E}$.

Sheets	Average Chromaticity	Standard Deviation	Ground Truth Truth
Pink	(0.61, 0.19)	(0.01, 0.00)	(0.61, 0.20)
Green	(0.15, 0.64)	(0.01, 0.02)	(0.16, 0.64)
Orange	(0.56, 0.32)	(0.02, 0.02)	(0.56, 0.31)
Red	(0.61, 0.21)	(0.00, 0.00)	(0.61, 0.20)
Yellow	(0.19, 0.62)	(0.01, 0.03)	(0.19, 0.62)

chromaticity and running the alternating iterations to see what kinds of chromaticity values would be converged upon. For the types of initializations tested, I choose a dense and uniformly distributed set of initializations for $\boldsymbol{E}$ from the space of possible chromaticities. For each channel n, the values of E_n is set from 0 to 1 in increments of 0.1 with the constraint that $E_1 + E_2 + E_3 = 1$. This amounted to 66 initializations[2] for the (E_1, E_2, E_3) values.

Table 3.1 shows average estimated chromaticities and their standard deviations for all 66 initializations for the 5 fluorescent sheets on the color wheel in Figure 3.2. The averages are shown in Table 3.1 to be close to the ground truth chromaticities. In addition, the standard deviations of the 66 initializations is very small for all the fluorescent sheets tested. This indicates that our estimation method is very robust to the choice of initialization values of $\boldsymbol{E}$.

[2]When E_1 is initialized to 0, E_2 will have 11 selections from 0 to 1 in 0.1 increments, E_3 will be $1 - E_1 - E_2$. When E_1 is initialized as 0.1, E_2^0 will have 10 selections from 0 to 0.9 in 0.1 increments, and so on. So there are $(11 + 10 + \cdots + 1) = 66$ possible initializations.

3.3.6 Summary of the Algorithm

I exploit the unique property of fluorescence that the chromaticity of fluorescent emissions are invariant under different illuminants to simplify our optimization in Equation (3.4) into 3 sub-problems: reflectance spectrum $\boldsymbol{s}$ recovery, fluorescence absorption spectrum $\boldsymbol{a}$ recovery, and fluorescence emission spectrum $\boldsymbol{e}$ recovery. However, the optimization problem in Equation (3.10) for reflectance spectrum $\boldsymbol{s}$ recovery is also challenging due to its nonconvexity from the bilinear correlation between $\boldsymbol{s}$ and $\boldsymbol{E}$. The global minimum for Equation (3.10) can be found via a two-dimensional exhaustive search but this would be extremely slow. Meanwhile, using certain local optimization methods would require a reasonable initialization. In practice, Equation (3.10) is minimized via a standard alternating minimization scheme with an initialized fluorescent chromaticity $\boldsymbol{E}$. In Section 3.3.5, the standard deviations of the recovered fluorescent chromaticities $\boldsymbol{E}$ under different initializations are very small for all the fluorescent sheets tested, which show that the proposed method converges well under different initializations and tends to avoid local minima.

In practice, the maximum number of iterations for the alternating minimization procedure was chosen to be 10 in all experiments. The fluorescent chromaticities $\boldsymbol{E}$ are exhaustively initialize by using the 66 possible settings and choose the one that minimizes $\sum_n \sum_m \|p_n^m - p_n^m(\boldsymbol{r}, \boldsymbol{E})\|$ as the estimated result for each pixel. The proposed method can be seen in Algorithm 1.

3.4 Results and Analysis

The performance of the proposed method was tested by using images taken by a CCD camera (SONY DXC-9000) under varied illuminants. The camera spectral sensitivity is shown in Figure 3.6. The types of illuminants used were 9 colored lights ranging from blue to red in the visible spectrum as shown in Figure 3.7(a), which were produced by a Nikon Equalized Light Source (ELS) in the experiments. The camera spectral sensitivity and the illuminant spectra were both calibrated in advance.

Algorithm 1: Reflectance, fluorescence absorption and emission spectra estimation

Input : Images captured under varied illuminants

Output: Recovered reflectance, fluorescence absorption and emission spectra for all pixels

```
for t = 1, 2, ··· , T do
    Set the fluorescent chromaticity E to the t^th initialization;
    for h = 1, 2, ··· , H do
        Estimate the reflectance spectrum s via Equations (3.16) and (3.6);
        Update the chromaticity of the fluorescent component E;
    end
    Estimate the absorption spectrum a via Equations (3.20) and (3.17);
end
Select the best estimated s, a and E, to minimize Equation (3.4) from all T estimations;
Estimate the emission spectrum e by the fluorescent chromaticity E according to Section 3.3.4.
```

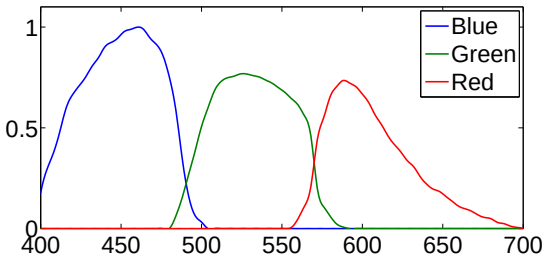

Figure 3.6: Camera spectral sensitivity used in the experiments.

3.4.1 Recovery of Spectra

The accuracy of the recovered spectral reflectance and fluorescence absorption and emission spectra is first evaluated on all 5 fluorescent sheets of the color wheel of Figure 3.2. The ground truth spectra of all these fluorescent sheets are captured by using the method described in Section 1.1.2. Figure 3.8 shows the recovered spectral reflectance and fluorescence absorption and emission spectra of all 5 fluorescent sheets. Compared with the ground truth, the recovered spectral reflectance (Figure 3.8(a)), absorption spectra (Figure 3.8(b)) and emission spectra (Figure 3.8(c)) of all fluorescent sheets approximate the ground truth well. All these results demonstrate that the proposed method can effectively recover spectral reflectance and fluorescence absorption and emission spectra by only using an RGB camera under multiple illuminations.

The proposed method is also compared against state-of-art work [FLS+13], which requires a hyperspectral camera and specialized illuminants. To allow for the fairest comparison under ideal conditions for both methods, synthetic tests are performed. In Figure 3.9, the proposed method and [FLS+13] both approximate the ground truth well. It shows that the proposed method can achieve competitive results with [FLS+13] and effectively recover all spectra for reflective-fluorescent scenes by using lower costing equipment.

Table 3.2: The errors between the ground truth and the relit results. "R Only" means only reflectance was considered. The "R+F" means reflectance and fluorescence were considered. "R+F 1", "R+F 2", "R+F 3" and "R+F 4" are the errors between the ground truth and the relighting results under different initialized fluorescent chromaticities, which are respectively, the exhaustive 66 initializations, the image captured under near UV light, average image from input 9 images, and the flat chromaticity $(1/3, 1/3, 1/3)$ for the R, G, and B Channels. "Max" and "Min" correspond to the maximum and minimum errors under 5 different illuminants, respectively .

Scene	R Only		R+F 1		R+F 2	
	Min	Max	Min	Max	Min	Max
Color Wheel	0.3434	0.4696	0.0265	0.0404	0.0273	0.0481
Duck	0.3858	0.5739	0.0216	0.0489	0.0238	0.0552
Cup	0.2286	0.3007	0.0220	0.0330	0.0288	0.0371
Train	0.3336	0.6381	0.0333	0.0670	0.0362	0.0679
Gun	0.3411	0.6376	0.0283	0.0522	0.0302	0.0543
Scene	R+F 3		R+F 4			
	Min	Max	Min	Max		
Color Wheel	0.0290	0.0502	0.0268	0.0490		
Duck	0.0240	0.0501	0.0222	0.0513		
Cup	0.0220	0.0372	0.0222	0.0379		
Train	0.0347	0.0672	0.0344	0.0682		
Gun	0.0300	0.0571	0.0298	0.0547		

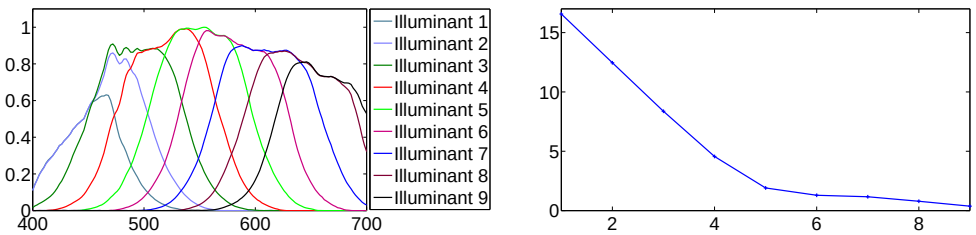

(a) 9 Illuminations (b) Singular Values

Figure 3.7: The spectra of the 9 colored illuminants and corresponding singular values.

3.4.2 Relighting Results

Since the proposed method is able to recover the full spectral reflectance, fluorescence absorption, and fluorescence emission spectra for an entire reflective-fluorescent scene, the scenes can be separated into reflective and fluorescent components, and relit for different illuminations, as shown in Figures 3.10-3.14.

Figure 3.10 shows the separation of reflectance and fluorescence for a reflective-fluorescent scene as well as relighting results with different initializations of the fluorescent chromaticity. In Figures 3.10(c) and (e), the recovered reflective and fluorescent components. In the scene, the notebook on the left only has ordinary reflectance so its colors in the recovered reflective component (Figure 3.10(c)) are the same as those seen under white light (Figure 3.10(a)).

The ground truth for the color wheel scene under the 5 illuminants can be seen in Figure 3.10(f) and the corresponding relighting results (Figure 3.10(f) (h) (j) and (l)) are rendered by the recovered spectra $\boldsymbol{s}$, $\boldsymbol{a}$, and $\boldsymbol{e}$ under different initialization conditions for fluorescent chromaticities $\boldsymbol{E}$. Figure 3.10(f) shows the best results for each pixel chosen from the the 66 possible initializations described in the exhaustive tests in Section 3.3.5. It can be seen that these relighting results (Figure 3.10(f)) approximate the ground truth well (Figure 3.10(b)).

To further demonstrate that the proposed method is robust to the fluorescent chromaticity initializations, the relighting results (Figure 3.10(h) (j) and (l)) are shown under 3 other initialized fluorescent chromaticities, which

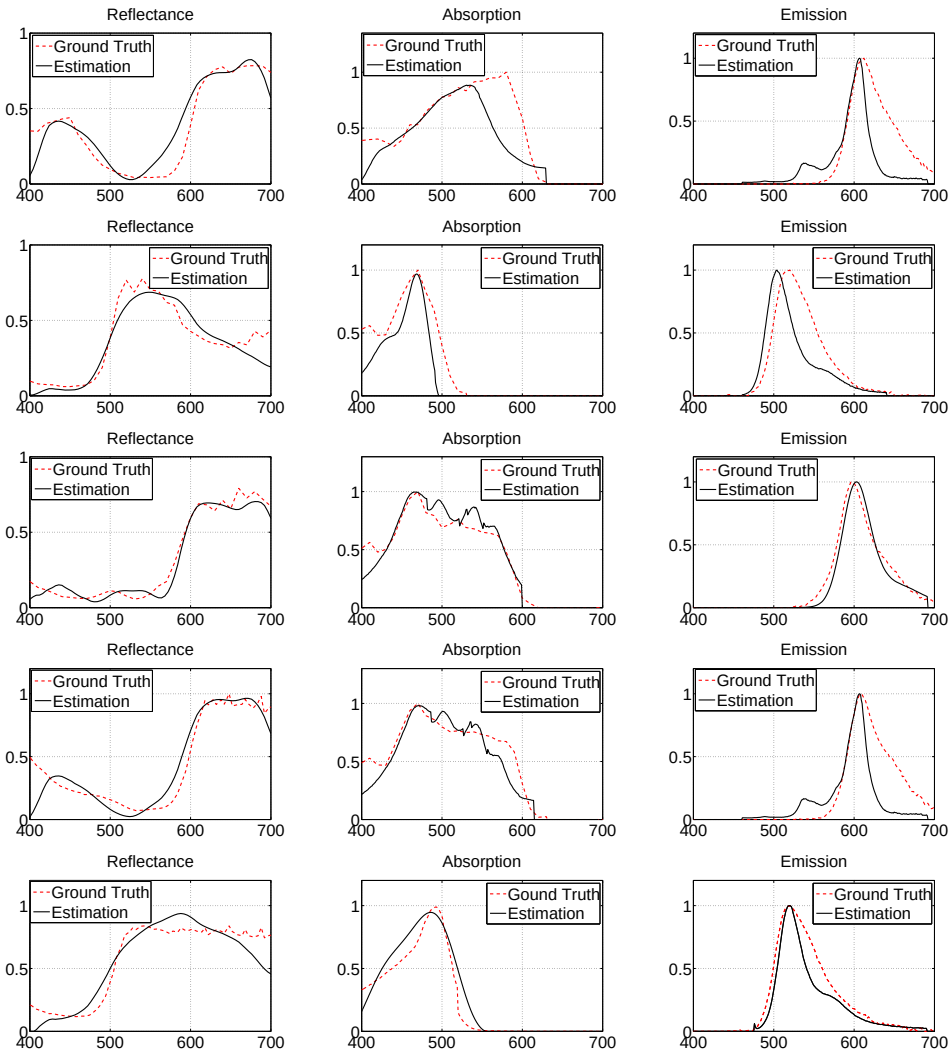

(a) Recovered $r(\lambda)$ (b) Recovered $a(\lambda)$ (c) Recovered $e(\lambda)$

Figure 3.8: Recovered reflectance $r(\lambda)$, fluorescence absorption $a(\lambda)$ and emission $e(\lambda)$ spectra of the 5 fluorescent sheets in the color wheel of Figure 3.2. The recovered results for 5 fluorescent sheets from top to bottom in the color wheel are shown from in the rows from top to bottom.

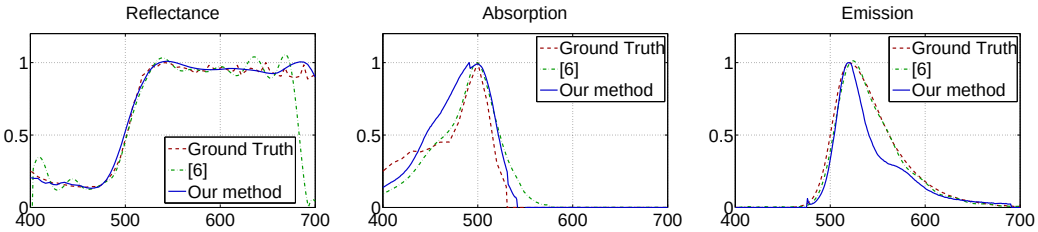

(a) Recovered $r(\lambda)$ (b) Recovered $a(\lambda)$ (c) Recovered $e(\lambda)$

Figure 3.9: Comparison between [FLS+13] and the proposed method using synthetic data.

are the image captured under near UV light (Figure 3.10(g), it is a close approximation to observing the ground truth chromaticity), average image from the 9 input color images (Figure 3.10(i), it is similar to the image captured under white light), and the flat chromaticity $(1/3, 1/3, 1/3)$ for the R, G, and B channels (Figure 3.10(k)), respectively. These relighting results (Figure 3.10 (h) (j) and (l)) are close to the ground truth (Figure 3.10(b)). In fact, all the visual relighting results (Figure 3.10(f) (h) (j) and (l)) are virtually indistinguishable and match the ground truth well.

When the scene is relit without considering fluorescent effects in the scene (Figure 3.10(g)), this leads to many fluorescent materials appearing as black, especially under blue-green light (the first column in Figure 3.10(g)). For the parts of the image that are not black, it is only observed the colors that are present in the illuminant. For example, under blue-green light, Figure 3.10(g) only shows blue and green colors.

Figures 3.11-3.14 show additional separation of reflectance and fluorescence on 3 other fluorescent scenes and their relighting results. It is found all relighting results under different initializations to be nearly identical so the relighting results from the best estimated spectra under the 66 initializations for these 3 scenes are only shown. The relighting results were all close to the ground truth and the fluorescent parts were well separated from the reflective parts. For example, Figure 3.11 shows highly fluorescent objects such as the fluorescent pen at the bottom. In the reflectance only image (Figure 3.11(b)), those objects are very dark while they are very bright in the fluorescence only image (Figure 3.11(g)). Similar results can be observed from the other scenes. These additional results on real scenes show that the

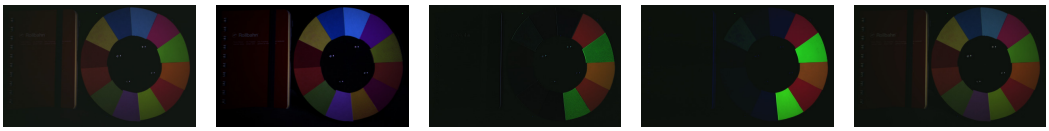

(a) White light (b) Reflectance (c) Fluorescence (d) Near UV Light (e) Average image

(f) Ground Truth

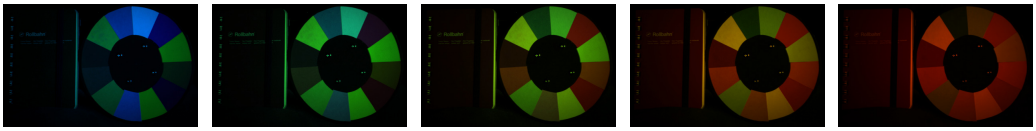

(g) Relit without Fluorescence

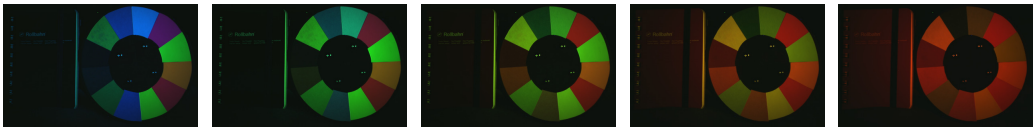

(h) Relit with Fluorescence (Best results from among the 66 initializations.)

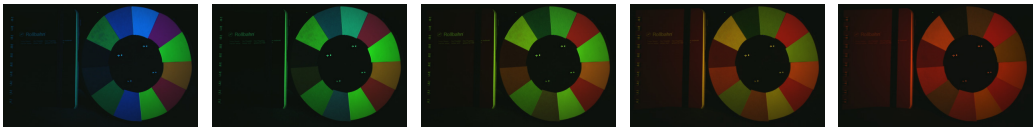

(i) Relit with Fluorescence (Image captured under near UV light as initialization.)

(j) Relit with Fluorescence (Average Image from M illuminants as initialization.)

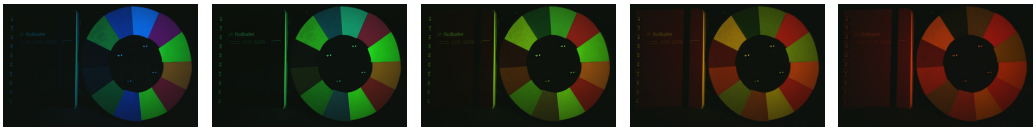

(k) Relit with Fluorescence (Chromaticities $(1/3, 1/3, 1/3)$ as initialization.)

Figure 3.10: Relighting results for the fluorescent color wheel.

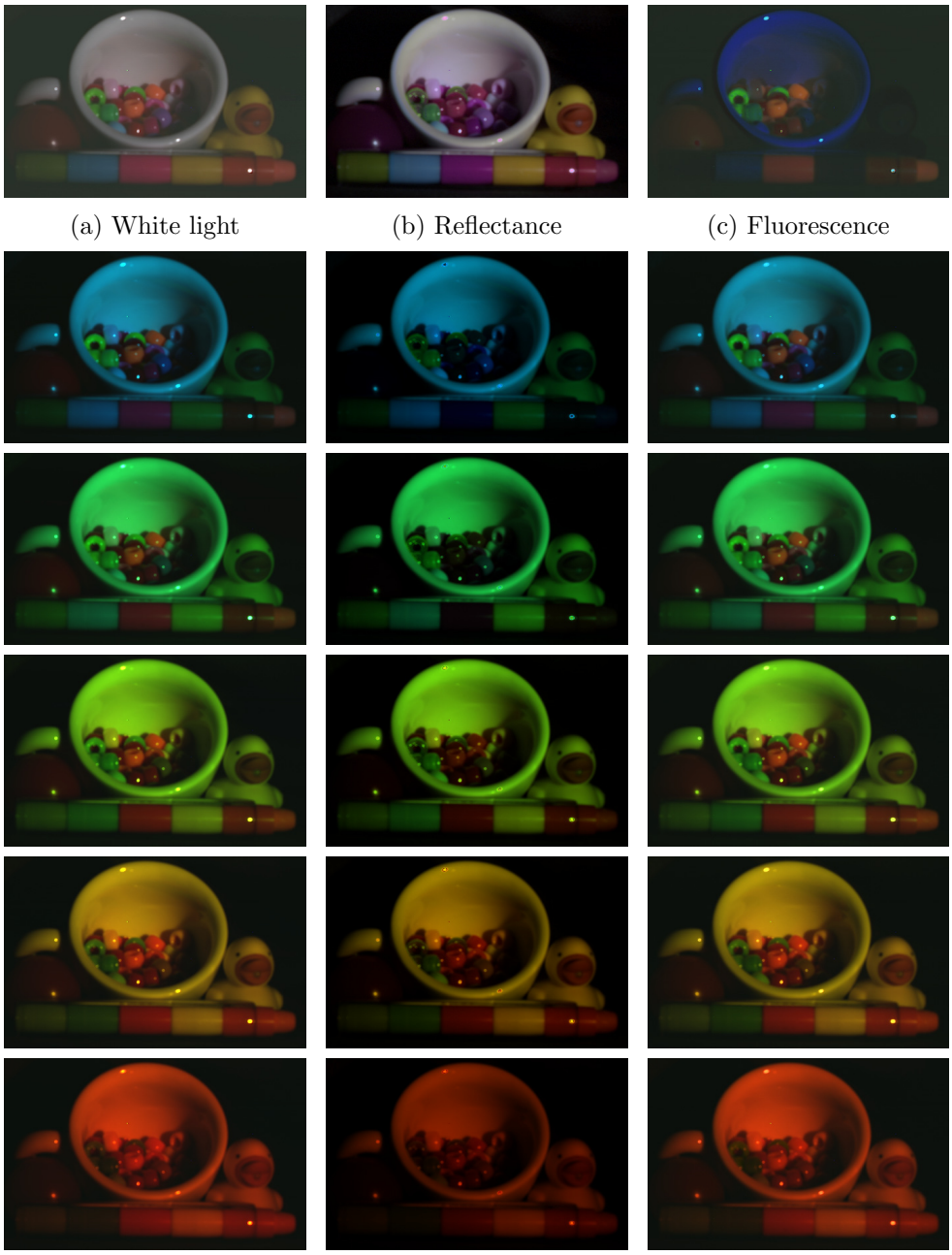

(a) White light (b) Reflectance (c) Fluorescence

(d) Ground Truth (e) Relit without Fluorescence (f) Relit with Fluorescence

Figure 3.11: Relighting results for the fluorescent cup scene.

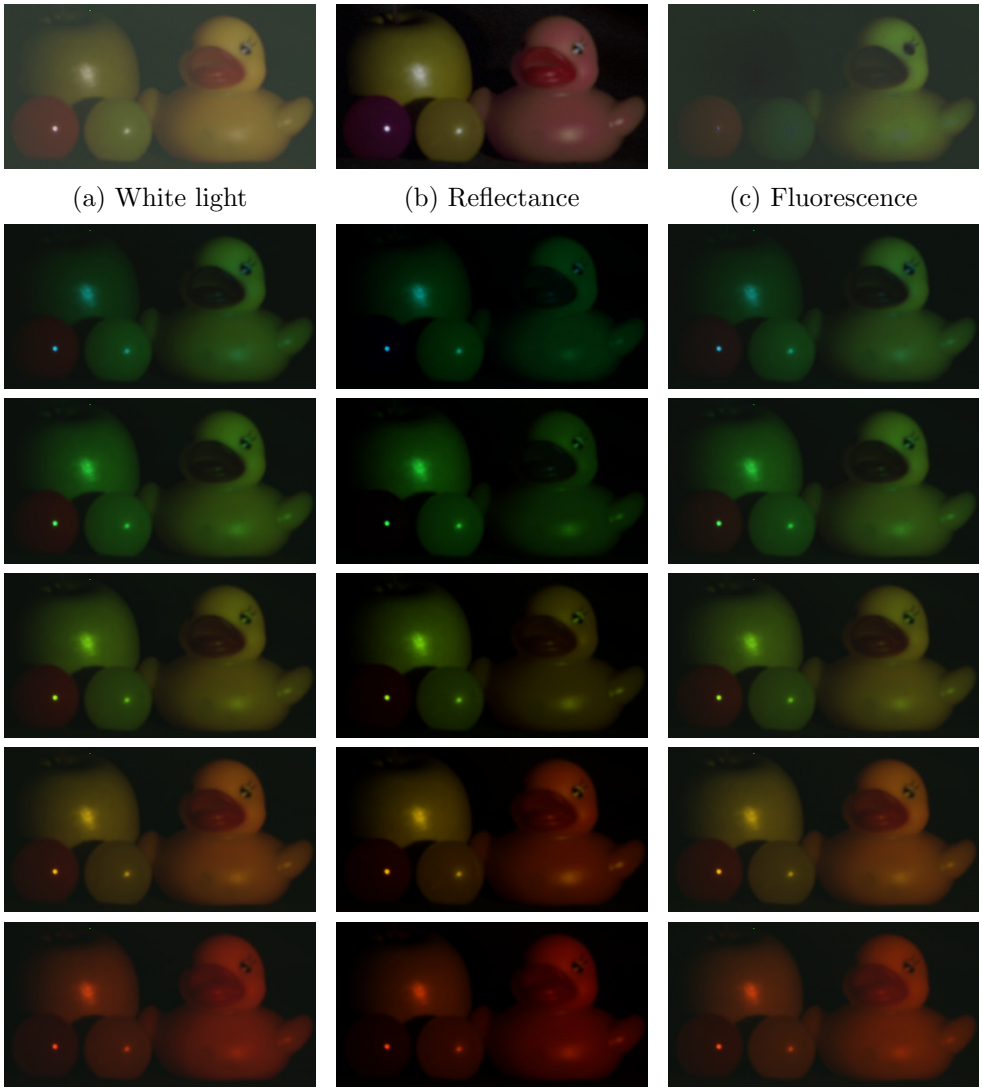

(a) White light (b) Reflectance (c) Fluorescence

(d) Ground truth (e) relit without fluorescence (f) relit with fluorescence

Figure 3.12: Relighting results for the fluorescent duck scene.

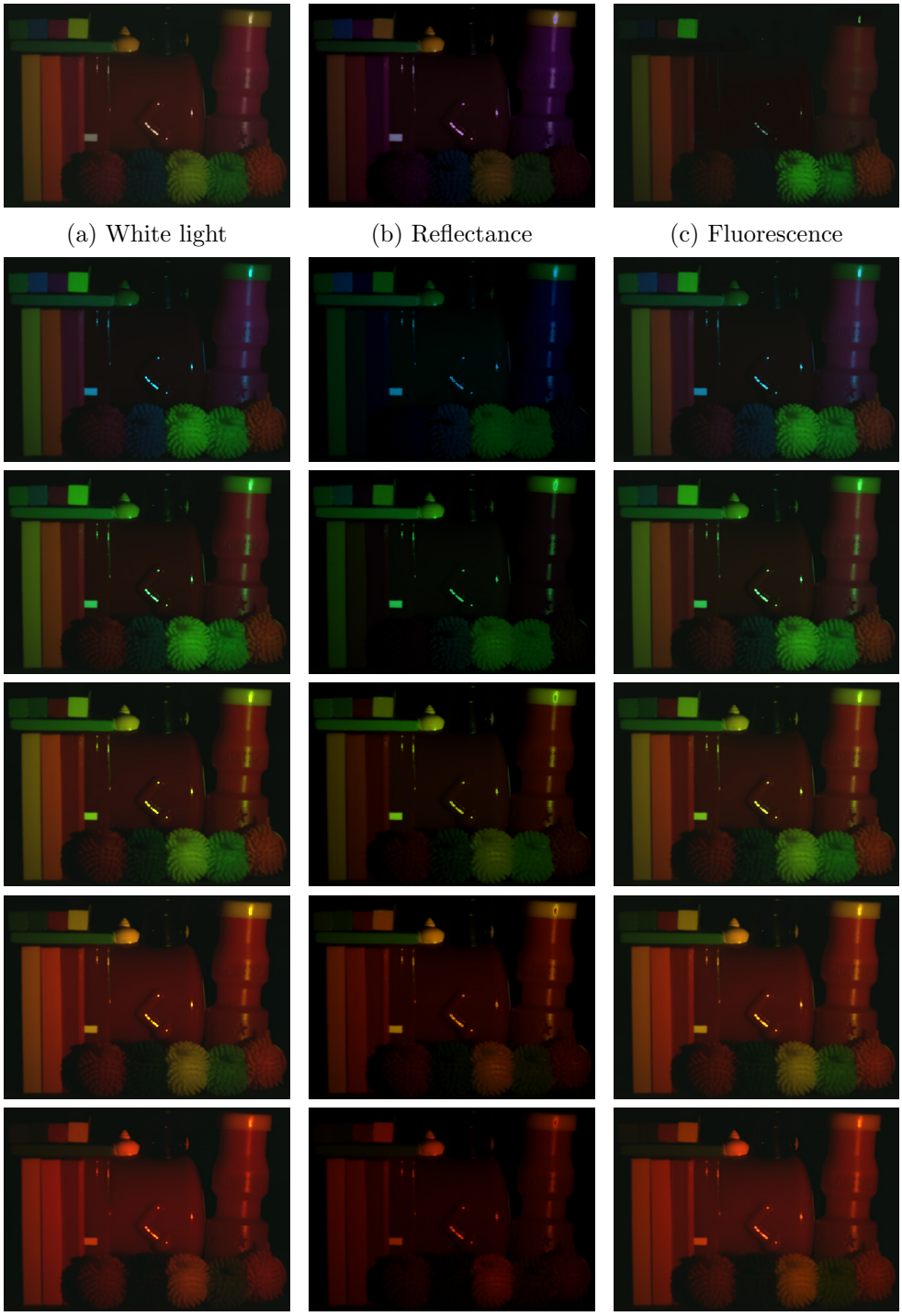

(a) White light (b) Reflectance (c) Fluorescence

(d) Ground Truth (e) Relit without Fluorescence (f) Relit with Fluorescence

Figure 3.13: Relighting results for the fluorescent train scene.

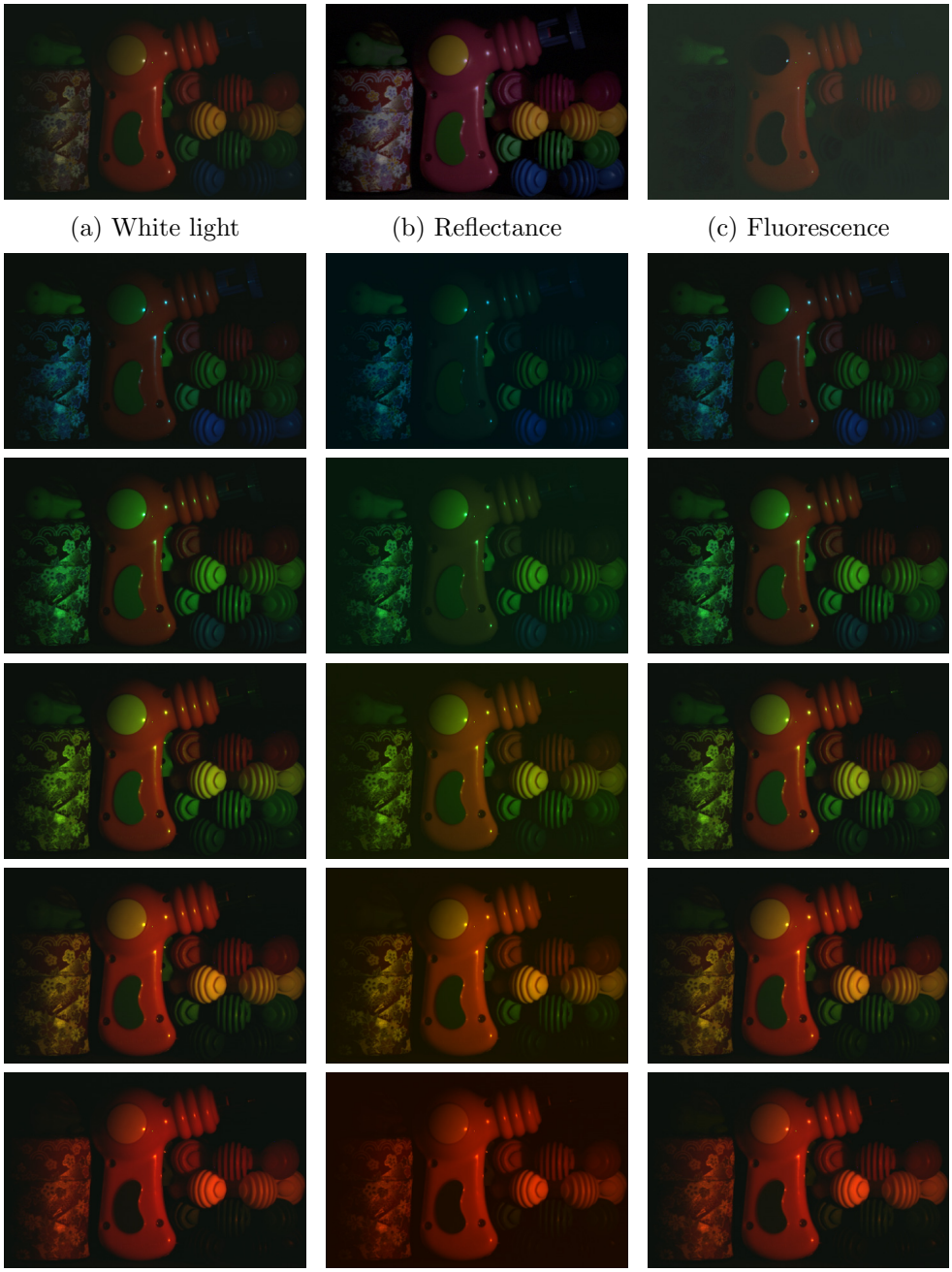

(a) White light (b) Reflectance (c) Fluorescence

(d) Ground Truth (e) Relit without Fluorescence (f) Relit with Fluorescence

Figure 3.14: Relighting results for the fluorescent toy gun scene.

proposed method is robust to different types of materials and initialization conditions in the optimization.

The errors are also quantitatively evaluated between the virtual relighting of all these 4 reflective-fluorescent scenes and their ground truth. Errors are computed between the ground truth and the relit results as

$$\sqrt{\sum_n (p_n^{gt} - p_n^{re})^2 / \sum_n (p_n^{gt})^2}. \tag{3.21}$$

where p_n^{gt} is the ground truth (corresponding images in Figures 3.10-3.14(f)) and p_n^{re} is the relighting result. Table 3.2 shows the maximum and minimum errors for 4 scenes under 5 illuminants and under different initializations. "R Only" means only reflectance was considered. The "R+F" means reflectance and fluorescence were both considered. "Max" and "Min" correspond to the maximum and minimum errors under the 5 different illuminants, respectively. "R+F 1", "R+F 2", "R+F 3" and "R+F 4" are the errors between the ground truth and the relighting results under different initialized fluorescent chromaticities, which are respectively, from the 66 possible initializations in the exhaustive test, the image captured under near UV light, average image from the 9 input images in the proposed method, and the flat chromaticity $(1/3, 1/3, 1/3)$ for R, G, and B channels. The errors are large when only reflectance is considered. When fluorescence is considered, the errors are small and show that the predicted colors are very close to their ground truth images. The errors for relighting results from the 4 fluorescent chromaticity initializations strategies are also very similar. The "R+F 1" with he best estimated spectra from the 66 initializations is only a little better than other results. This slightly better accuracy is visually indistinguishable in the relit images (Figure 3.10). These quantitative results reconfirm that our method is robust and converges well under different fluorescent chromaticity initializations.

3.5 Discussion on Illuminants

The illuminants used in the experiments can be produced by LEDs or other light sources. For testing purposes, a programmable light source (Nikon

ELS) is employed to produce the 9 colored lights in the experiments. To be effective, the light sources need to satisfy 2 conditions:

First, the spectra of all the illuminants should be linearly independent as images captured under linearly correlated illuminants cannot provide new information. In Equation (3.3), if the spectrum of one illuminant can be described as a linear combination of 2 other illuminants as

$$l_3(\lambda) = \tau_1 l_1(\lambda) + \tau_2 l_2(\lambda), \tag{3.22}$$

then substituting Equation (3.22) into Equation (3.3), the intensity for the nth channel of the reflective-fluorescent scene can be represented as

$$\begin{aligned} p_n^3 &= \int c_n(\lambda) l_3(\lambda) s(\lambda) \mathrm{d}\lambda \\ &+ \left(\int l_3(\lambda^{'}) a(\lambda^{'}) \mathrm{d}\lambda^{'} \right) \int c_n(\lambda) e(\lambda) \mathrm{d}\lambda \\ &= \int c_n(\lambda)(\tau_1 l_1(\lambda) + \tau_2 l_2(\lambda))(\lambda) s(\lambda) \mathrm{d}\lambda \\ &+ \left(\int (\tau_1 l_1(\lambda^{'}) + \tau_2 l_2(\lambda^{'})) a(\lambda^{'}) \mathrm{d}\lambda^{'} \right) \int c_n(\lambda) e(\lambda) \mathrm{d}\lambda \\ &= \tau_1 p_n^1 + \tau_1 p_n^2 \end{aligned} \tag{3.23}$$

This means that the image captured under illuminant l_3 can be expressed as a linear combination of the images captured under illuminants l_1 and l_2. The third image captured under l_3 would thus provide no additional information beyond that found in the images captured under under l_1 and l_2.

A second requirement is that the spectra of all illuminants combined should, as much as possible, uniformly cover the visible spectrum. If some range of wavelengths were not covered by any illuminants, it would affect the recovery of reflectance and absorption spectra in that range. This is because it is not known in advance where along the spectrum the fluorescence absorption spectra will be present. If the illuminants span the entire visible spectrum, it can be assured that the proposed method would be robust to different materials and their different spectra.

The 9 illuminants (Figure 3.7(a)) used in the experiments are evenly distributed in the spectral domain and cover all visible wavelength. The linear independence of these 9 illuminant spectra can be evaluated by their

singular values and condition number. Their singular values are shown in Figure 3.7(b) and their condition number is 44.57. The condition numbers of the W in Equation (3.16) and H in Equation (3.20) are 45.95 and 74.06 under these illuminants and using the RGB camera with spectral sensitivity shown in Figure 3.6, respectively. The closer the condition number is to 1, the stronger the linear independence. The results indicate that this level of linear independence of light sources is good enough to provide accurate estimation of reflectance and fluorescence absorption spectra.

In the experiments, the illuminants are produced by using a programmable light source. The proposed approach is also evaluated by performing an analysis using the spectra of off-the-shelf LEDs. In Figure 3.15, the spectra of these 9 off-the-shelf LED light sources and their corresponding singular values are shown. These light sources also satisfy the requirements for effective imaging of all spectral components. The condition number for these 9 illuminants is 9.50, which is much less than the 44.57 condition number of our original illuminants. The condition numbers of the W and H are 15.92 and 22.57 under these illuminants, respectively. The condition numbers of the W and H under the off-the-shelf LED light sources are also much lower than those of the original illuminants used in our experiments, so theory shows better experimental results can be obtained under these LEDs than with the illuminants produced by the programmable light source.

To evaluate the proposed method under the used illuminants and off-the-shelf LED light sources, one color from the 16 color patches on the Macbeth ColorChecker is first randomly selected as the reflectance spectrum. As for the absorption and emission pair, one pair from the fluorescence spectral dataset [MGR+06] from among the 183 materials is randomly selected. All spectra were normalized such that the maximum value was 1 for each spectrum. The proposed method is then simulated on these spectra under the used illuminants and the off-the-shelf LED light sources. After the simulation, the errors are calculated between the recovered spectra and the ground truth like in the Section 3.3.4. The mean errors for the recovered reflectance and fluorescence absorption spectra are 0.012 and 0.007 under the used illuminants, while the mean errors are 0.009 and 0.007 under off-the-shelf LED lights. The mean errors from using these two sets of illuminants are close.

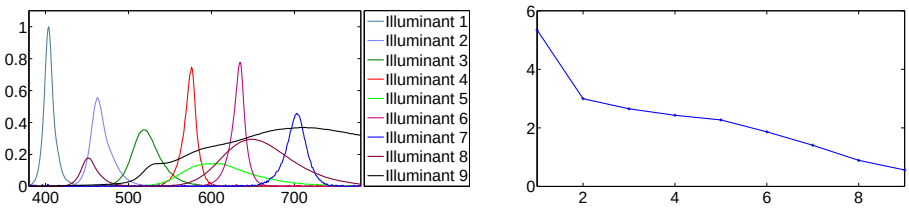

(a) 9 LED Light Sources (b) Singular Value

Figure 3.15: The spectra of off-the-shelf LED light sources and corresponding singular values.

Therefore, the proposed method can be directly applied using off-the-shelf light sources.

3.6 Summary

In this chapter, an effective method is presented to simultaneously recover the reflectance and fluorescence absorption and emission spectra of an entire scene by using RGB images under varied illuminants. Making use of the illuminant-invariant chromaticity of fluorescence, the proposed method is capable of estimating the reflectance spectrum and chromaticity of the fluorescent component. Moreover, the fluorescence absorption and emission spectra are estimated accurately by exploiting the basis representation of absorption spectra and a strong correlation between fluorescent chromaticity and emission spectra, respectively. The effectiveness of the proposed method was successfully demonstrated with experiments on real data taken under varied illuminants. In addition, the recovered spectra were used to accurately relight scenes.

There are still some limitations in the proposed method that are worth further investigation in the future. Estimating all three spectra from RGB values observed under different illuminants is a difficult task. To overcome these difficulties, 9 colored illuminants are employed in the proposed method. This is time consuming and makes it impractical to directly extend the proposed method to moving fluorescent scenes. To solve this problem, I will investigate how the constraints might be relaxed to reduce the number of required input images. In addition, a high speed camera is also used to capture

multiple images in a short amount of time. A dataset for emission spectra estimation is also required. One of the extensions of our approach will be to employ multi-channel cameras (e.g. 5 channels) with more narrow-band sensitivities and investigate how emission spectra can be estimated without relying on a dataset. Another issue is that the proposed method needs to be calibrated to the camera spectral sensitivity and the illuminant spectra in advance. There are existing methods that can be used to calibrate camera spectral sensitivity [HMS+12, JLGS13] and illuminants [JG12]. In the future, it is worth investigating how we can estimate all reflectance, absorption, and emission spectra under unknown camera spectral sensitivity or illuminant spectra by combining those existing methods as well as considering the fluorescent property for camera spectra sensitivity and illuminant recovery.

Chapter 4

Interreflection Removal Using Fluorescence

4.1 Overview

Interreflection is a global light transport process whereby light reflected from a surface point illuminates other points. In the presence of interreflections, an intensity observation of a scene consists of the directly reflected light rays after a single-bounce on a surface (direct component) and light rays that bounce off of the scene surface multiple times before they reach the camera (indirect component). Modeling and removing interreflections is of broad interest for making shape-from-intensity methods to work properly, because most of them are designed to take only the direct component as input.

Recent studies on this problem provide deeper understandings about the inverse light transport and show that the direct and indirect components can be separated for static scenes image [SMK05, NKGR06, LHY11]. In addition, some papers have tackled the problem for dynamic scenes but the capture process may require specialized masks [NKGR06, OMK14] or motion compensation [ANN13].

In this chapter, it is shown that separation can be achieved for dynamic scenes by capturing only a single image using *fluorescence* (see Fig. 4.1). Fluorescent materials[1] not only reflect incident light but also absorb and

[1]In practice, fluorescent materials show both ordinary reflection and fluorescent emis-

emit light at longer wavelengths [Lak06] (see Fig. 4.2). This physical property allows us to obtain single-shot images that contain reflective-only images at the same wavelength as the illuminant and wavelength-shifted images that are a mixture of fluorescent emission and interreflections of those emissions. This wavelength-shifted image is called a fluorescent-reflective image. These concepts are illustrated with an example. If a scene is illuminated by a blue light source, the reflective-only image is recorded in the blue channel, and the fluorescent-reflective image could be captured in the red channel (see Fig. 4.1). Interreflections still exist in both channels but using this bispectral measurement, a direct-indirect decomposition method is developed by deriving a new interreflection model for fluorescence and extending Liao *et al.* [LHY11] where they used varying light colors and multiple images. Unlike Liao *et al.*'s method, the proposed method only requires a single image with an assumption of commonly available fluorescent materials, which enables interreflection removal from a dynamic scene.

In summary, the main contributions are that we

- derive a general interreflection model for fluorescent materials,
- develop a method to separate direct-indirect components from reflective-only and fluorescent-reflective measurements, and
- show that a single-shot measurement is sufficient for the decomposition using fluorescence.

4.2 Related Work

Fluorescence Fluorescent analysis has received attention in recent years in computer vision. Examples of such work can be found in color rendering [JF99, WWLP06], reflectance and re-radiation modeling [HHA+10], camera spectral sensitivity estimation [HMS+12], 3D reconstruction [SOS12, TMMK12], immersion range scanning [HFI+08], and color relighting of real scenes [FLS+13, LS13]. In many of these methods, a phenomenon of fluorescence known as Stokes shift is exploited to achieve results. Specifically,

sion.

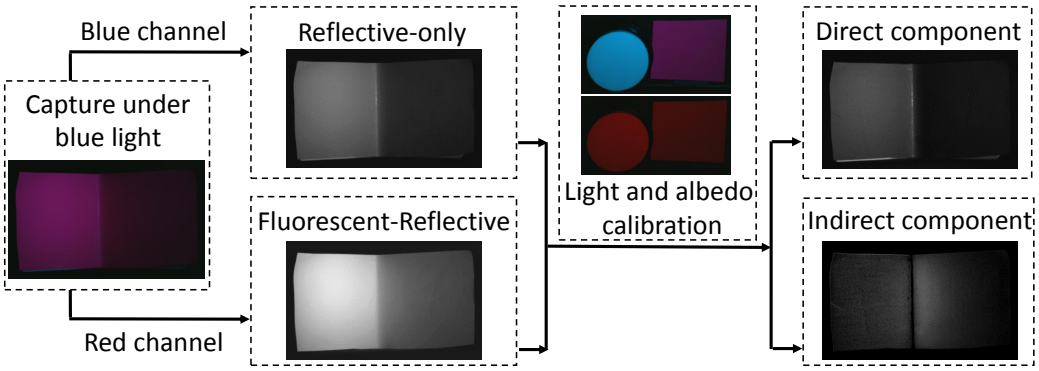

Figure 4.1: Overview of the proposed method. A fluorescent object is captured under blue light, whose blue channel is a reflective-only image and red channel is a wavelength-shifted fluorescent-reflective image. The lighting and albedo are calibrated by images of the flat white target and fluorescent sheet captured under blue and red light. After calibration, direct and indirect components can be recovered.

Stokes shift can be described simply as the absorption of light at shorter wavelengths and emission of light at longer wavelengths [Lak06]. The way this works is that when incident light hits a fluorescent surface, the surface's absorption spectrum will determine how much of the light is absorbed. Some of the absorbed energy is then released in the form of an emission spectrum at longer wavelengths than the incident light. The remainder of the absorbed energy is released as heat. In this chapter, I take advantage of Stokes shift to assist with interreflection removal.

Interreflection There have been a number of methods that analyze interreflection and demonstrate applications such as shape recovery. Koenderink and Doorn [Kv83] presented a general model for diffuse interreflections. Forsyth *et al.* [FZ90, FZ89] studied how interreflections affect shape recovery. Later, Nayar *et al.* [NIK91] addressed the interplay between interreflections and shape by iteratively refining the shape and reflectance of surfaces. They then extended their algorithm to colored and multi-colored surfaces [NG92].

Despite the effectiveness of past approaches such as [NIK91] and [NG92],

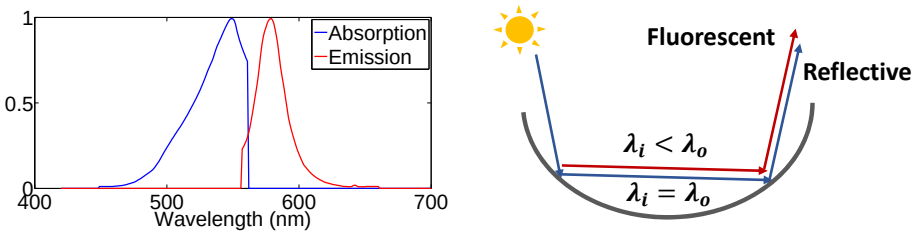

(a) (b)

Figure 4.2: (a) An example of absorption and emission spectra in the McNamara and Boswell fluorescence spectral dataset [MGR+06]. (b)When the fluorescent material is illuminated, it will reflect at the same wavelength and emit light at longer wavelengths.

the modeling and separation of interreflections is of broader interest because most shape-from-intensity methods assume only direct lighting. Thus solving the problem of separating out interreflections would allow for improving an entire body of methods in the literature. An early example of such work was presented by Funt *et al*. [FDH91, FD93] where the color different effect in interreflections was used to separate interreflections from direct lighting. Later, Seitz *et al*. [SMK05] proved the existence of an inverse light transport operator capable of separating m-bounced light from scenes with uniform albedo and Lambertian surfaces. However, their method requires a laser and scene capture is very time consuming. In addition, their method is not robust to complex shapes. Nayar *et al*. [NKGR06] were able to separate direct and global lighting components for complex scenes using spatially high frequency illumination. In principle, their method would be very fast but in practice, they require additional images or reduce the resolution.

More recently, Liao *et al*. [LHY11] removed interreflections by using spectrum-dependent albedo in scenes but their method still needs two images captured under different illuminations. In this chapter, we show that by exploiting properties of fluorescence, interreflections can be removed using only using one color image under one illumination. The proposed method also does not require a highly specialized setup and images can be captured using a standard RGB camera in a straightforward manner. This provides an advantage over other methods for interreflection removal on dynamic scenes

that need more specialized setups such as masks [NKGR06, OMK14] or motion compensation [ANN13]. Like Liao *et al.* [LHY11], the main drawback is that the object needs to be homogeneously colored with the reflective and fluorescent component. However, even when objects do not satisfy this condition, it is possible to color it using commonly available paint.

4.3 Bispectral Model for Interreflection Removal

In this section, the bispectral model for fluorescent materials is first introduced. I then briefly review the interreflection model for ordinary reflective materials with a uniform albedo and Lambertian surface and derive the interreflection model for fluorescence. After that, the model is proposed to separate direct and indirect lighting based on fluorescence. Finally, we describe the practical issues of lighting and albedo calibration.

4.3.1 Bispectral Model

In general, the appearance of fluorescent materials consists of both reflective and fluorescent components [SZ13]. If a Lambertian surface is assumed, the local reflection of the reflective component can be described as

$$E_r(x, \lambda) = \rho(x, \lambda) L(\lambda) \cos\theta, \tag{4.1}$$

where $\rho(x, \lambda)$ is the albedo of the surface point x at wavelength λ, $L(\lambda)$ is the incoming radiance from the light source, and θ is the angle between the surface normal and light source directions. In the following, $\rho(x, \lambda)$ is called as the *reflective albedo*.

Unlike the reflective component that reflects light rays at the same wavelength as the incident light, the fluorescent component absorbs and emits light at different wavelengths from the incident one [WWLP06, HHA+10, SZ13]. Another interesting property is that, as shown by Glassner [Gla95], fluorescence emissions have no directional characteristics and are uniformly radiated in all directions. In other words, fluorescence emissions behave like

light reflected from a Lambertian diffuse surface. Therefore, the outgoing radiance E_f from a fluorescent material under the light $L(\lambda_i)$ can be written as

$$E_f(x, \lambda_i, \lambda_o) = \eta(x, \lambda_i, \lambda_o) L(\lambda_i) \cos\theta, \tag{4.2}$$

where λ_i and λ_o represent the incident and outgoing wavelengths, respectively, and $\eta(x, \lambda_i, \lambda_o)$ is a direction-invariant function that describes the re-radiation property of the fluorescence. According to the characteristics of fluorescence [SZ13], $\eta(x, \lambda_i, \lambda_o)$ can be factored as

$$\eta(x, \lambda_i, \lambda_o) = \mu(x, \lambda_o) a(x, \lambda_i), \tag{4.3}$$

where $a(x, \lambda_i)$ and $\mu(x, \lambda_o)$ define the absorption and emission factors of the fluorescent material, respectively. In the following, we call $\mu(x, \lambda_o)$ the *fluorescent albedo*. The incoming radiance energy is absorbed by $a(x, \lambda_i)$ as $\int a(x, \lambda_i) L(\lambda_i) d\lambda_i$; therefore, Eq. (4.2) can be rewritten as

$$E_f(x, \lambda_o) = \mu(x, \lambda_o) \left(\int a(x, \lambda_i) L(\lambda_i) d\lambda_i \right) \cos\theta. \tag{4.4}$$

Finally, the observation $E(= E_r + E_f)$ becomes

$$\begin{aligned} E(x, \lambda_o) = \Big[& \rho(x, \lambda_o) L(\lambda_o) \delta(\lambda_i - \lambda_o) \\ & + \mu(x, \lambda_o) \int a(x, \lambda_i) L(\lambda_i) d\lambda_i \Big] \cos\theta, \end{aligned} \tag{4.5}$$

in which E_r and E_f are independently observed at two distinct wavelengths λ_i and λ_o, respectively. The delta function $\delta(\lambda_i - \lambda_o)$ is associated with the reflective component because an ordinary reflective component only reflects light at the same wavelength as its incident light ($\lambda_i = \lambda_o$).

4.3.2 Bispectral Interreflection Model

We briefly review the interreflection model for the ordinary reflective component on a Lambertian surface [Kv83] and extend the interreflection model for the fluorescent component.

Interreflection model for reflective component.

The interreflection geometry [Kv83] between points $x \in \mathbb{R}^3$ and $x' \in \mathbb{R}^3$ is described by a kernel K as

$$\begin{aligned} K(x, x') &= \frac{Pos[n(x)^T(x' - x)]Pos[n(x')^T(x - x')]}{\|x' - x\|^2}, \\ Pos[a] &= \frac{a + |a|}{2}, \end{aligned} \tag{4.6}$$

where $n(x) \in \mathbb{R}^3$ is the surface normal at point x. The outgoing radiance of the reflective component $I_r(x, \lambda)$ can be expressed as the sum of direct and indirect components as

$$\begin{aligned} I_r(x, \lambda) = &\frac{\rho(x, \lambda)}{\pi} P(x, \lambda) \\ &+ \frac{\rho(x, \lambda)}{\pi} \int K(x, x') I_r(x', \lambda) dx', \end{aligned} \tag{4.7}$$

where $P(x, \lambda)$ is the irradiance from the light source towards the surface point x at wavelength λ. By defining iterated kernels K_m as

$$\begin{aligned} K_1(x, x') &= \frac{K(x, x')}{\pi}, \\ K_m(x, x') &= \int \frac{K(x, y)}{\pi} K_{m-1}(y, x') dy \ (m > 1), \end{aligned} \tag{4.8}$$

Eq. (4.7) can be rewritten as the polynomial function of ρ as

$$\begin{aligned} I_r(x, \lambda) = &\rho(x, \lambda) \frac{P(x, \lambda)}{\pi} \\ &+ \sum_{m=2}^{\infty} \rho^m(x, \lambda) \int K_{m-1}(x, x') \frac{P(x', \lambda)}{\pi} dx'. \end{aligned} \tag{4.9}$$

By defining

$$\begin{aligned} R_1(x, \lambda) &= \frac{P(x, \lambda)}{\pi}, \\ R_m(x, \lambda) &= \int K_{m-1}(x, x') \frac{P(x', \lambda)}{\pi} dx' \quad (m > 1), \end{aligned} \tag{4.10}$$

Eq. (4.9) becomes

$$I_r(x, \lambda) = \sum_{m=1}^{\infty} \rho^m(x, \lambda) R_m(x, \lambda). \tag{4.11}$$

as described in [LHY11]. Interested readers can refer to [Kv83], [NIK91] and [LHY11] for more details.

Interreflection model for fluorescent component.

Analogous to interreflections of the reflective component, the direct component of the fluorescent component is

$$\mu(x, \lambda_o)\frac{\int a(x, \lambda_i)P(x, \lambda_i)d\lambda_i}{\pi}. \tag{4.12}$$

From Eq. (4.6), the interreflection geometry $K(x, x')$ is independent of the albedo of the objects and the energy absorbed from the light source. Also, the fluorescence emissions are typically not re-absorbed by the same fluorescent material again[2]; therefore, the interreflection of fluorescence emissions behaves like that of the reflective components except for the initial emission. Therefore, the second-bounce component can be written as

$$\mu(x, \lambda_o)\rho(x, \lambda_o)\int K_1(x, x')\frac{\int a(x', \lambda_i)P(x, \lambda_i)d\lambda_i}{\pi}dx', \tag{4.13}$$

where $\rho(x, \lambda_o)$ is the reflective albedo at the outgoing wavelength λ_o. The radiance of the fluorescent component at surface point x is, therefore represented as the sum of the direct component and interreflections as

$$\begin{aligned} I_f(x, \lambda_o) = \mu(x, \lambda_o)\frac{\int a(x, \lambda_i)P(x, \lambda_i)d\lambda_i}{\pi} + \\ \sum_{m=1}^{\infty}\mu(x, \lambda_o)\rho^m(x, \lambda_o)\int K_m(x, x')\frac{\int a(x', \lambda_i)P(x, \lambda_i)d\lambda_i}{\pi}dx'. \end{aligned} \tag{4.14}$$

By defining

$$\begin{aligned} F_1(x, \lambda_i) &= \frac{\int a(x, \lambda_i)P(x, \lambda_i)d\lambda_i}{\pi}, \\ F_m(x, \lambda_i) &= \int K_{m-1}(x, x')\frac{\int a(x', \lambda_i)P(x, \lambda_i)d\lambda_i}{\pi}dx', \ (m > 1), \end{aligned} \tag{4.15}$$

[2]The overlap between absorption and emission spectra is small. As a result, only a negligible amount of emitted light is re-absorbed.

the interreflection model for the fluorescent component can be written as

$$\begin{aligned} I_f(x, \lambda_o) &= \mu(x, \lambda_o) F_1(x, \lambda_o) \\ &\quad + \sum_{m=1}^{\infty} \mu(x, \lambda_o) \rho^m(x, \lambda_o) F_{m+1}(x, \lambda_o). \end{aligned} \tag{4.16}$$

Unlike the conventional interreflection model for the reflective component (Eq. (4.11)), the derived model includes both fluorescent and reflective albedos at the outgoing wavelength λ_o.

4.3.3 Separation of Direct and Indirect Components

In theory, one would need an infinite-bounce model to fully describe interreflections. Fortunately, in practice, a 2-bounce model is sufficient for accurately modeling interreflections [FD93]. The attention is restricted to the 2-bounce case. If the reflective component is observed at the same wavelength ($\lambda_i = \lambda_o$) as the illumination,

$$I_r(x, \lambda_i) = \rho(x, \lambda_i) R_1(x, \lambda_i) + \rho^2(x, \lambda_i) R_2(x, \lambda_i). \tag{4.17}$$

The fluorescent component can be observed at a longer wavelength as

$$\begin{aligned} I_f(x, \lambda_i, \lambda_o) &= \mu(x, \lambda_o) F_1(x, \lambda_i) \\ &\quad + \mu(x, \lambda_o) \rho(x, \lambda_o) F_2(x, \lambda_i). \end{aligned} \tag{4.18}$$

For convenience, I remove λ_i and λ_o in all functions in Eqs. (4.17) and (4.18) and use ρ_1 and ρ_2 to represent the reflective albedo at incident wavelength λ_i and outgoing wavelength λ_o, respectively. It is also assumed that the scene consists of a uniform material, so the albedos $\rho(x)$ and $\mu(x)$ will be the same for all points x and can be represented as ρ and μ. Therefore, Eqs. (4.17) and (4.18) can be rewritten as

$$\begin{aligned} I_r(x) &= \rho_1 R_1(x) + \rho_1^2 R_2(x), \\ I_f(x) &= \mu F_1(x) + \mu \rho_2 F_2(x). \end{aligned} \tag{4.19}$$

As will be detailed in Sec. 4.3.4, $P(x, \lambda_i) = \int a(x, \lambda_i) P(x, \lambda_i) d\lambda_i$ so $R_m(x) = F_m(x)$(m=1,2). Thus Eq. (4.19) can then be written as

$$\begin{bmatrix} I_r(x) \\ I_f(x) \end{bmatrix} = \begin{bmatrix} \rho_1 & \rho_1^2 \\ \mu & \mu\rho_2 \end{bmatrix} \begin{bmatrix} R_1(x) \\ R_2(x) \end{bmatrix}. \tag{4.20}$$

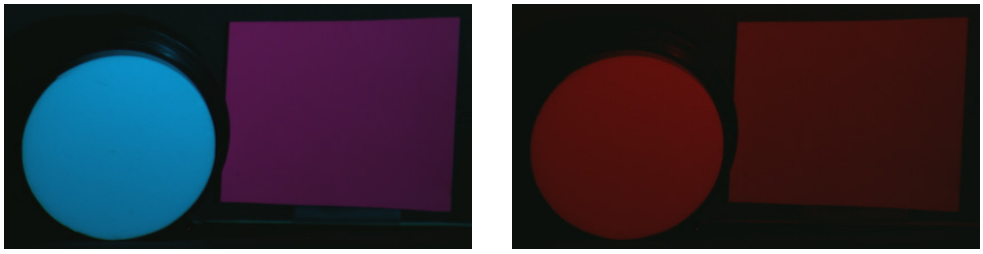

(a) Blue light (b) Red light

Figure 4.3: Lighting and albedo calibration.

It is later detailed how ρ_1, ρ_2 and μ can be determined but provided they are known, $R_1(x)$ and $R_2(x)$ can be solved in Eq. (4.20) by a matrix inverse. From this, $\rho_1 R_1(x)$ and $\mu R_1(x)$ would give us the direct component in the reflective and fluorescent parts respectively.

Compared with [LHY11], the proposed method requires one less image to capture. Since the 2-bounce model can accurately approximate interreflections in practice, the proposed method can remove interreflections only with a single image. As demonstrated in later in experiments, this allows the interreflection removal of a dynamic scene by the straightforward recording of a video using a standard RGB camera.

4.3.4 Lighting and Albedo Calibration

The equality $R_m(x) = F_m(x)$ holds only if $P(x, \lambda_i) = \int a(x, \lambda_i) P(x, \lambda_i) d\lambda_i$, which is not the general case. Furthermore, in order to solve Eq. (4.20), the value of the albedos are required. These will be addressed two issues in the following.

Light Intensity Calibration

As in Eq. (4.19), $R_m(x) = F_m(x)$ only when irradiance $P(x, \lambda_i)$ is equal to $A(x) = \int a(x, \lambda_i) P(x, \lambda_i) d\lambda_i$. To make these two values equal, it is necessary to calibrate the fluorescent absorption spectrum and control the light source carefully. This would be technically very challenging so a simpler calibration procedure is used. Let us assume $P(x, \lambda_i)$ is α times $A(x)$, then for every surface point x, the radiance $L(\lambda_i)$ from the light source for the

reflective component is also α times the absorbed energy $\int a(\lambda)L(\lambda_i)d\lambda_i$ for the fluorescent component with uniform albedo. That is,

$$\alpha = \frac{P(x,\lambda_i)}{\int a(x,\lambda_i)P(x,\lambda_i)d\lambda_i} = \frac{L(\lambda_i)}{\int a(\lambda_i)L(\lambda_i)d\lambda_i}. \tag{4.21}$$

Because of this relation, a single α for all points x can be calculated . As defined in Eqs. (4.10) and (4.15), $R_m(x)$ and $F_m(x)$ are linearly dependent on the irradiance $P(x,\lambda_i)$ and $\int a(x,\lambda_i)P(x,\lambda_i)d\lambda_i$, respectively:

$$R_1(x) = \alpha F_1(x), \text{ and } R_2(x) = \alpha F_2(x). \tag{4.22}$$

Therefore, Eq. (4.20) can be written as

$$\begin{cases} I_r(x) = \rho_1 R_1(x) + \rho_1^2 R_2(x) \\ I_f(x) = \frac{\mu}{\alpha}\left(R_1(x) + \rho_2 R_2(x)\right). \end{cases} \tag{4.23}$$

Albedo Ratio

With known reflective albedos ρ_1 and ρ_2 and fluorescent albedo μ discussed earlier, the direct and indirect lighting components can be solved. However, directly measuring these values is actually quite difficult. From from Eq. (4.1) and Eq. (4.4), reflective albedo ρ and fluorescent albedo μ can be described as

$$\begin{aligned} \rho(x,\lambda) &= \frac{E_r(x,\lambda)}{L(\lambda)\cos\theta}, \\ \mu(x,\lambda_o) &= \frac{E_f(x,\lambda_o)}{\left(\int a(x)L(\lambda_i)d\lambda_i\right)\cos\theta}. \end{aligned} \tag{4.24}$$

Determining the albedos from Eq. (4.24) is difficult because it is necessary to know θ, the angle between the incident light and the surface normal.

Fortunately, a simple calibration procedure can be used to obtain albedo ratios which would also be sufficient for the purposes[3]. If $\rho_1 R_1(x)$ and $\rho_1^2 R_2(x)$ are taken as the unknown variables, Eq. (4.20) can be reformulated as

$$\begin{bmatrix} I_r(x) \\ I_f(x) \end{bmatrix} = \begin{bmatrix} 1 & 1 \\ \frac{\mu}{\rho_1\alpha} & \frac{\mu}{\rho_1\alpha}\frac{\rho_2}{\rho_1} \end{bmatrix} \begin{bmatrix} \rho_1 R_1(x) \\ \rho_1^2 R_2(x) \end{bmatrix}. \tag{4.25}$$

[3]The scaled versions of R1 and R2 are solved but this is sufficient for analyzing direct and indirect lighting.

Then measuring the relative surface albedo for a point x as opposed to the absolute value of the albedo can be simply done with the following ratios derived from Eq. (4.24)

$$\frac{\mu}{\rho_1 \alpha} = \frac{E_f(x,\lambda)}{E_{r1}(x,\lambda)}, \quad \text{and} \quad \frac{\rho_2}{\rho_1} = \frac{E_{r2}(x,\lambda)}{E_{r1}(x,\lambda)} \frac{L_1(\lambda)}{L_2(\lambda)}, \tag{4.26}$$

where L_1 and L_2 are blue and red lights respectively[4].

In the calibration process, the objects used to compute the albedo ratios should be made of the same material as the object under consideration, as well as being flat or convex to avoid any interreflections. As shown in Fig. 4.3, flat fluorescent sheet and a spectrally flat white reflectance target are used to calibrate $\frac{\mu}{\rho_1 \alpha}$ and $\frac{\rho_2}{\rho_1}$. The scene is captured under blue and red light. $\frac{E_f}{E_{r1}}$ is the ratio of the intensity of the fluorescent sheet in the blue and red channels under the blue light. $\frac{E_{r2}}{E_{r1}}$ is the ratio of the intensity of the fluorescent sheet in the red channel under the red light and the blue channel under the blue light. $\frac{L_1}{L_2}$ is the ratio of the intensity of the white target in the blue channel under the blue light and the red channel under the red light.

So far, the possibility to make Eq. (4.25) work is based on the assumption that the surface reflective albedo cannot be constant across the entire spectrum ($\rho_1 \neq \rho_2$).

4.4 Experimental Results

The proposed method is tested on real fluorescent objects. To obtain both reflective and fluorescent components effectively, I used pink fluorescent objects where the reflective component is strong in the blue channel and the fluorescent emission is strong in red channel. Such color characteristics make reflective-only and fluorescent-reflective capture ideal for use with a standard RGB camera. In practice, capture with other colors can also be done but different light sources or camera filters would be needed to remove some wavelengths so that reflective-only and fluorescent-reflective images can be

[4]In the proposed method, L_1 should be in the short wavelength range, and L_2 should be the same appearance with the fluorescent emission spectrum so that it shows the spectral reflectance in the fluorescent emission area.

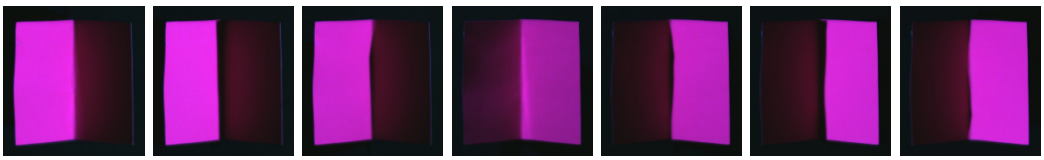

(a) Input color image

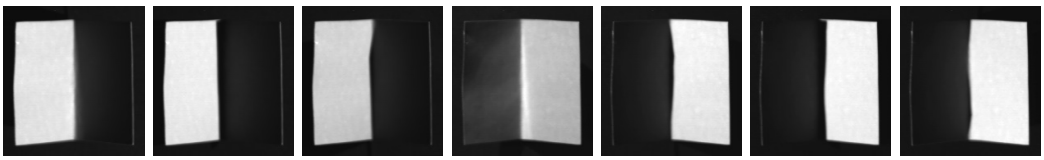

(b) Reflective-only

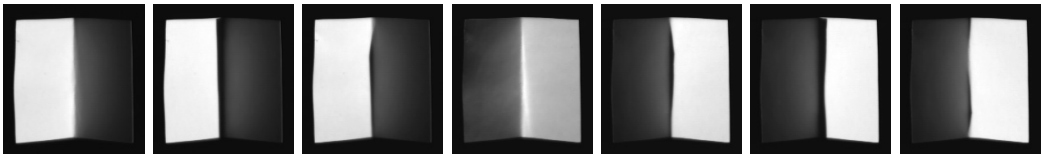

(c) Fluorescent-reflective

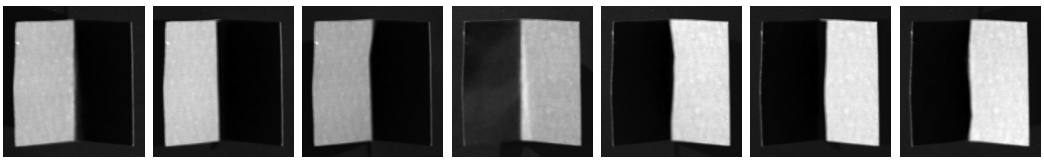

(d) Direct component

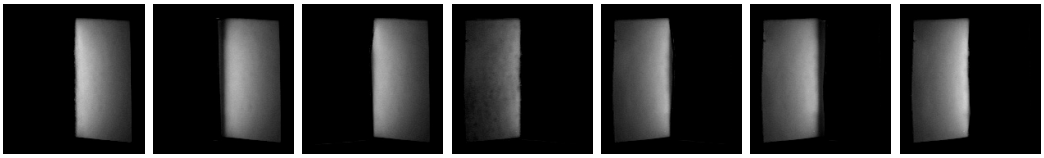

(e) Indirect component

Figure 4.4: Separation results for the v-shape. (a) The input image captured under blue light. (b) The reflective-only image from (a)'s blue channel. (c) The fluorescent-reflective image from (a)'s red channel. (d) The separated direct component. (e) The separated indirect component.

(a) Input color image

(b) Reflective-only

(c) Fluorescent-reflective

(d) Direct component

(e) Indirect component

Figure 4.5: Separation results for the moving fluorescent cloth. (a) The input image captured under blue light. (b) The reflective-only image from (a)'s blue channel. (c) The fluorescent-reflective image from (a)'s red channel. (d) The separated direct component. (e) The separated indirect component.

captured. The proposed method requires all surface points to exhibit the same color. In a real application, objects could be easily spray painted. The benefits of the proposed method's ability could then be got to separate direct and indirect components for moving objects. For the experiments, objects that naturally exhibit fluorescence and a leaf dish that was painted are used. These objects were all illuminated by blue light and captured in the blue and red channels of a CCD camera (SONY DXC-9000).

4.4.1 Separation Results

In this section, the results for the separation of direct and indirect components are shown. An overview of the entire process is first given. As shown in Fig. 4.1, an RGB image is first captured under blue light. Since the pink fluorescent color is used, the blue channel is a reflective-only image while the red channel is a fluorescent-reflective image. As described in Sec. 4.3.4, the lighting and albedo are then calibrated by images captured under blue and red light, where the calibration targets are both flat. After calibration, direct and indirect components are recovered by Eq. (4.25).

The first scene is a pink fluorescent v-shape object. The scene was first taken under blue light (Fig. 4.4 (a)). Its blue channel is then a reflective-only image (Fig. 4.4 (b)) and the red channel is a fluorescent-reflective image (Fig. 4.4 (c)). The lighting and albedo are calibrated by using the method in the previous section and found $\frac{\mu}{\rho_1 \alpha}$ and $\frac{\mu}{\rho_1 \alpha}\frac{\rho_2}{\rho_1}$ to be 1.10 and 2.07 for the pink fluorescent sheet, respectively. After calibration, the direct and indirect components were separated by Eq. (4.25) as shown in Fig. 4.4(d) and (e). In the figures, the indirect component has been scaled to $0 \sim 255$, for visualization purposes. It can be seen that when we light one side of the v-shape, the direct component is strong on one side while the indirect component is strong in other side. This observation fits our expectations of how interreflections would physically behave and demonstrates that the proposed method removes interreflection effectively.

As mentioned, the proposed method only requires a one-shot measurement to separate the direct and indirect component and so is applicable to dynamic scenes. In Fig. 4.5, seven successive video frames for a dynamic pink

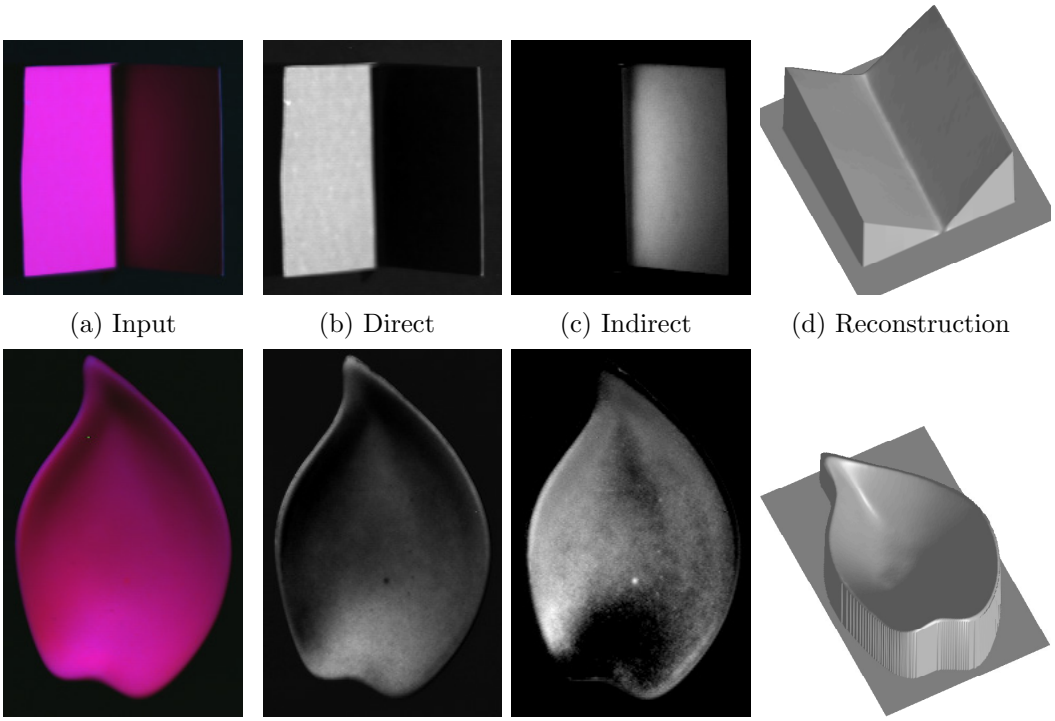

(a) Input (b) Direct (c) Indirect (d) Reconstruction

(e) Input (f) Direct (g) Indirect (h) Reconstruction

Figure 4.6: Reconstructed results for the fluorescent v-shape and leaf dish. (a)(e) One of the input images captured under the directional blue light. The corresponding separated direct and indirect components are shown (b)(f) and (c)(g). (d)(h) The recovered shape form the direct components.

fluorescent cloth are shown. The changing of direct and indirect components in Fig. 4.5 (d) and (e) as a result of the object's motion. The direct component is strong in the flat area (Fig. 4.5 (d)) and the indirect component is strong in the wrinkled area. As with the v-shape, these observations fit the expectations of how interreflections would physically behave and demonstrates the proposed method's effectiveness.

4.4.2 Photometric Stereo

To demonstrate a sample application and to further validate the separation results, the recovered direct component is used to perform photometric stereo [Woo80]. Photometric stereo also performs on reflective-only and

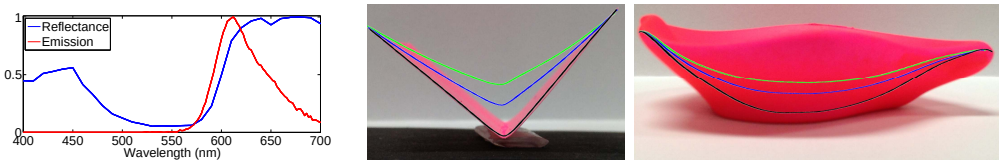

(a) (b) (c)

Figure 4.7: (a) The reflectance and emission spectra for the fluorescent pink sheet. (b) and (c) The cross-sectional view of recovered shapes from fluorescent-reflective images (green line), reflective-only images (blue line) and direct components (dark line) superimposed into the side view of the v-shape and leaf dish, respectively.

fluorescent-reflective images and show the recovered direct component provides the best results. In the experiments, for each object, 12 images were captured with the object illuminated from different light source directions. The light source was about 1 m away from the object, which was $4 \sim 10$ cm in diameter.

The proposed method is tested on the pink fluorescent v-shape sheet and a "leaf dish". Fig. 4.6 shows one of the input images and the corresponding separated direct and indirect components. The surface normals were recovered by photometric stereo and the shape was integrated from the normal map. Fig. 4.6(d)(h) show the recovered shapes by using the recovered direct components.

In [NIK91], Nayar *et al.* showed that interreflections cause recovered shapes to be shallow. The improvement in using the interreflection removal method is quantitatively shown by comparing against recovered shape depths from using the reflective-only images and fluorescent-reflective images as inputs to photometric stereo.

The shape recovered from the fluorescent-reflective images (Fig. 4.7(b) green line) is more shallow than that from the reflective-only images(Fig. 4.7(b) blue line). This is because the reflectance spectrum is stronger in the red channel than in the blue channel (Fig. 4.7(a)). Recall that the fluorescent indirect component shown in Eq. (4.25), $\frac{\mu}{\rho_1 \alpha}\frac{\rho_2}{\rho_1} = 2.07$ is greater than the reflective indirect component which is 1. Thus the indirect component $2.07\rho_1^2 R_2(x)$ in the fluorescent-reflective images is stronger than the $\rho_1^2 R_2(x)$ in the reflective-only images. From Fig. 4.7(a), we also see that the spectral

reflectance has a strong overlap with the fluorescence emission spectrum. In the fluorescent photometric stereo work of [SOS12] and [TMMK12], they both assume that spectral reflectance does not overlap with the fluorescent emission spectrum. This is not always the case and the proposed method addresses situations where spectral reflectance does overlap with the fluorescent emission spectrum.

Finally, the recovered shape from the direct component (Fig. 4.7(b) dark line) is deepest one, which indicates that the proposed method removes the indirect component effectively. The ground truth angle between the two sides for the v-shape is about 90 degrees. The recovered angles for the shape from the direct component, reflective-only and fluorescent-reflective cases are 91, 101 and 114 degrees, respectively. Thus the recovered direct component provided a result very close to the ground truth. Similar results can be seen for the leaf dish in Fig. 4.7(c).

4.5 Summary

A novel method is presented for separating direct and indirect components using the phenomenon of fluorescence. By exploiting Stokes shift, separated reflective and fluorescent components are able to be simultaneously observed in two channels of an RGB camera. While both channels still contained interreflections, a simple but effective decomposition method is devised for separating out interreflections. From this, a general interreflection model is derived for fluorescent materials and it is shown that a single shot measurement is sufficient for the decomposition. In contrast to existing methods, this single shot ability allowed for effective operation on complex dynamic scenes as demonstrated in the experiments. In addition, I showed that the proposed method's effective recovery of the direct component greatly improved an existing photometric stereo method. Although this is only demonstrated on the photometric stereo method, our method can be easily applied to any methods that assume direct lighting and a uniform Lambertian surface. In the future, I would like to explore the benefits of separating for dynamic scenes through applications such as dynamic color relighting.

Chapter 5

Conclusions

5.1 Summary

Fluorescence does frequently occur in many objects, such as natural gems and corals, fluorescent dyes used for clothing, and plant containing chlorophyll to name a few. In fact, Barnard shows that fluorescent surfaces are present in 20 of randomly constructed scenes. This is a significant proportion of scenes that have not been considered by past methods. Another important point is that reflective and fluorescent components behave very differently under different illuminants. Thus to accurately predict the color of objects, separate modeling of all spectral properties of both reflective and fluorescent components is essential. Specifically, when a reflective surface is illuminated by incident light, it reflects back light of the same wavelength. Fluorescent surfaces on the other hand, first absorb incident light and then emit at longer wavelengths. As the properties of fluorescence are very different from ordinary reflectance, neglecting fluorescence can result in completely incorrect color estimation. The goal of the research is to model the full spectral reflective and fluorescent components of an entire scene, and apply the fluorescence in our computer vision field.

Firstly, it is shown that the reflective and fluorescent spectra of a scene can be efficiently separated and measured through the use of high frequency illumination in the spectral domain. The proposed approach only assumes that the absorption spectrum of the fluorescent material is a smooth function

with respect to the frequency of the lighting in the spectral domain. With this assumption, it becomes possible to separate reflective and fluorescent components by just two hyperspectral images taken under a high frequency illumination pattern and its shifted version in the spectral domain. So the reflective and fluorescent emission spectra can then be fully recovered by the proposed separation method. In addition to recovering reflectance and fluorescent emission spectra, the observation is made that materials with similar emission spectra tend to have similar absorption spectra as well. Using this observation, a method is devised for taking the recovered emission spectra from high frequency lighting and estimate their corresponding absorption spectra.

Then, a more practical approach is proposed for hyperspectral imaging of reflective-fluorescent scenes using only a conventional RGB camera and varied colored illuminants. the proposed method takes as input RGB images under different lighting and effectively separates reflectance and fluorescence in the spectral domain. These separated results can then be used for tasks such as accurate color relighting of scenes under novel lighting. The key idea in the proposed approach is to exploit a unique property of fluorescence: the chromaticity of fluorescence emissions is invariant under different illuminants. Based on this property, we formulate a method that takes RGB images and performs pixel-wise estimation of spectral reflectance and fluorescent chromaticity. The method works by iteratively improving estimates of the spectral reflectance and fluorescent chromaticity in turn. The proposed method is robust to initialization conditions and converges onto accurate spectral reflectance and fluorescent chromaticity for real scenes. Then I propose methods for estimating the fluorescence absorption and emission spectra of the scene given the estimated spectral reflectance data and fluorescent chromaticities.

Finally, it is shown that separation of direct and indirect components can be achieved for dynamic scenes by capturing only a single image using fluorescence. Fluorescent materials not only reflect incident light but also absorb and emit light at longer wavelengths. This physical property allows us to obtain single-shot images that contain reflective-only images at the same wavelength as the illuminant and wavelength-shifted images that

are a mixture of fluorescent emission and interreflections of those emissions. Interreflections still exist in both channels by using this bispectral measurement. I derive a general interreflection model for fluorescent materials, develop a method to separate direct-indirect components from reflective-only and fluorescent-reflective measurements, and show that a single-shot measurement is sufficient for the decomposition using fluorescence.

5.2 Contributions

The main contributions of this dissertation are summarized as follow:

- *Separate the reflective and fluorescent components using two complement high frequency illuminations*
  An efficient method is devised for the separation and recovery of full reflectance and fluorescent emission spectra. Then, the absorption spectrum of a material is estimated by using its emission. Since the reflective and fluorescent emission and absorption spectra of the scene are completely recovered, the proposed method also can accurately predict the relighting of scenes under novel lighting.

- *Spectal modeling of refletive-fluorescent scence by using RGB color images*
  The illuminant-invariant chromaticity of fluorescence is exploited to estimate both spectral reflectance and fluorescent chromaticity from RGB images, devise a means for estimating fluorescence absorption and emission spectra from given spectral reflectance and fluorescent chromaticity. Ultimately, I present the first system capable of imaging all reflective and fluorescence absorption and emission spectra of real scenes using only a conventional RGB camera and varied colored illuminants.

- *Interrefletion removal using*
  I derive a general interreflection model for fluorescent materials, develop a method to separate direct-indirect components from reflective-only and fluorescent-reflective measurements, and show that a single-shot measurement is sufficient for the decomposition using fluorescence.

5.3 Future Directions

5.3.1 Separating Reflective and Fluorescent Components Using a Single Hyperspectral Image

In Chapter 2, the separation method for reflective and fluorescent components was proposed that employs the high frequency illumination in the spectral domain to keep the fluorescent component constant under different illumination. This method can effectively separate the reflective and fluorescent components in the scene, but it still need two hyperspectral images captured under two high frequency illuminations.

As stated in chapter [**?**], one of the important characteristics of fluorescence is its wavelength-shifting behavior: fluorescent component absorbs light at a certain wavelength and then reemit it at longer wavelengths, while the reflective component will reflect back light of the same wavelength with the illumination. Therefore, the reflective component can be modulated by the illuminant, which does not affect the fluorescent component except a scale. It is worth investigating how to separate the reflective and fluorescent method based on the signal modulation and demodulation. The potential approach only need to capture the scene under a single high frequency illumination and fast separate these components using signal processing method.

5.3.2 Spectral Modeling Under More General Conditions

In Chapter 3, the illuminations are linear independent but their independence is not so strong. It disclose that the demand for the independence of illuminations spectra is not so high in our method. It is because smooth regularization is employed on the reflectance and fluorescent absorption spectra recovery, and implies that it is possible use to less constraints in the proposed method when their condition number is high. Observing Figure 5.2 (a), there is an inflection point on five singular values. The 5 images captured under 5 illuminants are chosen as input images, which are illuminants 1, 3, 5, 7 and 9 in Figure 3.7. Their singular values are shown in Figure 5.2 and condition

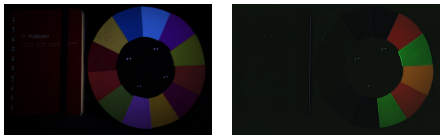

(a) Reflectance (b) Fluorescence

(c) Relighted with fluorescence

Figure 5.1: Relighting results for the fluorescent train scene.

number is 6.38.

The fluorescent color wheel scene is taken as an example and their separation and relighting results are shown in Figure 5.1. Compared with the ground truth in Figure 3.10, the relighting results (Figure 5.1 (c)) can approximate the ground truth well. The separation results in Figure 5.1 (a) (b) are also close to the Figure 5.1 (c) (e). Therefore, it is possible for the proposed method to use less color images to recover reflectance and fluorescence spectra in practice, but the unknown values are less than the constraints so that it become to a underdetermined system, and the proposed method can not guarantee that the results are good enough in any case. To solve this problem, I will use a high speed camera and investigate how the required constraints can be reduced in order to use less changing illuminants.

Besides, a trichromatic camera is used in Chaper 3, only 3 values are used to estimate the fluorescent emission spectra. To overcome this limitation, the proposed method relied on a fluorescent spectral dataset. If the dataset does not cover sufficient number of wavelengths for the application at hand, the proposed method will not work. Also, there is a ambiguity between the chromaticities and the spectra. It is still possible that two materials have the same chromaticities but with the different spectra. This problem only occurs in a small subset of the data but this is still an issue that needs to be addressed in the future. To make the proposed method more effective, we will employ multi-channel cameras(e.g. 4 or 5 channels) and investigate how emission spectra are estimated without relying on a dataset.

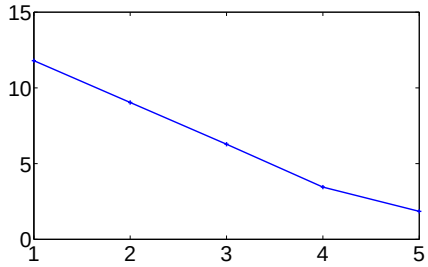

Figure 5.2: The singular values of the illumination spectra.

In addition, the proposed method needs to be calibrated to the camera spectral sensitivity and the illuminant spectra in advance. Han *et al.*[HMS+12] estimated camera spectral sensitivity from a single image under unknown illumination by using fluorescence. Jiang and Gu [JG12] recovered spectral reflectance under commonly available lighting conditions by using a color target which is used to calibrate the camera spectral sensitivity or the spectral distribution of illuminants. Jiang *et al.*[JLGS13] estimated camera spectral sensitivity by using a dataset of spectral sensitivity functions for 28 cameras under unknown the daylight spectra. All these methods require a color checker or a color target to assist with camera spectral sensitivity estimation. Despite the need for some type of calibration target, the mentioned methods can be directly applied to my problem, if the fluorescent-reflective scene is captured with the targets required in their methods. In the future, it is worth investigating to estimate all reflectance, absorption and emission spectra under unknown camera spectral sensitivity or illuminant spectra without the use of a color checker.

5.3.3 Separating the Direct and Indirect Components for Complex Scene by Using a Single-shot

In Chapter 4, the direct and global components are separated for the uniform fluorescent material and Lambertian surface. Nayar *et al.* [NKGR06] devised a way to separate direct and indirect components using high frequency lighting patterns in the spatial domain using multiple images.

The direct component is the light from the source that undergoes a single reflection in the scene before reaching the observer. The global component

is due to indirect lighting from interreflections, subsurface scattering, volumetric scattering and diffusion. When the scene is illuminated by the high frequency illumination in the spatial domain. The direct component is modulated by the high frequency pattern, while the global component still stay in the original frequency domain. If the frequency of the pattern is high enough, the direct and global components can be separated in the frequency domain directly. In the future, it is worth investigating to Separate the direct and indirect components for complex scene by using a single-shot.

Bibliography

[ANN13] Supreeth Achar, Stephen Nuske, and Srinivasa G. Narasimhan. Compensating for motion during direct-global separation. In *Proc. of International Conference on Computer Vision (ICCV)*, pages 1481–1488, Dec 2013.

[ASW10] M. Alterman, Y.Y. Schechner, and A. Weiss. Multiplexed fluorescence unmixing. In *IEEE International Conference on Computational Photography (ICCP)*, 2010.

[Bar99] Kobus Barnard. Color constancy with fluorescent surfaces. In *CIC,Proceedinds of the IS&T/SID Color Imaging Conference*, 1999.

[BPP+03] C. Balas, V. Papadakis, N. Papadakis, A. Papadakis, E. Vazgiouraki, and G. Themelis. A novel hyper-spectral imaging apparatus for the non-destructive analysis of objects of artistic and historic value. *J. Cult. Herit.*, 4(1), 2003.

[CT06] E.J. Candes and T. Tao. Near-optimal signal recovery from random projections: Universal encoding strategies? *IEEE Transactions on Information Theory*, 52(12), 2006.

[CYBE10] Cui Chi, Hyunjin Yoo, and Moshe Ben-Ezra. Multi-spectral imaging by optimized wide band illumination. *IJCV*, 86(2-3), January 2010.

[DTDS12] D.L. Donoho, Y. Tsaig, I. Drori, and J-L Starck. Sparse solution of underdetermined systems of linear equations by stagewise or-

thogonal matching pursuit. *IEEE Transactions on Information Theory*, 58(2), 2012.

[DXW01] Jeffrey M. DiCarlo, Feng Xiao, and Brian A. Wandell. Illuminating illumination. In *CIC*. IS&T/SID, 2001.

[EHJT04] Bradley Efron, Trevor Hastie, Iain Johnstone, and Robert Tibshirani. Least angle regression. *Annals of Statistics*, 32, 2004.

[FA99] H. Farid and E.H. Adelson. Separating reflections and lighting using independent components analysis. In *Computer Vision and Pattern Recognition (CVPR)*, Fort Collins, CO, 1999.

[FD93] B.V. Funt and M.S. Drew. Color space analysis of mutual illumination. *IEEE Trans. Pattern Analysis and Machine Intelligence (PAMI)*, 15(12):1319–1326, 1993.

[FDH91] Brian V. Funt, Mark S. Drew, and Jian Ho. Color constancy from mutual reflection. *International Journal of Computer Vision (IJCV)*, 6(1):5–24, 1991.

[FLM+14] Ying Fu, Antony Lam, Yasuyuki Matsushita, Imari Sato, and Yoichi Sato. Interreflection removal using fluorescence. In *European Conference on Computer Vision (ECCV)*, 2014.

[FLS+13] Y. Fu, A. Lam, I. Sato, T. Okabe, and Y. Sato. Separating reflective and fluorescent components using high frequency illumination in the spectral domain. In *Proc. of International Conference on Computer Vision (ICCV)*, pages 457–464, 2013.

[Fuc01] Eran Fuchs. Separating the fluorescence and reflectance components of coral spectra. *Applied Optics*, 40(21):3614–3621, July 2001.

[FZ89] D. Forsyth and A. Zisserman. Mutual illumination. In *Proc. of IEEE Conference on Computer Vision and Pattern Recognition (CVPR)*, pages 466–473, June 1989.

[FZ90] D. Forsyth and A. Zisserman. Shape from shading in the light of mutual illumination. *Image Vision Computing*, 8(1):42–49, 1990.

[Gat00] N. Gat. Imaging spectroscopy using tunable filters: A review. In *Wavelet Applications VII*, volume 4056. SPIE, 2000.

[Gla95] Andrew S. Glassner. A model for fluorescence and phosphorescence. In *Photorealistic Rendering Techniques*, pages 60–70. Springer Berlin Heidelberg, 1995.

[HFI+08] Matthias B. Hullin, Martin Fuchs, Ivo Ihrke, Hans-Peter Seidel, and Hendrik P. A. Lensch. Fluorescent immersion range scanning. *ACM Trans. Graph.*, 27, 2008.

[HHA+10] Matthias B. Hullin, Johannes Hanika, Boris Ajdin, Hans-Peter Seidel, Jan Kautz, and Hendrik P. A. Lensch. Acquisition and analysis of bispectral bidirectional reflectance and reradiation distribution functions. *ACM Trans. Graph.*, 29, 2010.

[HMS+12] Shuai Han, Y. Matsushita, I. Sato, T. Okabe, and Y. Sato. Camera spectral sensitivity estimation from a single image under unknown illumination by using fluorescence. In *IEEE Conference on Computer Vision and Pattern Recognition (CVPR)*, 2012.

[HP11] R. W. G. Hunt and M. R. Pointer. *Measuring Colour*. John Wiley & Sons, Ltd, 4th edition edition, September 2011.

[HSOS10] Shuai Han, Imari Sato, Takahiro Okabe, and Yoichi Sato. Fast spectral reflectance recovery using DLP projector. In *Proc. of Asian Conference on Computer Vision (ACCV)*, pages 323–335, 2010.

[JF99] G.M. Johnson and M.D. Fairchild. Full-spectral color calculations in realistic image synthesis. *IEEE Computer Graphics and Applications*, 19, August 1999.

[JG12] Jun Jiang and Jinwei Gu. Recovering spectral reflectance under commonly available lighting conditions. In *IEEE Computer Society Conference on Computer Vision and Pattern Recognition Workshops (CVPRW)*, 2012.

[JLGS13] Jun Jiang, Dengyu Liu, Jinwei Gu, and S. Susstrunk. What is the space of spectral sensitivity functions for digital color cameras? In *IEEE Workshop on Applications of Computer Vision (WACV)*, pages 168–179, 2013.

[Kv83] J. J. Koenderink and A. J. vanDoorn. Geometrical modes as a general method to treat diffuse interreflections in radiometry. *Journal of the Optical Soceity of America (JOSA)*, 73(6):843–850, 1983.

[Lak06] Joseph R. Lakowicz. *Principles of Fluorescence Spectroscopy.* Springer, 2006.

[LHY11] Miao Liao, Xinyu Huang, and Ruigang Yang. Interreflection removal for photometric stereo by using spectrum-dependent albedo. In *Proc. of IEEE Conference on Computer Vision and Pattern Recognition (CVPR)*, pages 689–696, 2011.

[LJA97] James E. Leland, Norbert L. Johnson, and Angelo V. Arecchi. Principles of bispectral fluorescence colorimetry. In *Proc. SPIE*, volume 3140, pages 76–87. SPIE, 1997.

[LS13] A. Lam and I. Sato. Spectral modeling and relighting of reflective-fluorescent scenes. In *IEEE Conference on Computer Vision and Pattern Recognition (CVPR)*, 2013.

[LSC01] Bore-Kuen Lee, Feng-Chi Shen, and Chun-Yen Chen. Spectral estimation and color appearance prediction of fluorescent materials. *Optical Engineering*, 40, 2001.

[MGR+06] George McNamara, Amit Gupta, James Reynaert, Thomas D Coates, and Carl Boswell. Spectral imaging microscopy web sites

and data. *Cytometry. Part A: the journal of the International Society for Analytical Cytology*, 69(8), 2006.

[MW86] Laurence T. Maloney and Brian A. Wandell. Color constancy: a method for recovering surface spectral reflectance. *JOSA A*, 3(1), 1986.

[NFB93] S.K. Nayar, X.S. Fang, and T. Boult. Removal of Specularities using Color and Polarization. In *IEEE Conference on Computer Vision and Pattern Recognition (CVPR)*, Jun 1993.

[NG92] Shree K. Nayar and Yitao Gao. Colored interreflections and shape recovery. In *Proceedings of the Image Understanding Workshop*, 1992.

[NIK91] S.K. Nayar, K. Ikeuchi, and T. Kanade. Shape from interreflections. *International Journal of Computer Vision (IJCV)*, 6(3):173–195, 1991.

[NKGR06] Shree K. Nayar, Gurunandan Krishnan, Michael D. Grossberg, and Ramesh Raskar. Fast separation of direct and global components of a scene using high frequency illumination. *ACM Trans. Graph.*, 24(3), July 2006.

[OMK14] Matthew O'Toole, John Mather, and Kiriakos N. Kutulakos. 3d shape and indirect appearance by structured light transport. In *Proc. of IEEE Conference on Computer Vision and Pattern Recognition (CVPR)*, Jun 2014.

[OWH96] Alan V. Oppenheim, Alan S. Willsky, and with S. Hamid. *Signals and Systems*. Prentice Hall, 2 edition, August 1996.

[PHJ89] J. P. S. Parkkinen, J. Hallikainen, and T. Jaaskelainen. Characteristic spectra of munsell colors. *Journal of the Optical Society of America A*, 6, 1989.

[PLGN07a] J. Park, M. Lee, M. D. Grossberg, and S. K. Nayar. Multispectral Imaging Using Multiplexed Illumination. In *ICCV*. IEEE, Oct 2007.

[PLGN07b] Jong-Il Park, Moon-Hyun Lee, Michael D. Grossberg, and Shree K. Nayar. Multispectral imaging using multiplexed illumination. In *Proc. of International Conference on Computer Vision (ICCV)*, pages 1–8, 2007.

[Ros92] F. W. D. Rost. *Fluorescence Microscopy.* Cambridge University Press, 1992.

[SBCD14] Jinli Suo, Liheng Bian, Feng Chen, and Qionghai Dai. Bispectral coding: compressive and high-quality acquisition of fluorescence and reflectance. *Optics Express*, 22(2):1697–1712, January 2014.

[SCC+06] I B Styles, A Calcagni, E Claridge, F Orihuela-Espina, and J M Gibson. Quantitative analysis of multi-spectral fundus images. *Medical Image Analysis*, 10(4), 2006.

[SHC07] Dougles A. Skoog, F. James Holler, and Stanley R. Crouch. *Principles of Instrumental Analysis.* Thomson Publishers, 2007.

[SMK05] Steven M. Seitz, Yasuyuki Matsushita, and Kiriakos N. Kutulakos. A theory of inverse light transport. In *Proc. of International Conference on Computer Vision (ICCV)*, pages 1440–1447, 2005.

[SOS12] I. Sato, T. Okabe, and Y. Sato. Bispectral photometric stereo based on fluorescence. In *Color Imaging Conference: Color Science, Systems, and Applications*, 2012.

[Spr99] Art Springsteen. Introduction to measurement of color of fluorescent materials. *Analytica Chimica Acta*, 380, 1999.

[SZ13] Imari Sato and Cherry Zhang. Image-based separation of reflective and fluorescent components using illumination variant and invariant color. *IEEE Trans. Pattern Analysis and Machine Intelligence (PAMI)*, 35(12):2866–2877, 2013.

[THK11] S. Tominaga, T. Horiuchi, and T. Kamiyama. Spectral estimation of fluorescent objects using visible lights and an imaging

device. In *Proceedinds of the IS&T/SID Color Imaging Conference*, 2011.

[TMMK12] Tali Treibitz, Zak Murez, B. Greg Mitchell, and David Kriegman. Shape from fluorescence. In *European conference on Computer Vision*, 2012.

[Tom96] Shoji Tominaga. Multichannel vision system for estimating surface and illumination functions. *JOSA A*, 13(11), Nov 1996.

[Woo80] Robert J. Woodham. Photometric method for determining surface orientation from multiple images. *Optical Engineering*, 19(1), 1980.

[WWLP06] Alexander Wilkie, Andrea Weidlich, Caroline Larboulette, and Werner Purgathofer. A reflectance model for diffuse fluorescent surfaces. In *International conference on Computer graphics and interactive techniques*, 2006.

[ZS11] C. Zhang and I. Sato. Separating reflective and fluorescent components of an image. In *IEEE Conference on Computer Vision and Pattern Recognition (CVPR)*, 2011.

[ZS13] C. Zhang and I Sato. Image-based separation of reflective and fluorescent components using illumination variant and invariant color. *IEEE Transactions on Pattern Analysis and Machine Intelligence*, 35(12):2866–2877, December 2013.

[ZSS14] Yinqiang Zheng, Imari Sato, and Yoichi Sato. Spectra estimation of fluorescent and reflective scenes by using ordinary illuminants. In *Proc. of European Conference on Computer Vision (ECCV)*, pages 188–202, 2014.

Publications

1. **Ying Fu**, Antony Lam, Imari Sato, Takahiro Okabe, and Yoichi Sato, Separating Reflective and Fluorescent Components using High Frequency Illumination in the Spectral Domain, In proc. *IEEE International Conference on Computer Vision (ICCV)*, pp.457-464, 2013.
2. **Ying Fu**, Antony Lam, Yasuyuki Kobashi, Imari Sato, Takahiro Okabe, and Yoichi Sato, Reflectance and Fluorescent Spectra Recovery based on Fluorescent Chromaticity Invariance under Varying Illumination, In proc. *IEEE conf. Computer Vision and Pattern Recognition (CVPR)*, pp.2171-2178, 2014.
3. **Ying Fu**, Antony Lam, Yasuyuki Matsushita, Imari Sato, and Yoichi Sato, Interreflectance Removal Using Fluorescence, In proc. *European Conference on Computer Vision (ECCV)*, pp.203-217, 2014.
4. **Ying Fu**, Antony Lam, Imari Sato, Takahiro Okabe, and Yoichi Sato, Reflectance and Fluorescent Spectra Recovery via Actively Lit RGB Images, to appear in *IEEE Trans. Pattern Analysis and Mahine Intelligence (PAMI)*,2015.
5. **Ying Fu**, Antony Lam, Imari Sato, Takahiro Okabe, and Yoichi Sato, Separating Reflective and Fluorescent Components using High Frequency Illumination in the Spectral Domain, to appear in *IEEE Trans. Pattern Analysis and Mahine Intelligence (PAMI)*, 2015.